

Modeling and Prediction of Pollutant Emissions in an Axial Turbine

Sneha Ravisankar

Technische Universiteit Delft



Modeling and Prediction of Pollutant Emissions in an Axial Turbine

by

Sneha Ravisankar

in partial fulfillment of the requirements for the degree of
Master of Science
in **Aerospace Engineering**
at the Delft University of Technology,

to be defended publicly on 31st March 2020

Student number: 4724143
Project duration: February 2019 – March 2020
Supervisors: Dr. Arvind Gangoli Rao
Dr. Andre A.V. Perpignan
Thesis Committee: Dr. Arvind Gangoli Rao
Dr. Dirk Roekaerts
Dr. Stephanie Cazaux
Dr. Alexis Bohlin

Abstract

The aviation market has seen a drastic rise in past decades, and is projected to follow a similar trend in the coming years. Stricter regulations and ambitious targets have been framed to effectively curtail the rise in emissions due to this surge in aviation. A multi-fuel blended wing body aircraft is being developed in TUDelft, with the goal of drastically reducing aircraft emissions. To this end, a dual-combustor configuration, which operates with a main combustion chamber and an inter-turbine burner has been proposed. The exhaust gas from the main combustion chamber passes through the high pressure turbine and then proceeds to the inter-turbine burner. It is important to accurately model the evolution of exhaust gas species, from the main combustion chamber through the high-pressure turbine, since this constitutes the species concentration at the inlet of the inter-turbine burner. This, in turn, can have impacts on its performance too. Therefore, this thesis aims to do a detailed parametric analysis to study the individual impact of the operating conditions on the chemical kinetics after the main combustor. The operating temperature has been identified as the most significant parameter that would have drastic impacts on the way emissions evolve after the combustor. The predictions of Turbine Inlet Temperatures for future aircraft have shown only a steady increase. Although the assumption of frozen chemistry after the combustor may have been valid for older engines, the same does not hold as good for futuristic configurations. Newer and different engine architectures like the hybrid engine, which are designed to operate on high cycle temperatures and pressures, cannot ignore the consequence of change in emissions after the combustor in order to retain accuracy in estimations.

Acknowledgement

The successful completion of this thesis would not have been possible without the help, support and encouragement from a number of people and I would like to take this opportunity to show my gratitude to them.

I would like to thank my supervisor, Prof. Arvind Rao for offering me this topic to work with. His critical feedback has been instrumental in shaping this work, and also my outlook and approach towards research in general. I also would like to thank my other supervisor, Andre A. V. Perpignan, for the direction, support and feedback that he have provided me with. Our conversations have always given me a lot of insight and a much-needed outsider's perspective.

I would also like to thank my best friends Siva Kumar and Vidyuth who have been my long-distance support back from India. Thank you for not only listening to my endless rambling, but also actively trying to help me out by providing suggestions to handle any and every sort of issue, be it academic or personal. I also would like to thank the amazing best friend I made in Delft, Adithya Baliga. You have been a pillar of support during some of the worst times and always strived to help me out in any way possible. Thank you for all the food, the good times and every interesting and insightful conversation we have had. You are one of the very few people who would engage with me in conversations of any kind and that is really appreciated.

I am indebted to my grandfather, Ramanathan who had helped me when I needed it the most. I would like to express my deepest and most sincere gratitude to my parents, Latha and Ravisankar. A masters in Aerospace Engineering would have remained only a dream if not for their struggles, hardships and sacrifices. I know no other parents as supportive, as motivating and as loving as you both. Amma, thank you for all your love and support that has made my life easier so many times in so many ways. Daddy, thank you for going through any mile possible to make sure I only see the bright side of life. Having you both as parents is the badge I have always worn proudly for as long as I can remember. I would also like to express my sincere gratitude to my other set of parents, my sister and brother-in-law - Priyamvatha and Viswanath. Priya, we becoming sisters is God's way of ensuring I have the most fun childhood. Thank you for being the biggest cheerleader in my life in everything I do. Wish, thank you for being the perfect combination of an elder brother, best friend, confidante and sometimes a father. I would also like to thank my companion for life, Vishal Venkatesh, for all that he has done. Coming to a different country for studying is an exciting and intimidating experience. Your presence has helped me feel only the former. Thank you for all the support you have shown in terms of academics, and more importantly food. Thank you for being the best friend you have always been, no matter what came in the way.

Thank you to everyone who has helped me inch closer towards my dream. I hope to have made you proud.

*Sneha Ravisankar
March 2020*

Contents

Abstract	iii
Acknowledgement	v
List of Figures	ix
Nomenclature	xi
1 Introduction	1
1.1 Context	1
1.1.1 Aviation industry - growing traffic and regulations	1
1.1.2 Trend of engine development	2
1.2 Research Background	3
1.2.1 Hybrid Engine Configuration	3
1.3 Research motivation	4
1.3.1 Research Question	5
1.4 Research Method: Chemical Reactor Network Modeling	5
1.5 Report structure.	5
2 Scientific Background and Literature Review	7
2.1 Fundamentals of combustion.	7
2.1.1 The Combustion Reaction	7
2.1.2 Stoichiometry	7
2.1.3 Equivalence ratio	7
2.2 Thermodynamics of Combustion	8
2.2.1 Gibbs free energy	8
2.2.2 Enthalpies	10
2.2.3 Heat/Enthalpy of combustion	10
2.3 Chemical Kinetics of Combustion.	11
2.3.1 Residence time.	11
2.3.2 Reaction time	11
2.3.3 Elementary reactions	12
2.3.4 Reaction rate.	13
2.3.5 Reaction rate constant	14
2.4 Reaction Mechanisms.	14
2.4.1 Reaction Mechanisms for methane combustion	15
2.4.2 Reduced mechanisms	16
2.5 NO _x formation mechanisms	18
2.5.1 Thermal NO _x (Zeldovich mechanism)	18
2.5.2 Prompt NO _x (Fenimore mechanism).	19
2.5.3 N ₂ O mechanism	20
2.5.4 Fuel bound NO _x	20
2.5.5 NNH pathway	21
2.6 CO emissions	21
2.7 Evolution of exhaust gas species downstream of the combustor	22
2.8 CRN models of the hybrid engine	28
2.8.1 Rao and Bhat CRN model	28
2.8.2 RQL combustion in the hybrid configuration	28
2.8.3 Model by Rosati	28
2.8.4 Model by Talboom	29
2.9 Summary	30

3	Modeling Tools, Method and Validation	31
3.1	Modeling tools	31
3.1.1	Reactor models used	31
3.2	Method	34
3.2.1	CRN Architecture	34
3.2.2	Cycle Parameters.	35
3.2.3	Reactor Dimensions	36
3.3	Chemical kinetics study.	37
3.4	Model Validation	37
3.5	Summary	39
4	Results and Discussion	41
4.1	Intent of the parametric analysis	41
4.1.1	Parameters considered.	41
4.2	Turbine Inlet Temperatures	42
4.2.1	Evolution of CO with TIT.	42
4.2.2	Evolution of NO _x for TIT	44
4.3	Inlet Pressures	45
4.3.1	Evolution of CO with inlet pressures	46
4.3.2	Evolution of NO _x with inlet pressures	47
4.4	Reaction mechanisms.	51
4.4.1	Evolution of CO with different mechanisms	51
4.4.2	Evolution of NO _x with different mechanisms	51
4.5	Residence time in the combustor	52
4.5.1	Evolution of CO with residence time	53
4.5.2	Evolution of NO _x with residence time	55
4.6	Temperature change in the HPT	55
4.6.1	Evolution of CO with temperature change	56
4.6.2	Evolution of NO _x with temperature change	56
4.7	Temperature and pressure change in the HPT.	56
4.7.1	Evolution of CO with temperature and pressure change in the HPT	58
4.7.2	Evolution of NO _x with temperature and pressure change in the HPT	58
4.8	Kerosene vs LNG	59
4.9	Evolution of emissions for a conventional turbofan engine	64
4.10	Summary	66
5	Conclusions and Recommendations	67
5.1	Summary	67
5.2	Conclusions.	68
5.3	Recommendations for future research	69
	Bibliography	71

List of Figures

1.1	Evolution of aircraft transport efficiency, Fig. courtesy: [11]	2
1.2	Evolution of TIT and future trend, Fig. courtesy: [11]	3
1.3	The multi-fuel, blended wing-body aircraft configuration, Fig. courtesy: [13]	3
1.4	Schematic of the hybrid, multi-fuel engine, Fig. courtesy: [16]	4
2.1	Gibbs free energy vs Reaction progress for 3 cases, Fig. courtesy [21]	9
2.2	Summary of four scenarios of enthalpy and entropy changes denoting the spontaneity of processes, Fig. courtesy [21]	10
2.3	Relationship between enthalpies of formation and reaction, Fig. courtesy [2]	11
2.4	Chemical species behaviour over time in case of stoichiometric combustion of gaseous fuel and oxygen and with exhaust gas recirculation, Fig. courtesy [23]	12
2.5	Major chemical pathways for methane oxidation involving C ₁ to C ₂ hydrocarbon orders for lean conditions. Fig. courtesy [70], [67]	17
2.6	Dependence of air number (equivalence ratio) on the NO production in a well-stirred reactor; Fig. courtesy [77], [78].	20
2.7	H-, N-, and S-containing gas species mole fractions (expressed as mole fraction*10 ⁿ ; n corresponds to the values on the y axis) in the post combustor flow of RB211 engine for Fluid Sulfur Content (FSC) = 0.04% (dashed curves), and = 0.3% (solid curves), Fig. courtesy [80].	23
2.8	The time evolution of concentration of NO _x species in the combustor and postcombustor region vs the APEX measured data, Figure courtesy [84].	24
2.9	The time evolution of concentration of sulfur-containing species in the combustor and post-combustor region vs the APEX measured data, Figure courtesy [84].	25
2.10	The time evolution of concentration of CO in the combustor and postcombustor region vs the APEX measured data, Figure courtesy [84].	25
2.11	Generalized flow path evolutionary trends after the combustor, for different species, as obtained from 1D simulations, Figure courtesy [88].	26
2.12	Comparison of 1D and 2D solutions through a single turbine blade row for SO ₃ , Figure courtesy [88].	26
2.13	The predicted NO and NO ₂ (lines in the figure) in the HES for both flight conditions, compared with measurement data (points in the figure), Figure courtesy: [104].	27
2.14	Reactor Network Model of the hybrid combustion system by Rao and Bhat, Fig. courtesy: [107]	28
2.15	The CRN of the main combustor as modeled by Rosati, Fig. courtesy: [108]	29
2.16	CRN for the main combustor developed in [20]	30
2.17	CRN for the inter-turbine burner developed in [20]	30
3.1	The illustration of a perfectly stirred reactor, Figure courtesy: [109].	32
3.2	The illustration of a plug flow reactor, Figure courtesy: [109].	33
3.3	The Bragg's combustor. Fig. courtesy: [110]	34
3.4	The CRN used for gas turbine combustion in [112]	35
3.5	The CRN used to model the main combustor of the hybrid engine configuration. Fig. courtesy [20]	35
3.6	The schematic of the main combustor + HPT CRN that has been modeled for this thesis	36
3.7	Emissions at takeoff - Bisson et al. vs CRN	37
3.8	Emissions at climbout - Bisson et al. vs CRN	38
3.9	Emissions at approach - Bisson et al. vs CRN	38
3.10	Emissions at idle - Bisson et al. vs CRN	39
4.1	The schematic of the main combustor + HPT CRN pertaining to the components of the hybrid engine configuration	42

4.2	CO at the stator inlet (blue curve) and the exit (orange curve) vs TIT	43
4.3	CO vs Residence time in the HPT (for different TITs)	43
4.4	CO vs Residence time for different equivalence ratios with combustor inlet conditions i.e. $T_{inlet} = 450K$ and $P = 4atm$. Fig. courtesy [121]	44
4.5	CO vs Residence time for different equivalence ratios and for two different combustor inlet pressures. Fig.courtesy [122]	44
4.6	NOx at the stator inlet (blue curve) and the exit (orange curve) vs TIT	45
4.7	Contribution of NOx pathways to the total NOx emissions from the main combustor with TIT	45
4.8	Contribution of NOx pathways to the total NOx emissions from the HPT with TIT	46
4.9	Increase of total NOx from the stator inlet to exit with respect to TITs	46
4.10	CO vs turbine inlet pressures for the highest and lowest TIT	47
4.11	NOx vs turbine inlet pressures for the highest and lowest TIT	47
4.12	Contribution of NOx pathways to the total NOx emissions from the combustor for the lowest TIT investigated (1657K)	48
4.13	Contribution of NOx pathways to the total NOx emissions from the HPT for the lowest TIT investigated (1657K)	48
4.14	Increase of total NOx from the stator inlet to exit with respect to turbine inlet pressures for the lowest TIT investigated (1657K)	49
4.15	Contribution of NOx pathways to the total NOx emissions from the combustor for the highest TIT investigated (2193K)	49
4.16	Contribution of NOx pathways to the total NOx emissions from the HPT for the highest TIT investigated (2193K)	50
4.17	Increase of total NOx from the stator inlet to exit with respect to turbine inlet pressures for the highest TIT investigated (2193K)	50
4.18	CO at the stator inlet and the exit assessed by three different mechanisms with respect to TITs	51
4.19	NOx at the stator inlet and the exit assessed by three different mechanisms	52
4.20	Relative contribution of NOx pathways at the combustor exit/stator inlet with TIT, as estimated by three different mechanisms	53
4.21	Relative contribution of NOx pathways at the stator exit with TIT, as estimated by three different mechanisms	54
4.22	Chemical and flow time scales in a turbulent reacting flow, Figure courtesy: [22, 125]	54
4.23	CO at the stator inlet and exit vs Residence time in the HPT for different combustor residence times	55
4.24	NOx at the stator inlet and exit vs Residence time in the HPT for different combustor residence times	56
4.25	CO vs Residence time in the HPT with and without temperature change for the lowest and highest temperature and pressure	57
4.26	NOx vs Residence time in the HPT with and without temperature change for the lowest and highest temperature and pressure	57
4.27	A blade row of the turbine of a typical aero-engine depicted along with the representative variation of temperature and pressure along the engine	58
4.28	CO vs Residence time in the HPT for four scenarios corresponding to the temperature and pressure change for the lowest and highest temperature and pressure	59
4.29	NOx vs Residence time in the HPT for four scenarios corresponding to the temperature and pressure change for the lowest and highest temperature and pressure	59
4.30	CO at the HPT stator inlet and the exit vs TIT compared for using kerosene and LNG in the main engine of the hybrid combustor	60
4.31	NOx at the HPT stator inlet and the exit vs TIT compared for using kerosene and LNG in the main engine of the hybrid combustor	61
4.32	CO at the HPT stator inlet and the exit vs turbine inlet pressure compared for using kerosene and LNG in the main engine of the hybrid combustor for the lowest and the highest TITs investigated	61
4.33	NOx at the HPT stator inlet and the exit vs turbine inlet pressure compared for using kerosene and LNG in the main engine of the hybrid combustor for the lowest and the TITs investigated	62
4.34	CO and NOx vs Residence time in the HPT for four scenarios corresponding to the temperature change and pressure expansion for the lowest and highest temperature and pressure	63
4.35	The cutaway drawing of the CF680C2 engine	64

4.36 Turbine Inlet Temperature and Residence time of the CF6-80 engine with operating conditions	65
4.37 The emissions at the stator inlet and exit for different operating conditions of the CF6-80 turbo-fan engine	66

Nomenclature

Abbreviations

<i>CRN</i>	Chemical Reactor Network
<i>HES</i>	Hot End Simulator
<i>HPT</i>	High Pressure Turbine
<i>ITB</i>	Inter-Turbine Burner
<i>LH2</i>	Liquefied Hydrogen
<i>LNG</i>	Liquefied Natural Gas
<i>OPR</i>	Overall Pressure Ratio
<i>PFR</i>	Plug Flow Reactor
<i>PSR</i>	Perfectly Stirred Reactor
<i>RQL</i>	Rich burn - Quick quench - Lean burn
<i>sfc</i>	specific fuel consumption
<i>TIT</i>	Turbine Inlet Temperature
<i>WSR</i>	Well Stirred Reactor

Subscripts and superscripts

"	corresponds to products
'	corresponds to reactants
<i>f</i>	forward
<i>f</i>	fuel
<i>i</i>	chemical species
<i>in</i>	inside the control volume
<i>j</i>	elementary reaction
<i>mix</i>	mixture
<i>out</i>	outside the control volume
<i>prod</i>	products
<i>r</i>	reverse
<i>reac</i>	reactants
<i>rxn</i>	reaction
<i>st</i>	stoichiometric
<i>t</i>	total

Greek Symbols

ϕ	equivalence ratio	
ρ	density	kg/m^3
τ	residence time	ms
$\dot{\omega}$	net rate of production of species	

Symbols

$[i]$	concentration of i-th species	
\bar{h}_i	specific enthalpy at given temperature	J/kg
$\bar{h}_{f,i}^0$	enthalpy of formation	J/kg
Δh	enthalpy of combustion/reaction	J/kg
$\Delta \bar{h}_{s,i}$	sensible enthalpy change	J/kg
\dot{Q}	heat transfer rate	J/s
\dot{m}	mass flow rate	kg/s
ν	stoichiometric coefficient	
A	area	m^2
A	pre-exponential factor	
A/F	Air-Fuel ratio	
C_p	heat capacity	J/K
c_p	specific heat capacity	J/kgK
C_xH_y	Hydrocarbon Fuel	
CO	Carbon Monoxide	
CO_2	Carbon dioxide	
E_a	activation Energy	J/mol
EI	Emission Index	g/kg
F/A	Fuel-Air ratio	
k	reaction rate constant	
m	mass	kg
MW	Molecular Weight	
N_2	Nitrogen	
NO_x	Nitrogen Oxides	
O_2	Oxygen	
P	pressure	bar
Pe	perimeter	m
PM	Particulate Matter	

R	rate of formation of species	
SO_x	Sulphur Oxides	
T	temperature	K
u	velocity	m/s
UHC	Unburnt HydroCarbons	
V	Volume	m^3
X	mole fraction	
Y	mass fraction	

1

Introduction

The intent of this report is to elucidate the research work that was carried out in assessing the behaviour of emissions *after* the combustor, in a high pressure turbine. This chapter introduces the context in which this thesis work was carried out, explaining the background and the motivation for this work. Further, the research objective and research question are described. This chapter concludes with a short note on the modelling approach, and the structure of this report.

1.1. Context

1.1.1. Aviation industry - growing traffic and regulations

The aviation industry has been seeing a steady growth due to increasing population (hence increasing demand) and the advancement of developing countries. According to the report made by Airbus [1], the rise in air traffic has been unaffected by fundamental factors like the fuel crisis. This is proved by the growth in air traffic capacity of as many as 117 countries, by at least 5% in 2017. With this trend, the forecast is that, from 2018 to 2037, a minimum of 39210 new aircraft should be brought into service in order to cater to the demands due to this steady growth.

This has resulted in the environmental impact of aviation becoming an inevitable focus. Aircraft emissions have varying detrimental impacts on the environment - locally and globally, in the form of pollutants which have an effect on the air quality, climate change, and human health [2]. The aircraft emissions that fall under this category are - Nitrogen Oxides (NO_x), Carbon Monoxide (CO), Carbon dioxide (CO₂), Sulphur Oxides (SO_x), Unburned HydroCarbons (UHC), and Particulate Matter (PM) [3]. Although most of these emissions have been considerably reduced as a result of improved engine designs [3], this is far from sufficient to counter the projected future trend. This ceaseless expansion results in an estimate that aviation emissions are bound to grow as much as 300% - 700% of the amount in 2005 [4].

The report - *Aviation and the Global Atmosphere* [5] made by the International Panel on Climate Change gave a thorough analysis of aviation emissions and their impacts - both short-term and long-term, on climate change. This report, was used by the International Civil Aviation Organization (ICAO) to draft three broad environmental goals in 2004 [6]:

- limit or reduce the number of people affected by significant aircraft noise
- limit or reduce the impact of aviation emissions on local air quality, and
- limit or reduce the impact of aviation greenhouse gas emissions on the global climate.

Based on these goals, the ICAO has devised much stricter emission regulations for aircraft engine certifications [7]. Apart from these regulations, in order to tackle with these estimates, the Advisory Council for Aviation Research in Europe (ACARE) has setup the following goals to be achieved by 2050, called the *Flightpath 2050* [8]:

- 75% reduction in CO₂ emissions

- 90% reduction in NO_x emissions
- 65% reduction in noise

with reference to the emissions of an aircraft from the year 2000.

These goals were set-up with the aim of achieving them through technological advancements in aircraft design and also by fuel options. An extensive study has been done on the impacts of various levels of attaining the ACARE goals, on the emissions by the year 2050 by Bethan et al. in [9]. It was found that the best results were corresponding to a specific scenario, B1. B1 comprised of improved engine configurations and fuel efficiencies that led to 0.8% and 0.1% decrease in rate of NO_x and CO emissions per year.

Consequently, modern engine designs have achieved considerably reduced CO and UHC levels at all low-power. Therefore most of the emissions from these engines are predominantly NO_x because of their significant numbers at cruise altitude conditions [10]. Although CO₂ is a greenhouse gas and has its own detrimental impact on the environment, it is not considered as a pollutant like other emissions, because it is a by-product of complete combustion. Nevertheless, CO₂ can be lowered by low (specific) fuel consumption (in case of hydrocarbon fuels) or by using alternative fuels which contain non-carbon species.

1.1.2. Trend of engine development

Another challenge facing aircraft manufacturers is the need of airline companies to increase or at least maintain their profitability, by means of reduced operating costs. Therefore, novel designs are needed to be made while considering the regulations imposed and also the operating costs that airlines would incur. One of the ways to achieve these two objectives together would be to consider the specific fuel consumption (SFC). Reduced SFC leads to better output in terms of CO₂ goals, and also decreased fuel costs for the airliner. The SFC can be improved by improving the thermal and propulsive efficiencies. Thus, throughout the years, aircraft engines have been innovated with designs leading to drastic reduction in fuel burn as seen in figure 1.1.

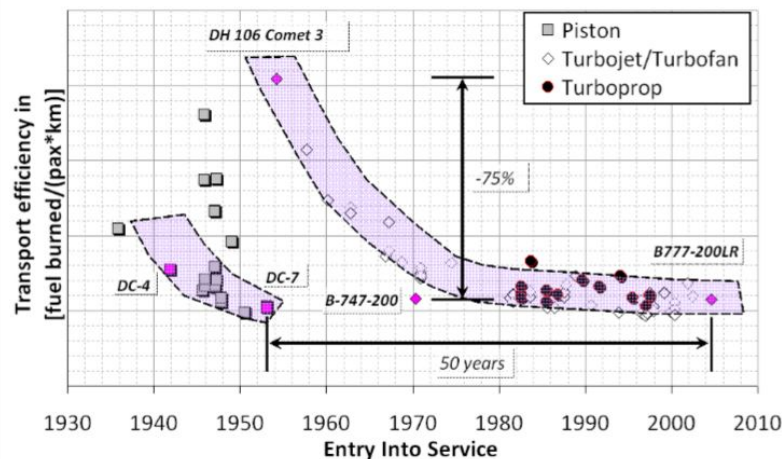


Figure 1.1: Evolution of aircraft transport efficiency, Fig. courtesy: [11]

The thermal efficiency is in turn dependent on the thermodynamic efficiency which can be raised by raising the Overall Pressure Ratio (OPR) of the engine. The increase in OPR means that the inlet pressures and temperatures increase too. This leads to higher Turbine Inlet Temperatures (TITs) which are limited by the metal temperatures of the turbine, especially during take-off and top of climb. These high temperatures are inherently adverse in an emission point-of-view, especially for NO_x emissions which increase due to these higher temperatures. Although the amount of NO_x with increasing OPR (and thus increasing TIT) has been lowered by incorporating and improving low emission combustor technologies, the trend of rising TITs is projected to increase steadily as shown in figure 1.2.

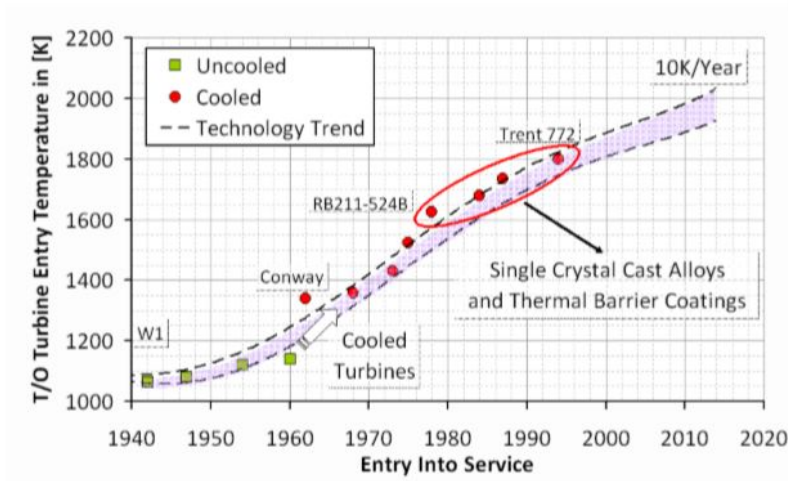


Figure 1.2: Evolution of TIT and future trend, Fig. courtesy: [11]

1.2. Research Background

1.2.1. Hybrid Engine Configuration

To meet with the ACARE goals, the novel hybrid engine concept has been developed as a result of the *Advanced Hybrid Engine for Aircraft Development (AHEAD)* project in the EU [12]. This engine has been developed for a new blended wing-body aircraft configuration. The layout of this blended wing-body aircraft is given below in figure 1.3.

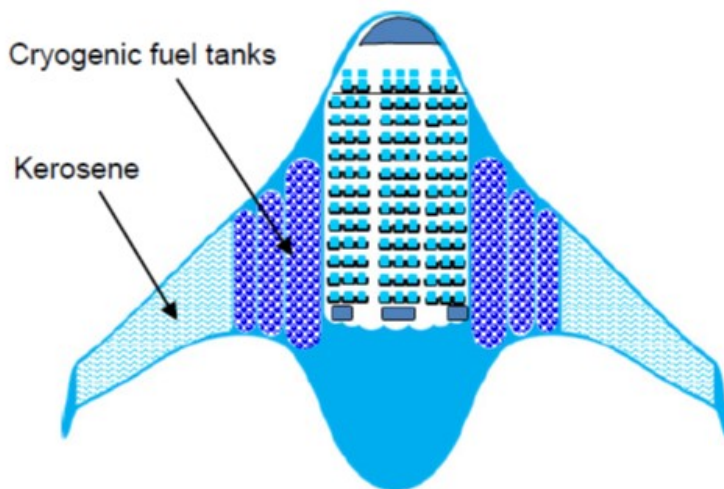


Figure 1.3: The multi-fuel, blended wing-body aircraft configuration, Fig. courtesy: [13]

Since one of the primary goals is CO₂ reduction, the inclusion of alternative aviation fuels becomes indispensable. These alternative fuels should not compromise on the quality and output of combustion, and have minimal CO₂ output. Since these are aviation fuels, the weight and storage issues due to the change in fuel should not outweigh the other advantages it could possibly provide.

This hybrid engine is a turbofan engine with contra-rotating fans, followed by the high and low pressure compressors. There is a gear box which proves as an advantage since the contra-rotating fans and the low pressure compressor can be driven at different rotational speeds for their favourable operation. The individualizing aspect of this engine is the dual combustion chamber design - a main combustor which operates on alternate fuels like Liquid Hydrogen or Liquefied Natural Gas. The second(ary) combustor is the Inter-Turbine Burner (ITB) located between the high and the low pressure turbines, and operates on conventional

or bio-fuels. There is also scope to use the Flameless Combustion regime in the ITB, which is advantageous in terms of NO_x emissions [14]. The schematic of this engine is shown in figure 1.4

The hybrid engine is therefore a turbofan engine with a ultra high bypass ratio which has also been conceived to operate with high overall pressure ratio. The result is that the core mass flow is low and the temperatures and pressures are high.

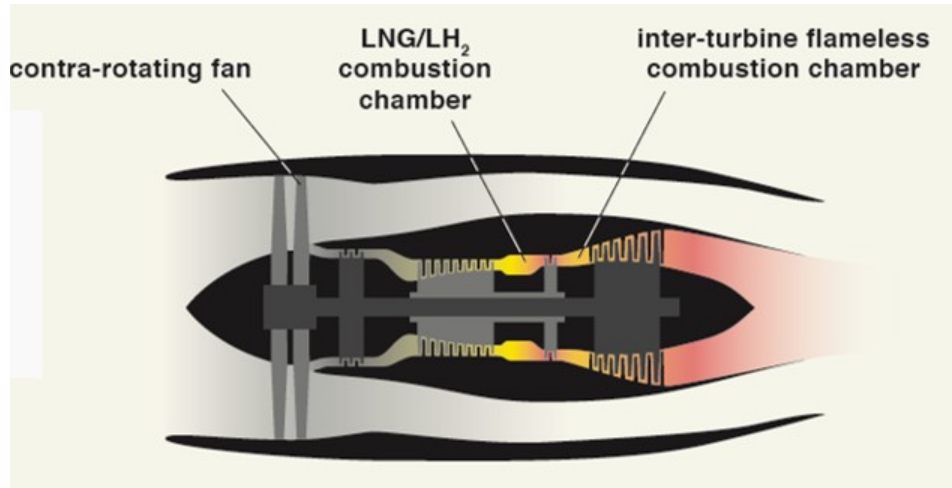


Figure 1.4: Schematic of the hybrid, multi-fuel engine, Fig. courtesy: [16]

Among the many candidates for alternate fuels, Liquid Hydrogen (LH₂) and Liquefied Natural Gas (LNG) are competent due to their higher mass energy density (/kg) compared to kerosene [13], [15], which makes these advantageous in terms of mass (weight). But due to their lower volumetric energy density (/litre) compared to that of kerosene, they demand more volume in terms of storage. This is satisfied by the blended wing-body design that can meet the storage demands [13], [15]. These alternate fuels are required to be stored in cryogenic conditions and therefore can also be used for cooling [15].

1.3. Research motivation

One of the prime motives of the development of this hybrid engine configuration is to meet with the aforementioned emission targets. Therefore it is equally important to study the resulting emissions, as much as its performance. Usually, in attempts to simulate the impact of aviation on the atmosphere and its processes, the engine emissions were assumed to correspond to the equilibrium composition of the species at the combustor outlet [17]. But this approach was found to be inaccurate in accounting for emissions in some cases, from various studies as explained in section 2.7.

The hybrid engine configuration is one with two combustion chambers. This means that the inlet of the ITB is not composed only of pure air but it is the exhaust from the upstream combustor which also passes through the high pressure turbine before entering the ITB. This exhaust, combined with the cooling air of the turbine forms the inlet of the ITB. This inlet mixture has lesser oxygen content (14-17.5%) when compared to fresh air (23%), and a higher water vapour content (6.7%), and is called vitiated air [18], [19].

The chemistry of the exhaust from the main combustor which passes through the high pressure turbine, cannot be considered frozen until the inlet of the ITB. The temperature and pressure in the high pressure turbine undergo drastic variation. Such a variation and its impact on the chemistry of the exhaust gases cannot be ignored if the performance of the ITB has to be modeled precisely. There have been research works done previously to investigate the main combustor and the ITB, both separately and together.

In [18], the dual combustor configuration is modeled together by considering the exhaust of the main combustor to be equivalent to the inlet of the ITB. In [19], there were both experimental and chemical kinetic studies conducted for the ITB. While the chemical kinetic study considered the vitiated air i.e. exhaust from the main combustor as the inlet for the secondary combustor, the experimental campaign was done for pure

air as the oxidiser and at atmospheric pressure conditions. The preliminary chemical kinetic study showed the considerable difference in CO and NO_x emissions from the ITB while considering pure air at the inlet vs vitiated air at the inlet. The hybrid engine CRN in [20] was made by combining both the combustors and with the HPT in between them. The temperature and pressure variations were imposed for four cases of the ITB energy fraction.¹ Although the HPT was considered and modeled, the Perfectly Stirred Reactor (PSR) model was used for the modeling which is not the most appropriate reactor to model the same. Apart from that, the detailed role of the HPT in the content of the inlet conditions of the ITB were also not investigated.

1.3.1. Research Question

Thus, the change in chemistry of the exhaust gases cannot be ignored, particularly while studying the hybrid engine configuration if the performance of the ITB has to be modeled well. While there have been earlier studies on modeling the change of emissions through the HPT [sec 2.7], they have been dedicated for only a few conditions of an engine. A detailed analysis on how emissions would behave as a result of different parameters has not been done earlier. Thus the following research question was framed for the purpose of this thesis:

How do CO and NO_x evolve after the combustor and what are the parameters that influence this evolution the most?

1.4. Research Method: Chemical Reactor Network Modeling

In order to answer the aforementioned research question, the Chemical Reactor Network (CRN) modeling was chosen. This is because CRNs are computationally viable while allowing the use of detailed chemical reaction mechanisms because of their simplified assumption of the flow-field. The CRN consists of both the main combustor and the HPT which are modeled using appropriate reactors as explained later. The network architecture and the conditions investigated are explained in detail in the forthcoming sections.

1.5. Report structure

The layout of this report is structured in the following way. The explanation of the scientific background and the literature review pertaining to this thesis are explained in chapter 2. The method and tools used for modeling are described in chapter 3. This chapter also describes the setup of the CRN analysis and its validation. The results are extensively presented and discussed in chapter 4. Using these results conclusions are drawn and recommendations for future work are suggested in 5.

¹The energy fraction of the ITB is defined as the ratio of the energy input of the ITB to the total energy input for the hybrid combustion system

2

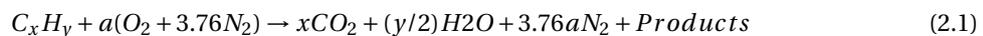
Scientific Background and Literature Review

This chapter aims to explain the scientific background underlying for the work pertaining to this thesis. A detailed literature review on some of the most important aspects have also been presented in this chapter.

2.1. Fundamentals of combustion

2.1.1. The Combustion Reaction

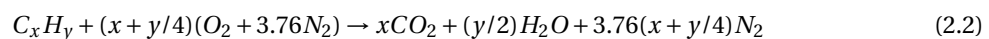
This section gives a brief description of the important aspects and parameters relating to combustion. Combustion is the chemical reaction between two reactants - fuel and oxidizer. It is an exothermic process which leads to the release of heat and light, and subsequently results in products which are mainly CO₂ and H₂O. In gas turbine systems, hydrocarbon fuels are usually used, which leads to the following reaction equation;



The reactants are usually fuel and air, which serves as the oxidizer. CO₂ and H₂O are the main outcome of the combustion reaction. The remaining "Products" indicate the other minor species which are formed as a result of not attaining complete combustion. These mainly include the pollutant species under consideration, and also other species which form the byproduct of incomplete combustion. The kind of pollutants that are obtained from this combustion reaction depends on the contents of the oxidiser.

2.1.2. Stoichiometry

The quantity of oxidiser precisely required for the complete oxidation of a specific quantity of fuel is called the stoichiometric oxidiser quantity. The availability of stoichiometric quantity of oxidizer does not necessarily guarantee that combustion in a practical system is complete. Nevertheless, in principle, a stoichiometric mixture of fuel and oxidizer would yield no products other than the ones mentioned in the following stoichiometric combustion reaction:



The above equation is based on the assumption that air is the oxidiser and consists of 21% of oxygen and 79% of nitrogen leading to 3.76 moles of N₂ for each mole of O₂. It must be noted that in most cases combustion is not stoichiometric. Therefore other parameters have to be defined in order to describe the actual combustion, in comparison to the stoichiometric combustion of the considered fuel and oxidizer.

2.1.3. Equivalence ratio

The amount of available fuel and oxidiser is one of the important factors which determine the nature of the combustion process and its outcome. They are described in the form of either air-fuel ratio or fuel-air ratio. A convenient way of defining these quantities is by using the equivalence ratio. The equivalence ratio is the ratio of the actual quantity vs the stoichiometric quantity. Thus, if fuel-air-ratio is considered, the equivalence ratio is,

$$\phi = \frac{\left(\frac{m_{fuel}}{m_{air}}\right)}{\left(\frac{m_{fuel}}{m_{air}}\right)_{st}} \quad (2.3)$$

If the air-fuel-ratio is considered, the equivalence ratio is,

$$\phi = \frac{\left(\frac{m_{air}}{m_{fuel}}\right)_{st}}{\left(\frac{m_{air}}{m_{fuel}}\right)} \quad (2.4)$$

where the stoichiometric air-fuel-ratio is calculated for hydrocarbon fuels used in equations 2.1 and 2.2 as,

$$(A/F)_{st} = \frac{4.76(x + y/4) MW_{air}}{1 MW_{fuel}} \quad (2.5)$$

where MW_{air} and MW_{fuel} are the molecular weights of air and the fuel respectively.

And,

$$(F/A)_{st} = \frac{1}{(A/F)_{st}} \quad (2.6)$$

Irrespective of whether the air-fuel-ratio or the fuel-air-ratio is used, the definition of equivalence ratio helps to identify and compare the proportion of fuel and oxidizer. An equivalence ratio of greater than unity means a fuel-rich mixture i.e. there is excess fuel content, whereas an equivalence ratio of less than unity means a fuel-lean mixture. If the equivalence ratio equals unity, the fuel-air mixture is stoichiometric.

2.2. Thermodynamics of Combustion

2.2.1. Gibbs free energy

The Gibbs free energy is a state function which can be calculated for physical and chemical reactions. The change in Gibbs free energy during a chemical reaction is calculated by using the change in enthalpy and change in entropy. Thus,

$$\Delta G = \Delta H - T\Delta S \quad (2.7)$$

where,

ΔG = change in Gibbs free energy;

ΔH = change in enthalpy i.e. for combustion means the enthalpy of reaction (which has been explained in the forthcoming sections);

ΔS = change in entropy of the reaction.

The change in Gibbs free energy can be interpreted as a driving force to reaction progress, which is represented in the following figure 2.1. There are three cases of the free energy change which can be associated to three outcomes.

1. **when $\Delta G < 0$** the process is called *exergonic* and it represents a spontaneous driving force in the forward direction i.e. towards the formation of products
2. **when $\Delta G > 0$** the process is said to be *endergonic* which ends up favouring the reverse direction i.e. the formation of reactants spontaneously
3. **when $\Delta G = 0$** the process is said to be in *equilibrium* and the concentration of the reactants and products remain constant

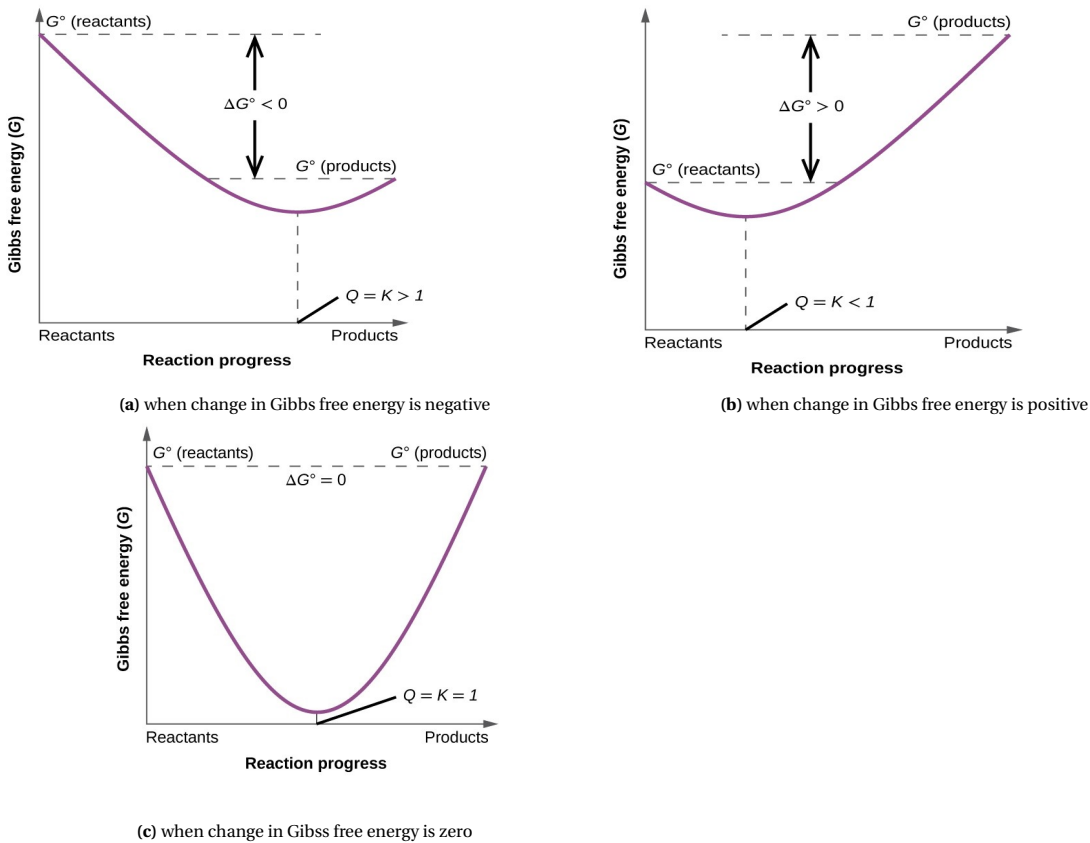


Figure 2.1: Gibbs free energy vs Reaction progress for 3 cases, Fig. courtesy [21]

Spontaneity of a reaction

Depending on whether ΔH and ΔS are positive or negative, the spontaneity of a process can be understood. The sign of ΔH helps to determine whether a process or a reaction is exothermic (heat giving) or endothermic (heat absorbing). It must be noted that combustion is an exothermic process which gives out heat from the fuel that is used as an energy source in a system. Thus, there are four possible scenarios for positive and negative enthalpy and entropy changes, which subsequently reflect as the change in Gibbs free energy. These four scenarios, as shown in figure 2.2 are:

- when ΔH and $\Delta S > 0$ - This scenario is pertinent to an endothermic process that has an increase in the system entropy. This scenario leads to two possibilities of the change in Gibbs free energy. ΔG is negative if the magnitude of $T\Delta S$ is greater than ΔH , and therefore the process is spontaneous at high temperatures. A non-spontaneous process is the result of $T\Delta S$ being lesser in magnitude than ΔH leading to ΔG being positive.
- when ΔH and $\Delta S < 0$ - This scenario is pertinent to an endothermic process that involves a decrease in system entropy. This scenario also leads to two possibilities of the change in Gibbs free energy. ΔG is negative if the magnitude of $T\Delta S$ is lesser than that of ΔH and therefore the process is spontaneous at low temperatures. When ΔG is positive as a result of $T\Delta S$ being greater in magnitude than ΔH , this leads to non-spontaneous process at high temperatures
- when ΔH is > 0 and $\Delta S < 0$ - This scenario means an endothermic process which has a decrease in entropy thus leading to ΔG being positive at all temperatures and hence leading to non-spontaneous process at all temperatures
- when ΔH is < 0 and $\Delta S > 0$ - This scenario corresponds to an exothermic process which involves an increase in entropy which leads to ΔG being negative irrespective of the temperature and thus the process is spontaneous at all temperatures

	$\Delta H > 0$ (endothermic)	$\Delta H < 0$ (exothermic)
$\Delta S > 0$ (increase in entropy)	$\Delta G < 0$ at high temperature $\Delta G > 0$ at low temperature Process is spontaneous at high temperature	$\Delta G < 0$ at any temperature Process is spontaneous at any temperature
$\Delta S < 0$ (decrease in entropy)	$\Delta G > 0$ at any temperature Process is nonspontaneous at any temperature	$\Delta G < 0$ at low temperature $\Delta G > 0$ at high temperature Process is spontaneous at low temperature

Figure 2.2: Summary of four scenarios of enthalpy and entropy changes denoting the spontaneity of processes, Fig. courtesy [21]

2.2.2. Enthalpies

Chemically reacting systems form the core of combustion and there are certain enthalpies associated with the same. As mentioned earlier, the process of combustion leads to the formation of the major products CO_2 and H_2O . The *standardized enthalpy at temperature T* or the absolute enthalpy at T, of these species is defined as the sum of two other enthalpies - the enthalpy of formation and the sensible enthalpy change. The *enthalpy of formation* of a certain species refers to the amount of heat evolved when one mole of that species forms from its constituent elements at the standard temperature and pressure (295K and 1atm). The *sensible enthalpy change* refers to the heat released when the temperature of the species changes from the standard temperature to temperature T. Thus,

$$\bar{h}_i(T) = \bar{h}_{f,i}^0(T_{ref}) + \Delta\bar{h}_{s,i}(T) \quad (2.8)$$

where,

\bar{h}_i = absolute enthalpy at temperature T;

$\bar{h}_{f,i}^0(T_{ref})$ = enthalpy of formation;

$\Delta\bar{h}_{s,i}$ = sensible enthalpy change.

2.2.3. Heat/Enthalpy of combustion

The heat of reaction or the heat of combustion of the fuel is a way to evaluate the energy content of a fuel. The heat of reaction is assessed by burning the fuel under specific conditions. In case of burning it under constant volume, it is known as internal energy of reaction, whereas constant pressure burning is called as enthalpy of reaction. Assuming complete combustion during the burning of a fuel with an oxidizer, the *enthalpy of combustion* is defined as the amount of energy required to be removed such that the products of the system are in the same temperature as the reactants. Thus,

$$\Delta h_{rxn} = h_{prod} - h_{reac} \quad (2.9)$$

where,

Δh = enthalpy of combustion reaction;

h_{prod} = enthalpy of the products;

h_{reac} = enthalpy of the reactants The relationship between enthalpies of formation and reaction are shown in figure 2.3.

Heating/Calorific value

The heating value of a fuel which is a measure of the amount of energy release achievable from it, is numerically the same as the heat of the reaction and bears the opposite sign. The two heating values defined for a fuel are the upper and the lower heating values. The heat of reaction which is calculated under the assumption that all the H_2O of the combustion process has condensed to a liquid, is called the *upper heating value* of the fuel. This assumption pertains to the scenario of the highest heat released from the fuel. If the assumption is that the H_2O from the combustion has not condensed at all, the heat of combustion in such a

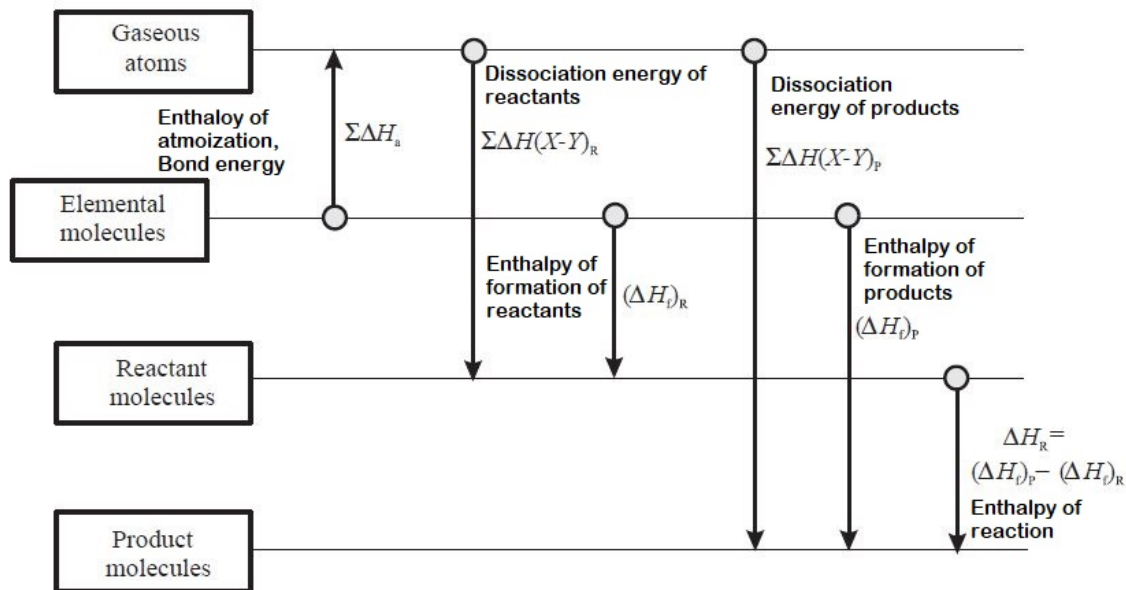


Figure 2.3: Relationship between enthalpies of formation and reaction, Fig. courtesy [2]

case corresponds to the *lower heating value* of the fuel. The heat of combustion and thus both these heating values are usually denoted in MegaJoules. The heating values which are assessed by specifically burning 1kg of fuel are called calorific values which is usually denoted in MegaJoule/kg.

2.3. Chemical Kinetics of Combustion

Chemical kinetics can be defined as the study of the chemical reaction rates and of the other factors on which these rates depend. These other factors are mainly the temperature, pressure and concentration of the species involved. A part of chemical kinetics is also about the elucidation of reaction mechanisms which are the empirical kinetic laws that describe the governing chemical pathways from reactants to products. This is achieved by experimental study of reaction rates which are coupled with theoretical models, such that the outcome of future chemical reactions and experiments can be predicted.

2.3.1. Residence time

One of the main factors which has a role in the outcome of the chemical kinetics in a combustor is the residence time. The chemical reactions in the combustor can happen as long as the reactant mixture resides in the combustor. Thus, the fuel and oxidizer mixture undergo chemical kinetic reactions as long as they stay in a prescribed volume, in this case, the combustor volume. In general, the residence time is defined as the time spent by the reacting mixture in a considered volume. The residence time is related to the considered volume by the following relation,

$$\tau = \frac{\rho V}{\dot{m}} \quad (2.10)$$

where,

τ is the residence time;

ρ is the density of the mixture;

V is the volume considered, and

\dot{m} is the mass flow rate of the mixture.

2.3.2. Reaction time

While the residence time is defined by the time spent in a considered volume, the chemical reaction time is defined by the time of change of concentration of a considered species. Thus, the chemical reaction time of species i is defined as,

$$\tau_{rxn,i} = \frac{[i]}{d[i]/dt} \quad (2.11)$$

where,
 $\tau_{rxn,i}$ is the chemical reaction time of the species i ;
 $[i]$ is the concentration of the i -th species, and
 $d[i]/dt$ is the rate of change of concentration of the i -th species.

Due to the scale of residence time in typical gas turbine combustors and the corresponding reaction time scales, it is not possible for all species in a combustion chamber to attain equilibrium. Due to this, chemical kinetics would be the governing factor in knowing the behaviour of chemical reactions. A comparison of reaction time scales for different species with the typical residence time in a combustor is given in figure 2.4. Although the figure is pertaining to a gas turbine system with exhaust gas recirculation, it is still representative of a typical, conventional gas turbine combustor.

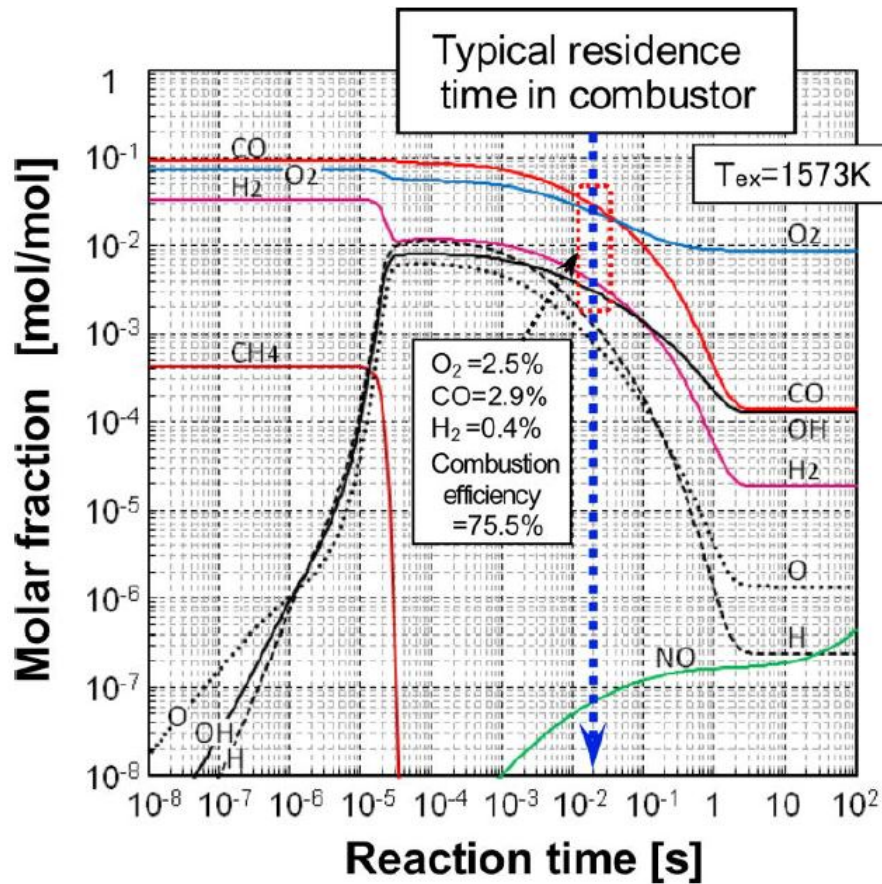
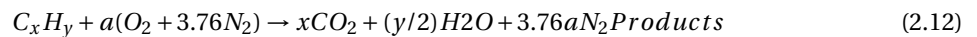


Figure 2.4: Chemical species behaviour over time in case of stoichiometric combustion of gaseous fuel and oxygen and with exhaust gas recirculation, Fig. courtesy [23]

2.3.3. Elementary reactions

The general combustion reaction from 2.1.1 has been reproduced here,



As mentioned earlier, although the complete combustion of fuel and oxidizer should lead to only CO_2 and H_2O , there are other resulting products from combustion, which also includes the pollutant species. This is because, the combustion process is not just the single straightforward reaction as mentioned in equation 2.12, but consists of a number of elementary reactions which subsequently leads to the overall reaction as mentioned above.

An elementary reaction is a single reaction that happens on a molecular level exactly as described by the chemical reaction. This means that it is a single step reaction and has no intermediates. A number of elementary reactions form the overall/global or net reaction described by equation 2.12. Elementary reactions are usually classified on the basis of molecularity, which means the number of reactant species involved in the elementary reaction. This classification can be listed as:

- **Unimolecular reactions:** This kind of reaction happens when a single reactant molecule rearranges itself to form one or more products. This is of the form:



- **Bimolecular reactions:** A bimolecular reaction is said to be one where the reactants involve two species. This is of the form:



- **Termolecular reactions:** When there are three reactant species reacting simultaneously, the underlying reaction is called a termolecular reaction. Thus, it can be described as:



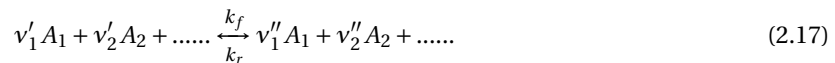
The combustion of any fuel and oxidizer consists of a number of elementary reactions of all the three kinds which constitute the overall global reaction.

2.3.4. Reaction rate

The reaction rate is the parameter that quantifies the speed in which an elementary reaction proceeds in a certain direction - forward or reverse. An elementary reversible reaction is defined in the following way:



or



where,

k_f and k_r are the forward and reverse reaction rate constants respectively;

v' and v'' are the stoichiometric coefficients of the reactant and product species respectively.

The forward reaction rate of the species A_1 is defined as,

$$\frac{dA_1}{dt} = -k_f \cdot [A_1]^{a_1} \cdot [A_2]^{a_2} \dots \quad (2.18)$$

where,

$[A_1]$, $[A_2]$... are the concentrations of the species A_1 , A_2 ..., and

a_1 , a_2 ... are the *reaction orders* with respect to the species A_1 , A_2

The sum of all the exponents or the order of the species forms the *overall reaction order*. The reaction order is a quantification of the dependency of the reaction rate on the amount of reactant species available. Therefore, similarly the reverse reaction rate of species A_1 is defined as,

$$\frac{dA_1}{dt} = k_r \cdot [A_1]^{a_1} \cdot [A_2]^{a_2} \dots \quad (2.19)$$

Rate of production or formation

The equation 2.17 can be generalised for the j th reaction in set of s reactions, as



where, q = total number of considered species and i represents the i th species and j represents the j th reaction in a set of s elementary reactions.

The **law of mass action** states that, the rate of production or consumption of a species is proportional to the product of molar concentrations of the reactants, each raised to the power of its stoichiometric coefficient. Hence, for a species i for the j th elementary reaction, the rate of formation can be defined as,

$$R_j \propto [A_1]^{v_{1j}} [A_2]^{v_{2j}} \dots [A_q]^{v_{qj}} \quad (2.21)$$

or, for a total of s elementary reactions, the rate of formation of the i th species from the j th elementary reaction can be written as,

$$R_j \propto \prod_{i=1}^q [A_{ij}]^{v_{ij}} \text{ for } (j = 1, \dots, s) \quad (2.22)$$

This above equation gets modified by introducing the proportionality constant called **reaction rate constant** in the following way,

$$R_j = k_j \prod_{i=1}^q [A_i]^{v_{ij}} \text{ for } (j = 1, \dots, s) \quad (2.23)$$

The net rate of formation of the species A_i can be represented as,

$$\left(\frac{d[A_i]}{dt} \right)_{net} = \Delta v_{ij} \left[k_{fj} \prod_{i=1}^q [A_i]^{v'_{ij}} - k_{rj} \prod_{i=1}^q [A_i]^{v''_{ij}} \right] \quad (2.24)$$

where k_{fj} is the forward rate constant of the j th reaction and k_{rj} is the reverse rate constant of the j th reaction and,

$$\Delta v_{ij} = (v'_{ij} - v''_{ij}) \quad (2.25)$$

2.3.5. Reaction rate constant

The reaction rate constant k which is related to the ability of molecules to combine, is defined by the Arrhenius equation as,

$$k = AT^b \cdot \exp\left(\frac{-E_a}{RT}\right) \quad (2.26)$$

The Arrhenius equation consists of the *preexponential factor*, A which is an experimentally determined value for different elementary reactions. This term is also called the collision frequency based on the collision theory. The term 'b' usually lies in the range of -1 to 1. And the term E_a corresponds to the *activation energy* which is an energy barrier required to be overcome during the reaction, by the reacting molecules. The maximum value of the activation energy corresponds to the bond energy of the molecule. Thus the activation energy is the minimum energy required by molecules to react. The collision model states that the activation energy is acquired from the kinetic energies of colliding molecules. The kinetic energy upon collision can then stretch, bend and eventually break bonds thus leading to chemical reactions.

The reaction rate constant also has a dependence on pressure which is not straightforward. The dependence of the reaction rate constant on pressure is determined by the molecularity of the reaction considered. Among them, the effect of pressure on the rate constant of unimolecular reactions are relatively studied more. It is found that for unimolecular reactions at lower pressures, increasing pressure has positive effect on the rate constant whereas for unimolecular reactions at high pressures, rate constant is found to be independent of increasing pressures.

2.4. Reaction Mechanisms

The prediction/calculation of emissions includes chemical kinetics as a rudimentary concept because chemical reactions and their rates determine the progress of combustion, and hence the formation and/or destruction of chemical reactions. Chemical kinetics combines the importance of reaction rates, reaction coefficients and their time scales. The formation of emissions from combustion has a complex dependence on

the temperature, residence time, detailed chemical kinetics, equivalence ratio etc. The importance of chemical kinetics modeling in experimental and numerical combustion has been proved in lot of research works in many applications. A good knowledge on the suitable chemical reaction mechanism is crucial for correct prediction of emissions [24].

A chemical model combining detailed chemical kinetics of methane oxidation has been used in order to predict NO_x, CO_x, CH₄ and HC emissions of an engine which uses natural gas as the fuel [25]. The GRI-Mech 3.0 with 325 elementary reactions and 53 species, which is a widely used mechanism for natural gas combustion and includes NO_x and CO formation schemes has been used in this study. The CRN in [26] is based on a semi-detailed chemical kinetics mechanism with 76 species and 327 reactions [27] to formulate the fuel burning rate, among which 6 reactions correspond to soot formation and 14 correspond to NO_x formation. A CFD study employed detailed chemical kinetics by means of a reaction mechanism with 84 reactions and 21 species [28], by Zhen et al. [29]. The NO_x and CO emissions from the model in [30] was studied using the reaction mechanism which pertains to the combustion of n-heptane and has 42 species with 57 reactions [31]. The use of detailed chemical kinetic mechanisms enables to capture all the chemical aspects of the particular fuel undergoing combustion.

The choice of suitable chemical reaction mechanism depends on the fuel and the operating conditions. In this thesis, since the evolution of exhaust species from the combustion of natural gas is to be analysed, mechanisms pertaining to methane combustion, in the operating conditions of the high pressure turbine are to be employed. Reaction mechanism files for usage usually contain the set of elementary reactions pertaining to that mechanism and the experimentally found values of the preexponential factor A, temperature exponent b and activation energy E_a . These values are found for a comprehensive range of experimental conditions for which they are *validated*. Although in general a reaction mechanism can be used for investigation of any conditions, better quantitative accuracy is expected when a specific mechanism is used for investigations pertaining to the conditions in which it was validated.

2.4.1. Reaction Mechanisms for methane combustion

There has been a large amount of research on methane combustion, and since natural gas is predominantly composed of methane, many studies on natural gas combustion are also modeled as methane combustion - both using detailed and semi-detailed/reduced reaction mechanisms. In [32], seven chemical reaction mechanisms were used, to compute burning velocities and compare with experimental data. Among these schemes, the one with 14 species and 39 reactions, and the one with 20 species and 63 reactions, resulted in good agreement for lean to slightly rich flames, at 298K and 1atm. But these schemes were still not considered validated even with this agreement as it was found that the measured burning velocities were realised to be insensitive of the mechanism. The 14 species mechanism was used in the LES study of a hydrogen-enriched methane/air meso-scale combustor by Benard et al. [33].

A core methane jet diffusion flame was simulated using a numerical model which used a chemical kinetics mechanism with 25 species and 121 reaction steps [34] based on GRI-Mech 2.11, which is validated between temperatures of 900K and 1400K [35]. This combination of the numerical model and the reaction mechanism was shown to have a good agreement with the results of the experimental model from [36]. In [36] experimental studies were conducted and compared to numerical results employing the GRI-Mech 2.11 and GRI-Mech 3.0, which is validated for temperature range of 300K - 5000K [37], but for a bigger range of pressures [38]. This study was done in order to quantify the variation in using different mechanisms [since 2.11 consists of 50 species and 275 elementary reactions whereas 3.0 consists of 53 species and 325 elementary reactions]. An open cycle CFD simulation coupled with detailed chemical kinetics using the GRI-Mech 3.0 mechanism [39] was done by Zaker et al. [40] to investigate the effect of hydrogen addition to a methane fueled engine. Detailed chemical kinetic modeling was the focus on the NO_x emissions in a toroidal well-stirred reactor undergoing methane combustion [41]. This mechanism pertains to the chemical kinetic modeling for perfectly stirred reactors [42], along with CHEMKIN-II [43], and comprises of 51 species and 235 elementary reactions.

The Leeds mechanism is another detailed mechanism representing the oxidation of methane [44], which was also validated for experimental conditions similar to that of the GRI mechanisms. The validation mostly showed good agreement, and has been used in several research papers working on the combustion of methane / natural gas [45, 46]. The San Diego mechanism which consists of 57 species and 268 reactions [37] is also commonly used for hydrocarbon combustion and even combustion of hydrogen and syngas [47, 48]. It can

be used between temperatures of 300K to 5000K. The Konnov mechanism [49] is also a widely used mechanism for small hydrocarbon and hydrogen combustion [50, 51]. This mechanism has been improved over the years for accuracy over a broader range of applications [52, 53].

The USC mechanism was developed by Prof. Hai Wang for and consists of 111 species and 784 reactions. This was developed for a wide range of combustion scenarios and has been well-validated by a number of tests [54]. This USC mechanism served as the base, to develop the JetSurf mechanism, which pertains to jet fuel combustion, in the form of surrogates. The JetSurf mechanism is also intended to be used for high temperature chemistry of n-alkanes upto n-dodecane [55] and consists of 348 species and 2163 reactions. The Caltech mechanism or the Blanquart mechanism was developed by Blanquart et al. [56–58] and was improved over the years to account for all major pathways of PolyAromatic Hydrocarbon formation [59] and consists of 174 species and 1896 reactions. This mechanism is optimized to include the combustion of hydrocarbons with upto 4 carbon species, for wide range of combustion scenarios [37]. The AramcoMech 2.0 has been developed for a large number of C₁-C₄ hydrocarbon and oxygenated fuels. It is built to characterise the kinetic and thermochemical properties of these fuels over a wide range of experimental conditions, consisting of 493 species and 2716 reactions [37, 60, 61]. The same group has worked on the development of a number of methane and natural gas mechanisms, for a broad range of combustion conditions pertinent to gas turbine combustion. These can be found in [61].

The Foundational Fuel Chemistry Model (FFCM) was developed to model the combustion of small hydrocarbon fuels using an advance reaction model which was built based on the latest kinetic knowledge, and accounted for well-defined predictive uncertainties. It consists of 38 species and 291 reactions which can be used for fuels containing C₁ to C₄ species [62]. The Lawrence Livermore National Laboratory has built a large number of mechanisms for research, among which the C₁ to C₄ mechanism was developed and validated between 600K and 1100K to describe the effect of hydrocarbons on NO to NO₂ conversion, and contains 126 species and 639 reactions [63]. The Chemical Reaction Engineering and Chemical Kinetics Lab has developed several detailed and semi-detailed chemical kinetic mechanisms, among which the C1-C3 mechanism with NO_x which has 115 species and 2141 reactions is validated for high temperatures [64].

2.4.2. Reduced mechanisms

The advancement in computational capabilities has brought about the evolution of detailed chemical reaction mechanisms to simulate the combustion of complex hydrocarbon fuels. There have also been reduced chemical reaction mechanisms which have been developed for obtaining good accuracy even with limited computational resources. The requirements of ample computational effort is indispensable while solving the time-dependent conservation equations pertaining to the flow field. It can be decreased by making use of reduced chemical mechanisms. These mechanisms are reduced in such a way that they do not fail to encapsulate the most important facets of the combustion process, while discarding the relatively unnecessary details inherently in the complex mechanisms.

Reduced mechanisms are obtained by creating a skeletal mechanism from a detailed one, by means of eliminating relatively inconsequential species and elementary reactions. This is done mainly by using sensitivity analysis, and other techniques also. Thus, the reduced mechanism is a skeletal one of the detailed mechanism consisting only the most important elementary steps. The process of eliminating species and/or reactions is highly application-specific. Another way to further reduce this is to consider steady-state approximation for the applicable elementary reactions

Reduced mechanisms for methane

Elaborate information on obtaining reduced mechanisms, (specifically for methane) have been described by Peters et al. in [65]. The oxidation of methane has been reduced in different levels and finally to a 4-step mechanism that has been used in calculating burning velocities, and estimating the flame structure, both of which in comparison with experimental values show very good agreement. Further, reduced mechanisms for the combustion of natural gas, has been combined with the thermal NO_x mechanism, to be able to provide the thermal NO_x formation from natural gas combustion [66]. A semi-detailed reaction mechanism for methane combustion with 14 species and 39 reactions [32] has been used for the LES study of a hydrogen-enriched methane/air meso-scale combustor by Benard et al.[33]. For LNG as the fuel in the main combustion chamber of the hybrid engine configuration, the mechanisms pertaining to methane are of primary

importance since the major compound in the composition of natural gas is methane. The complex reaction mechanism pertaining to methane can be segregated into two main pathways based on whether methane burns in rich or lean conditions [67–69]. Rich conditions require the full description of C₁ to C₄ pathways but lean (and stoichiometric) conditions require the description of C₁ to C₂ pathways for the oxidation process. The reaction pathway for lean and stoichiometric conditions can be seen in the following figure 2.5.

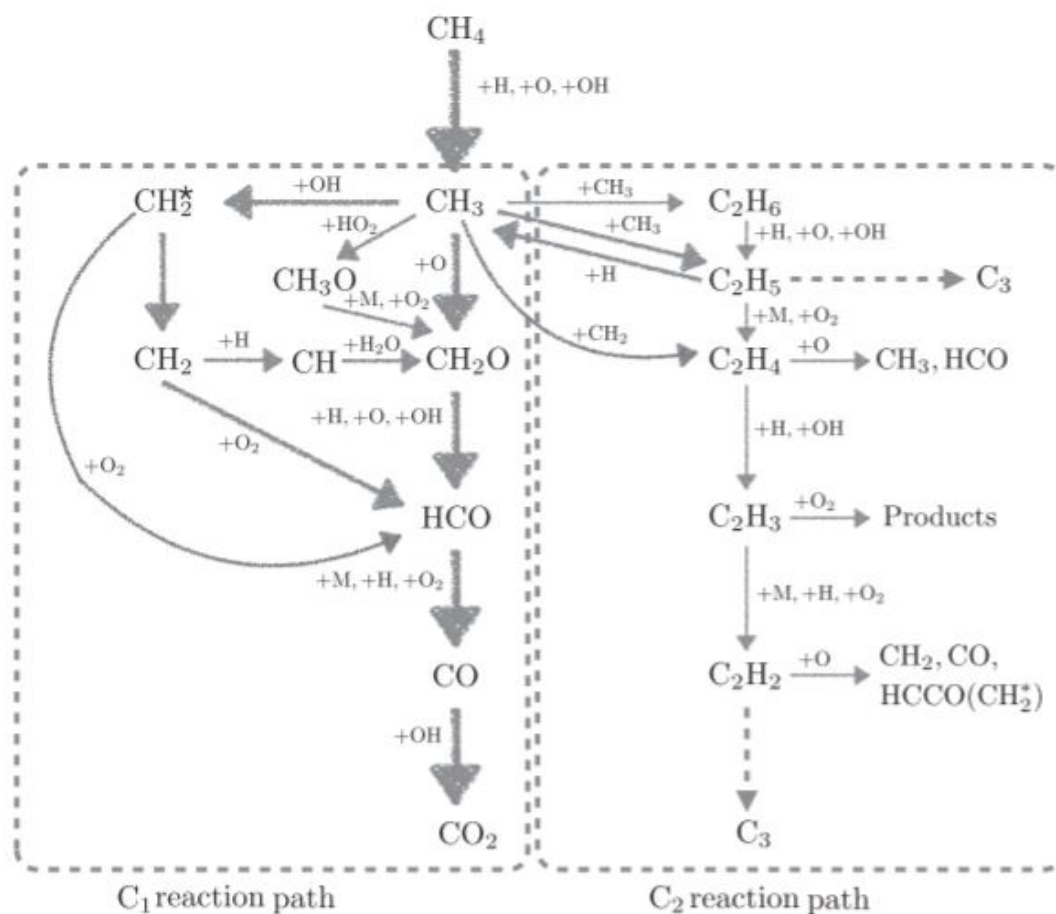


Figure 2.5: Major chemical pathways for methane oxidation involving C₁ to C₂ hydrocarbon orders for lean conditions. Fig. courtesy [70], [67].

Using this methane reaction pathway, a reduced mechanism for ultra-lean methane combustion has been derived by Jiang et al. in [67]. The optimization of the geometry of a jet stirred reactor combustor, for minimum NO emissions, for methane oxidation was carried out by Mazaheri et al. in [71]. This optimization also included finding out a corresponding reduced mechanism for methane oxidation from the GRI-Mech 3.0 mechanism. This reduced mechanism with 5 reactions and 17 species was validated for experimental NO and CO emissions. Detailed studies on the contribution of various NO_x mechanisms in diffusion combustion of methane was studied [72]. Two-, three- and four-step mechanisms for methane combustion had been derived previously for diffusion flames in order to study flame extinction and burning rates for premixed flames, which were not enough for modeling fuel-derived radicals that are crucial for prompt and reburn chemistry. Whereas, for nitrogen chemistry pertaining to these diffusion flames, six- and one-step reduced mechanisms were obtained for NO_x emissions. A reduced mechanism of 16 species and 12 steps derived from GRI-Mech 1.2 for methane oxidation which was validated previously, was further improved by deriving twelve-, fourteen-, fifteen-, seventeen-step mechanisms for NO_x emissions from methane combustion, from the complex GRI-Mech 3.0 mechanism [73]. These reduced mechanisms were effective in producing a good validation and excellent performance for different combustion predictions and expansive variations of

thermodynamic parameters.

Pollutant formation mechanisms All studies on the emissions of pollutant species have emphasized the importance of being aware of the fundamental mechanisms pertaining to them. A brief description of these mechanisms has been presented in the following sections.

2.5. NO_x formation mechanisms

NO_x emissions consist of NO and the product of the oxidation of NO i.e. NO₂. There are 4 mechanisms of formation of NO_x emissions which have been described here - Thermal NO_x, Prompt NO_x, N₂O route, Fuel NO_x (Fuel-bound NO_x) [10]. The contribution of each mechanism to the overall NO_x formation in the combustor and thereafter depends on the operating conditions [74]. Apart from these, NO_x can also be formed by the NNH route, which has also been discussed.

2.5.1. Thermal NO_x (Zeldovich mechanism)

This mechanism, proposed by Zeldovich, is the predominant source of NO_x formation in case of high temperature (above 1850K) combustion, when there is no fuel-bound nitrogen present [74]. Thermal NO_x is the product of the oxidation of atmospheric nitrogen of the combustion gases in the high-temperature regime [10]. This mechanism is named so because the reactions pertaining to it only happen at high temperatures, due to the very high activation energy owing to the triple bond in the N₂ molecule [70]. The elementary reactions of this mechanism are given as:



with reaction rates k_1 , k_2 and k_3 respectively.

Among these reactions, the reaction 2.27 is the rate-limiting step because of its high activation energy [74] (low rate [70]).

The formation of thermal NO_x is an exponential function of temperature due to the fact that the atomic oxygen in the flame front also has a similar relationship with temperature [74]. Thus, thermal NO_x formation is found to increase exponentially with temperature. But the peak formation occurs on the fuel-lean side of equivalence ratio, as opposed to the fuel-rich side where the temperature is the highest, because of the fact that the high amount of oxygen available in these conditions is consumed by the fuel itself [10]. In case of liquid and gaseous fuels, the NO_x formation is higher for liquids for the same flame temperature [10] due to local stoichiometric temperature conditions formed near the fuel drops, which consequently leads to high NO_x formation inspite of lean overall average equivalence ratios [10].

Rate of formation of NO

The rate of formation of NO can be obtained from the reactions mentioned in equation 2.27, as follows [70]:

$$\frac{d[\text{NO}]}{dt} = k_1[\text{O}][\text{N}_2] + k_2[\text{N}][\text{O}_2] + k_3[\text{N}][\text{OH}] \quad (2.30)$$

Assuming that the nitrogen atoms are in a quasi-steady state, i.e. $d[\text{N}]/dt = 0$, the above equation 2.30 simplifies to the following form:

$$\frac{d[\text{NO}]}{dt} = 2k_1[\text{O}][\text{N}_2] \quad (2.31)$$

This equation 2.31 shows that, the formation of NO can be reduced by decreasing k_1 (i.e. the temperature), or $[\text{N}_2]$ and $[\text{O}]$. $[\text{N}_2]$ can be easily and precisely measured by means of a probe, or estimated by an assumption of equilibrium in the medium. But the same equilibrium measurement of $[\text{O}]$ is not possible because, the assumption of equilibrium leads to underprediction of $[\text{O}]$ upto almost a factor of 10. Therefore, a relatively better assumption for $[\text{O}]$ is that of partial-equilibrium, which leads to estimating $[\text{O}]$ by means of finding $[\text{H}_2\text{O}]$, $[\text{O}_2]$ and $[\text{H}_2]$ which are also easy to measure or estimate.

Influence of operating conditions on thermal NOx formation

As mentioned earlier, the formation of thermal NOx is highly dependent on the flame temperature, and in turn is also dependent on the inlet air temperature, irrespective of the mean fuel droplet diameter [10]. The thermal NOx formation also has a direct relation with residence time. However, this relation is more pronounced in case of higher equivalence ratios. Therefore, for low equivalence ratios, thermal NOx formation is almost independent of residence time [10].

2.5.2. Prompt NOx (Fenimore mechanism)

The prompt NOx mechanism proposed by Fenimore, is the reaction of smaller hydrocarbon radicals like CH with N₂ molecule [74]. It is called "prompt" NOx because of it is the manifestation of rapid production of NO in a flame front [75]. It was observed when [NO] did not approach zero when the flame was studied with a probe from the downstream side as predicted by the Zeldovich mechanism [70]. As a result, in a plot of NO against the residence time, an extrapolation of NO concentration to zero time, or distance from the flame front, gives a positive intercept [75]. The CH radical is formed as an intermediate of a complex reaction scheme, at the flame front only, and reacts with molecular nitrogen [70]. As a result, amines and cyano compounds are formed, which react further and form NO [74].

Most texts report that the elementary reaction of this mechanism is as follows:



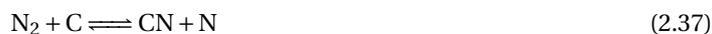
But there has been a disagreement to the validity of the above reaction, by quantum chemists on the grounds that it does not conserve electron spin [74]. Based on the work of Moskaleva et.al [76], the following reaction resulting in the intermediate species NCN that conserves electron spin, was finalised as the elementary reaction.



This intermediate species would result in the formation of NO by means of fast oxidation with O and OH radicals as follows [74]:



Another pathway is the reaction of NCN with H to form HCN and nitrogen atoms which would react with O and OH radicals and lead to the formation of NO [74], whereas the cyano-compounds react with oxygen-bearing species and result in NO.



The formation of prompt NOx is observed also at relatively low temperatures (below 1000K) because, the activation energy of the elementary reaction of this is much lower as compared to that of the Zeldovich mechanism [70]. Since the concentration of the hydrocarbon radicals are important to assess the NOx formation by this mechanism, the process of the fuel combustion also must be authentic and must be captured well, along with the reaction rates for the elementary reaction [75]. Although this mechanism is not seen significantly in the post-flame zone, formation of NOx in the flame-zone increases for rich conditions due to the availability of large quantities of hydrocarbon radicals [74].

The comparison of thermal and prompt NOx formation mechanisms, in a well-stirred reactor for different air number λ where $\lambda = 1/\phi$ is given in Figure 2.6.

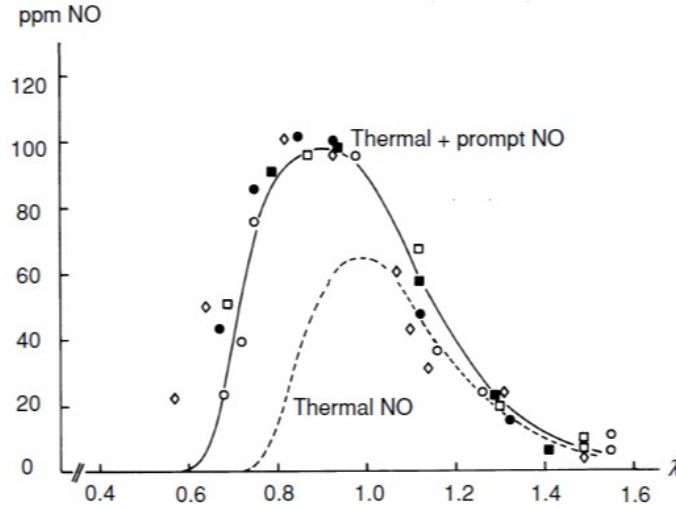
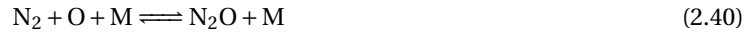


Figure 2.6: Dependence of air number (equivalence ratio) on the NO production in a well-stirred reactor ; Fig. courtesy [77], [78].

2.5.3. N_2O mechanism

The reaction between oxygen atom and molecular nitrogen (similar to the elementary reaction in thermal NO_x mechanism) occurs in the presence of a third molecule M which leads to the formation of N₂O [70]. This N₂O can react with O and H atoms in the following ways and lead to the formation of NO [74].



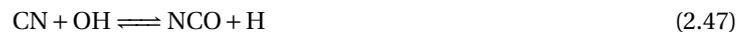
It is important to account for the accurate branching ratio of the multiple alternative reaction channels of N₂O with O and H atoms, like the following [74].



This mechanism often has a negligible contribution to the total NO_x amount, compared to the Thermal and Prompt pathways due to its slow kinetic rates [74]. But in case of low temperature conditions (suppressed thermal pathway) and lean conditions (suppressed prompt pathway), this mechanism becomes a significant contributor to the total NO_x [70]. It is still significant at low temperatures because of the low activation energy [70]. It also becomes appreciable at high pressure conditions which is typical for a three-molecule reaction [70]. Therefore, in cases of lean and low temperature combustion, this mechanism is the major source of NO_x [70].

2.5.4. Fuel bound NO_x

Another source of NO_x formation is the chemically present nitrogen in some fuels (solid and liquid). The nitrogen concentration in fuels vary between 0 to 0.65 weight percentage [79]. Although the reaction pathways are different and complex based on the nitrogen bonding in the fuel, the main intermediate species in most cases are HCN and/or NH₃ [74]. The main forerunner of NO formation from HCN is NCO and for that from NH is NH₃. The reactions for NO from HCN are as follows [74]:



The oxidation of NH_3 to NH_2 , NH and N is given as:



These NH and N radicals are further oxidised which leads to the formation of NO :



It must be noted that there are several secondary reaction pathways that lead to NO from HCN and NH_3 which are a part of the detailed chemical kinetic mechanisms of HCN and NH_3 [74].

2.5.5. NNH pathway

Another pathway for the formation of NO by the reaction of N_2 and H is via the formation of the intermediate NNH species [74]. This pathway becomes significant at low temperatures and sometimes also shares its NO pathway with fuel-bound NO_x (also dominant at low temperatures) [74].



This mechanism also shares its pathway with prompt- NO_x and hence its contribution increases with increasing equivalence ratio [74]. In case of high temperatures, the formation of NO_x by this NNH pathway depreciates, and instead the following reactions are seen to occur [74].



2.6. CO emissions

CO emissions in gas turbines occur due to the oxidation of fuels. But the level of oxidation and the oxidation conditions decide the outcome of the level of CO . The formation of CO emissions can be attributed to the following factors [10]:

- in fuel-rich conditions - due to the insufficient oxidation of the fuel to CO_2 as a result of incomplete combustion (due to inadequate burning rate, inadequate fuel-air mixing, quenching of post-flame products etc.)
- in fuel-lean and stoichiometric conditions - due to the dissociation of CO_2 to CO [10]

The oxidation of hydrocarbon fuels happens in different pathways [74] - low temperature oxidation, intermediate temperature oxidation, high temperature oxidation, based on the combustion temperature. These pathways also depend on operating pressures [74]. The high temperature oxidation pathway applies for combustion temperatures above 1200K and hence is the relevant pathway for gas turbine combustion [74]. In this pathway, combustion radicals are dominated by the chemical chain-branching reaction between the H atom and O_2 molecule.

In high-temperature oxidation, the long-chained hydrocarbon fuel molecules break down into smaller hydrocarbon molecules by means of initiation, propagation and termination reactions [74]. The following branching reaction is indispensable to the high-temperature oxidation of any hydrocarbon fuel, followed by the recombination reaction.



The characteristic of high-temperature oxidation is the dominance of the first reaction over the second [74]. Before the oxidation of the higher-order fuel molecule, it first becomes an alkyl radical by means of the following reaction:



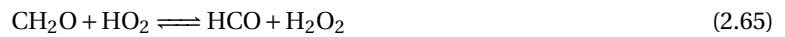
where X represents species like O, H, OH, HO₂, O₂ or CH₃.

The resulting alkyl radicals further undergo chain reactions and form smaller hydrocarbon molecules, which subsequently reacts with other oxygenated combustion species and forms formaldehyde (CH₂O) which is one of the main intermediate species of the oxidation of hydrocarbon fuels [74]. Further, formaldehyde dissociates as follows:



where M represents a third colliding species.

Apart from the above, formaldehyde also reacts with oxidation species to form HCO, which due to its reaction with O₂, becomes the main source of CO emissions as shown below [74].



CO, although resistant to oxidation [10], at high temperatures gets removed by means of oxidation to CO₂ after reacting with the oxidation species, as follows:



Among these, the reaction with OH is the main pathway for the oxidation of CO compared to the other reactions which are relatively slow at high temperature [74].

In order to reduce CO emissions, the combustion efficiency must be high. This depends on factors like the engine and combustor inlet temperatures, the combustion pressure and the equivalence ratio in the primary zone [10].

2.7. Evolution of exhaust gas species downstream of the combustor

The evolution of chemistry *after* the combustion chamber has been studied over the years in several ways. The creation of sulfur-containing gases and chemiions in the combustor of an aircraft engine, and its evolution along the turbine, between the combustor exit and the engine exit was computed by Starik et al. [80]. In this work, the combustor was modeled using an adiabatic, closed reactor assuming homogenous fuel-air mixture at low equivalence ratio. The species with sulfur and the chemiions in the core flow of the engine, was simulated using a chemical kinetic scheme with 152 species and more than 1000 reversible reactions. For the investigation inside the turbine section two models were used -

- a quasi-1D model with flow field variation corresponding to the turbine and including blade effects, and
- a box model¹ with pre-given temperature and pressure variations.

¹thermodynamic variations and chemical kinetic scheme is applied to in a simple, expanding box, to simulate the conditions after the combustor

This was implemented in order to have different kinds of treatment of the flow inside the turbine. The variation of the gaseous species along the region after the combustor can be seen in figure 2.7 from [80]. This variation was obtained for the quasi-1D model. The effect of the temperature profile on the chemistry was also computed for the same combustor exit conditions. It was found that the results from both are different by upto a factor of 3, indicating that the flow-field dynamics and the temperature profile along the region after the combustor are parameters that can impact the resulting emissions.

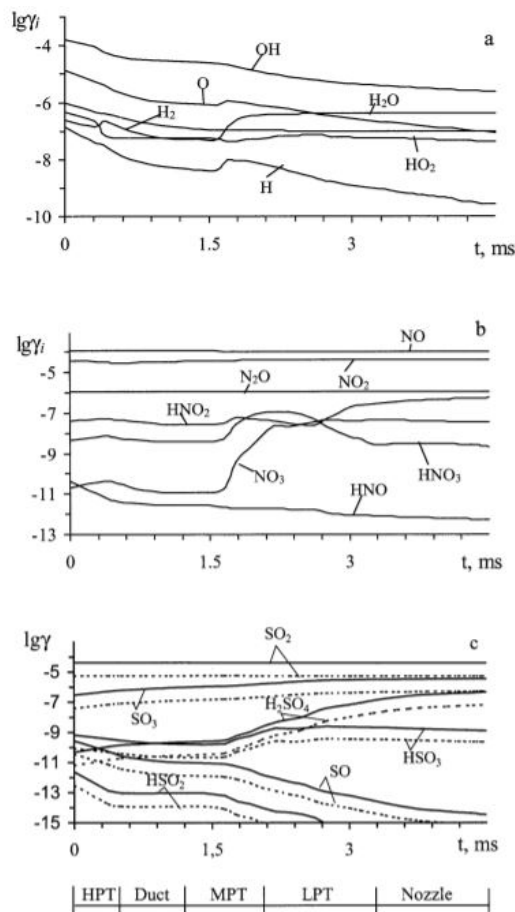


Figure 2.7: H-, N-, and S-containing gas species mole fractions (expressed as mole fraction $\cdot 10^n$; n corresponds to the values on the y axis) in the post combustor flow of RB211 engine for Fluid Sulfur Content (FSC) = 0.04% (dashed curves), and = 0.3% (solid curves), Fig. courtesy [80].

A 0D/1D gas turbine model consisting of the combustor, turbine and nozzle, using a Chemical Reactor Network (CRN) was developed, for different engine operating conditions, and incorporated a kerosene kinetics scheme and a soot kinetics model [81]. This CRN model was validated for the APEX experiment [82]. While the CRN modeled the combustor into its three different zones (primary, secondary and dilution) using a combination of Perfectly Stirred Reactors (PSRs) and Plug Flow Reactors (PFRs), the evolution of combustion products post the combustor in the HPT, LPT and Nozzle was simulated by modeling them with 3PFRs, with the assumption that the flow properties follow a 1D flow at a given pressure ratio. For the Jet A-1 fuel considered for this study, a three-component surrogate jet fuel was used. The NOx chemistry was included by the San Diego mechanism [83], and a sulfur scheme was used for SOx. It was found that the sulfur-containing emissions and the organic particulate matter had significant concentration variations through the postcombustor regions too, for all the considered power settings except the idle one.

The evolution of emissions during and post combustion, and their impact on the radiative forcing has been given studied by Chowdhury et al. [84]. A 0D multi-gas-parcel emission model, incorporating detailed jet-fuel chemistry was developed. It was capable of predicting the time evolution of emission species, and validated for the APEX experiment [82]. The combination of mechanisms for PolyAromatic Hydrocarbons, soot, NOx and sulfur resulted in a mechanism of 369 species and 2657 reactions, which was coupled with

CHEMKIN. This study was done for idle power setting condition. It was found that while the change (increase) in H_2SO_4 , starting from the combustor dilution zone through the turbine till the engine exit, was by a factor of 10 (due the oxidation of SO_3 in the combustor dilution zone and after), the change (decrease) in NO_x and soot emissions was by a factor less than 2, for *idle operating conditions*. These results compared with the APEX experiments is shown in figures 2.8, 2.9 and 2.10. These results are in terms of residence time, and the residence time corresponding to turbine and after it is from 10ms.

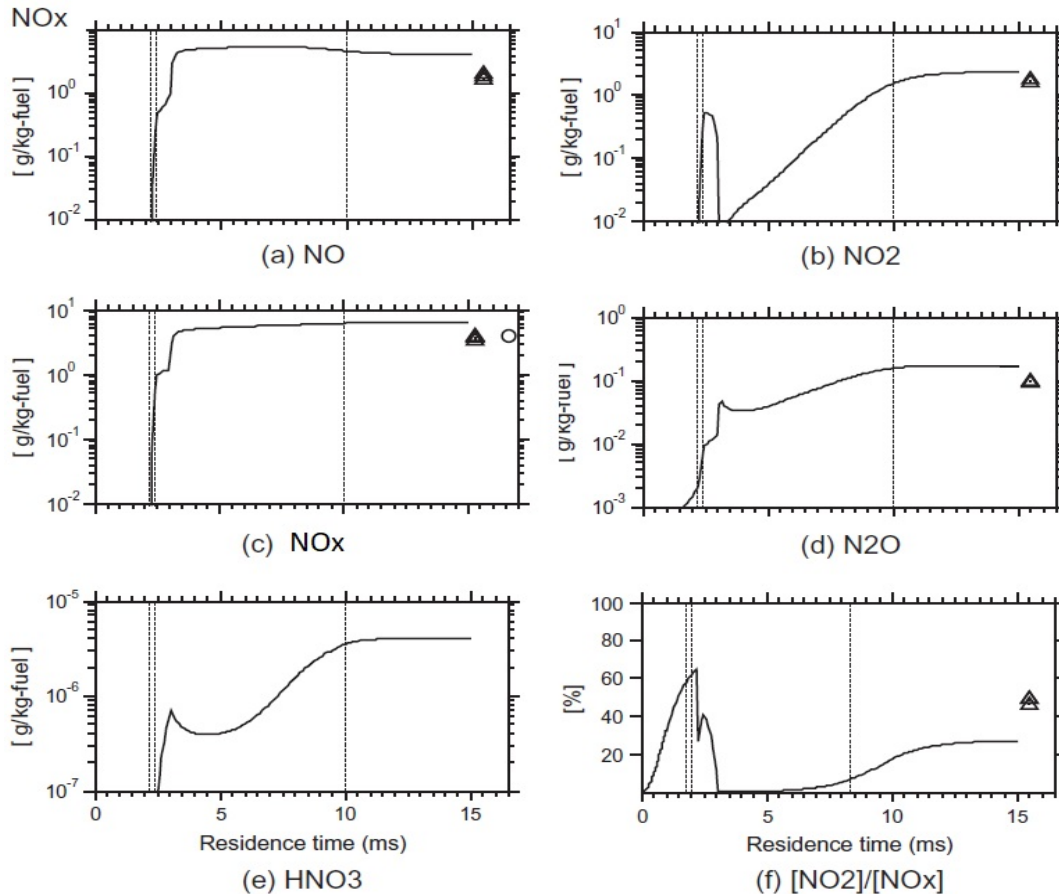


Figure 2.8: The time evolution of concentration of NO_x species in the combustor and postcombustor region vs the APEX measured data, Figure courtesy [84].

The influence of postcombustion thermodynamic characteristics in an aircraft engine particulate emissions was studied in detail by means of modeling the microphysical process and interactions between these species for relevant and representative temperatures and pressures [85]. Detailed soot chemistry including coagulation growth, ion-soot attachment, and vapor condensation was analysed, along with a high-fidelity microphysics kinetics used to estimate the evolution of the soot properties. The differences in thermodynamic environment and characteristic time scale pertaining to combustor, turbine and nozzle has been modeled for this study. It was found that, while the combustor exit conditions are representative of the engine exit conditions in case of non-volatile particulate emissions, the same does not hold for gas phase emissions because of their significant evolution through the conditions after the combustor.

The European PartEmis project described in [86] was implemented in order to obtain an acute understanding of the composition and transformation of combustion gases and particles passing from the combustor to the turbine, engine exit, into the external plume and the wake. One of their goals was to study particle properties as they progress through the engine turbine stages, for two engine operating conditions. This was an experimental study in which a combustor was coupled with a Hot End Simulator (HES), to simulate the thermodynamic expansion processes in the turbine and nozzle. The results of this study were spatially resolved (unlike previously reported ones which were resolved temporally based on residence time) and it

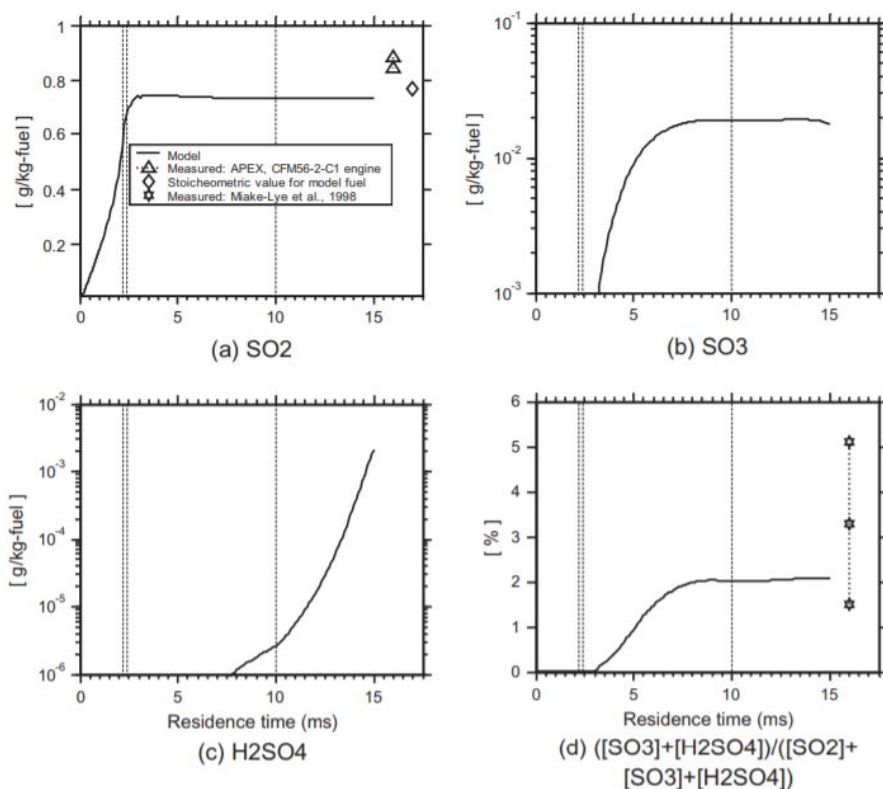


Figure 2.9: The time evolution of concentration of sulfur-containing species in the combustor and postcombustor region vs the APEX measured data, Figure courtesy [84].

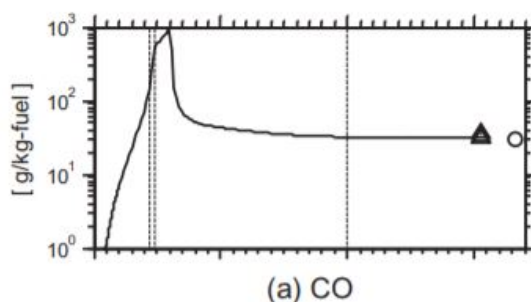


Figure 2.10: The time evolution of concentration of CO in the combustor and postcombustor region vs the APEX measured data, Figure courtesy [84].

was found that the sulfur-containing emissions varied considerably through the combustor and the turbine. This HES was also numerically created in [87] and validated for the experiments of the PartEmis project [86]. This HES was combined with a numerical combustor model, and detailed chemical kinetic model containing 47 species and 77 reactions was used to study the species evolution.

The 1D and 2D simulations for a range of flow and chemistry conditions were carried out and the resulting sulfur oxidation through the post combustion region were compared by Lukachko et al. in [88]. The most important aspect of this work is that the effect of both aerodynamics and chemical kinetics on the sulfate aerosol precursors were studied, *including turbine blade cooling and simplified representations of flow non-uniformities*. The 1D simulations were run for three different species initial conditions. It showed that irrespective of the initial conditions, it is incorrect to assume equivalence between the combustor exit and the nozzle exit, for sulfur-species concentrations. These results highlight the prominent activity of these species in the turbine. The high temperature and pressure gradients in the turbine were found as the major factor

in the evolution of emissions species post the combustor, as shown by the generalised flow path evolutionary trends after the combustor, in figure 2.11.

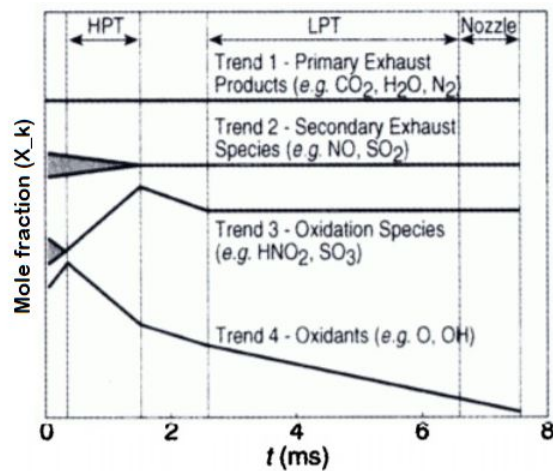


Figure 2.11: Generalized flow path evolutionary trends after the combustor, for different species, as obtained from 1D simulations, Figure courtesy [88].

The 2D simulations were done for two cases - an adiabatic blade, and a blade with constant wall temperature to simulate internal cooling. These resulted in an increase in NO and SO₃ species from the turbine inlet to the exit. It was also found that the turbine blade cooling has a significant role in aerosol precursor formation. The 1D simulations produced correct trends but quantitatively underestimated the sulfur oxidation by upto 47% as compared to the 2D simulation results. The results of SO₃ predictions for 1D vs 2D simulations is given in figure 2.12. 1D simulations were reportedly sufficient for concentration predictions in case of an uncooled turbine, whereas for turbines with cooling, resorting to 2D simulations is indispensable because of the impact of the temperature non-uniformities on the chemical kinetics evolution.

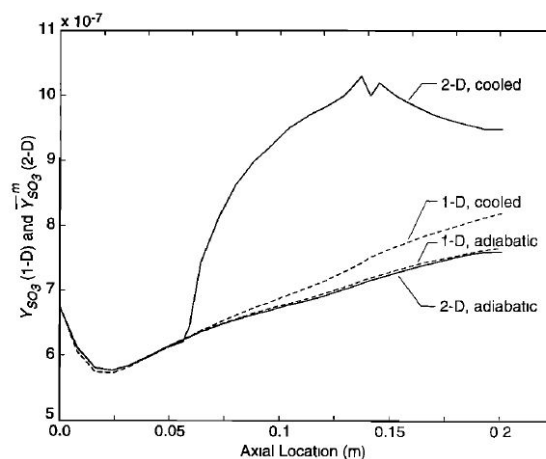


Figure 2.12: Comparison of 1D and 2D solutions through a single turbine blade row for SO₃, Figure courtesy [88].

Savel'ev et al. [89] used a quasi 1D flow model to analyse the non-equilibrium chemical processes from the combustor to the nozzle exit, and showed that the chemical reactions in the zone post the combustor resulted in the increase in formation of H₂SO₄ and NO₃ along with large amounts of H₂O, CO₂, CO, NO, NO₂, SO₂, HNO₂, N₂O, HNO₃, NO₃, H₂SO₄. This model used an inviscid and a non (heat-)conducting gas. This inviscid assumption led to important flow-field effects (flow separation on the leading edge of the turbine blades, "pair vortex" formation in the interblade channel etc.) related to the flow in the turbine being disregarded. A detailed chemical kinetic scheme with 273 reversible reactions was used for two turbofan engines using nC₈H₁₈ for two different conditions. The calculations were done for both equilibrium and

non-equilibrium mixture composition variation, and showed that the latter agreed very close to experimental emission indices. A simple emission prediction model which combines a reactor network (for simulation of the pollutant formation inside the combustor), and a quasi-1D model (for modeling the transformation inside the postcombustor region) was developed in [90], and found that the NO_x and CO variation during the expansion across the turbine is relatively less compared to the significant SO_x variation. The use of 1D models with detailed mechanisms have also been done in various other references [91–102].

The importance of using 3D CFD for capturing the interaction of the chemical mechanisms with the three-dimensional flow field was realised and was implemented in [103]. A 3D CFD model for the expansion in the turbine and nozzle was made by means of the validated Hot End Simulator of [104] using which simulations were done for two flight conditions - cruise and modern cruise conditions (defined in [103] as conditions under which the engine operates at lower power and with higher temperature and pressure respectively). Due to the inclusion of detailed nitrogen mechanisms, the values of NO and NO₂ at different stations after the combustor agree well with experimental results as seen in figure 2.13.

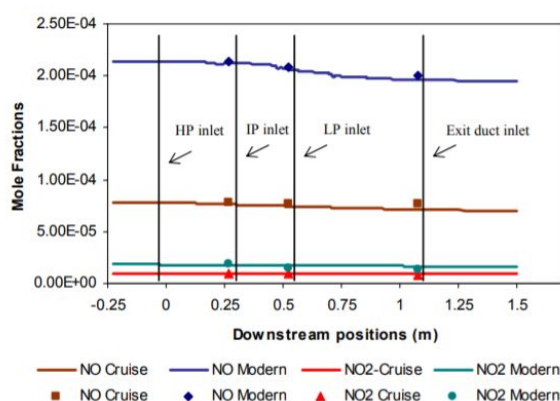


Figure 2.13: The predicted NO and NO₂ (lines in the figure) in the HES for both flight conditions, compared with measurement data (points in the figure), Figure courtesy: [104].

The results showed an important conclusion that the conversion of sulfur species in the postcombustor region is higher than in the combustor itself. The 3D blade design of the stator and the rotor of the first stage of the high pressure turbine of the CFM56 engine, was made by Nguyen et al.[105]. This was made to study the influence of the flow through turbomachinery, on the chemical processes leading to emissions. The results showed that the evolution of pollutant species beyond the combustor is a complex process involving interactions among the flow evolution in the geometry, the HPT geometry itself, the temperature variation and chemical reactions. Nguyen et al. extended their research of [105] into the work as described by [106] where a 3D modeling of a high pressure turbine (without including cooling effects) was performed, to find the effect of the aero-thermodynamics and the flow field of the turbine on the chemical processes involving emission species. This led to finding that, over a single stage of the HPT, the aero-thermodynamics changed by upto 17% and consequently the nitrogen oxidation changed by upto 48%. The flow field simulations were performed including chemical reactions corresponding to both detailed and reduced mechanisms. This was also compared to the simulations run without including the chemical reactions, to study the differences created due to the interactions between the flow processes and the chemical reactions, and their impacts on each other. This study also highlighted the importance of considering comprehensive details of the flow field (turbulence, wake interaction, secondary flows etc.) for their interaction with the chemical processes.

The study of evolution of emission species after the combustor, is a relatively less-ventured subject. Though it has been studied over the years, the number of research works and researchers focusing on it have been comparatively low. Nevertheless, the crux from all of these research works is that, based on the fuel and operating conditions, the evolution of certain emission species downstream of the combustor is not a negligible phenomenon.

The literature presented in this section studied the variation of emissions from *after* the combustor for specific operating conditions of certain specific engines. The study of the behaviour of emissions after the

combustor with respect to various parameters has not been presented in any of them. There has not been a detailed analysis on what parameters determine the evolution of emissions in the postcombustor region, and to what extent these parameters play a role in this behaviour, which is the research gap intended to be filled by this thesis. Using this parametric analysis, a better decision of whether to include the chemistry after the combustor or not, can be made depending on the operating conditions. Thus, this thesis intends to answer the research following research question in order to fill the aforementioned research gap:

How do CO and NO_x evolve after the combustor and what are the parameters that influence this evolution the most?

2.8. CRN models of the hybrid engine

2.8.1. Rao and Bhat CRN model

The hybrid engine configuration has been studied by using various CRN models previously. Rao and Bhat [107] studied the important characteristics of the hybrid configuration by performing a chemical kinetic analysis. The results pertaining to the hybrid engine from this study were compared with a conventional turbofan in terms of CO₂ and NO_x emissions for different design parameters and operating conditions. This CRN consists of both the main combustor and the inter-turbine burner with the HPT in between them. In this study, the main combustor operated with LH₂ as fuel and the CRN was validated for experimental results for the inter-turbine burner which operates in the flameless combustion regime. The hybrid engine CRN is fully made of PSRs except the HPT as shown in figure 2.14.

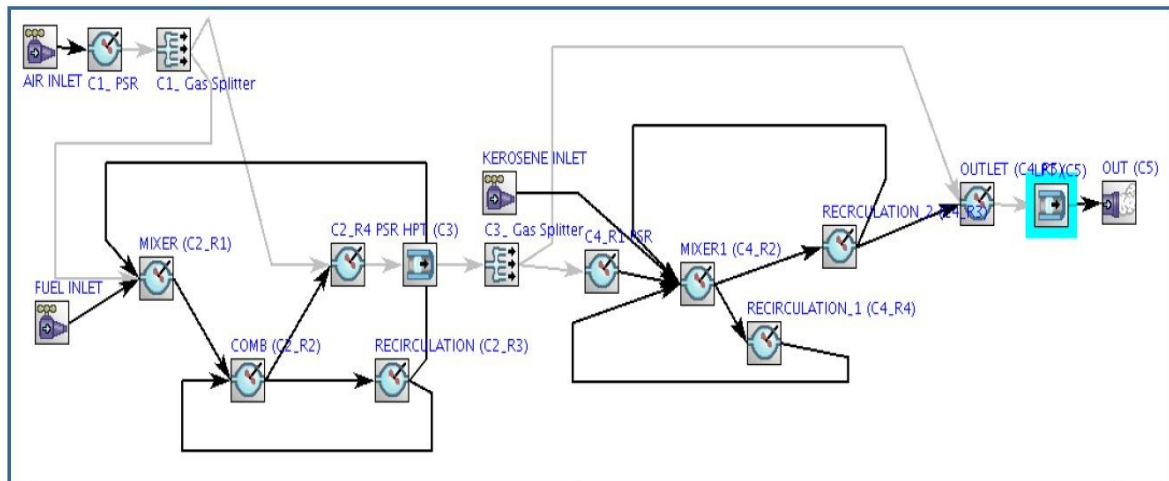


Figure 2.14: Reactor Network Model of the hybrid combustion system by Rao and Bhat, Fig. courtesy: [107]

2.8.2. RQL combustion in the hybrid configuration

An emission prediction tool for an RQL combustor was built using a multi-reactor network model in [18]. This tool, which was built based on the cycle values of the CF6-80 engine was validated for the emissions from the same. The CRN consisted of PSRs for all the regions of combustion. The hybrid engine configuration with and without the inter-turbine burner was investigated using the same tool, and thus both the combustors were assumed to be RQL-type combustors. When both the combustors were considered, the exhaust from the main combustor was directly given as the input of the inter-turbine burner *without* considering the HPT.

2.8.3. Model by Rosati

While studying the prediction of emissions from different combustion systems, the main combustor of the hybrid combustion system was also investigated by Rosati [108]. The CRN for the main combustor was built based on the network suggested for gas turbines in ANSYS CHEMKIN. This network is similar in structure

to that of the main combustor in 2.14, with the exception that there is no recirculation to the mixer reactor. This CRN was built to emulate experimental conditions and hence incorporated a heat loss model based on certain assumptions. This CRN was used to find the most influential parameters for NO_x emissions. The CRN is shown in figure 2.15.

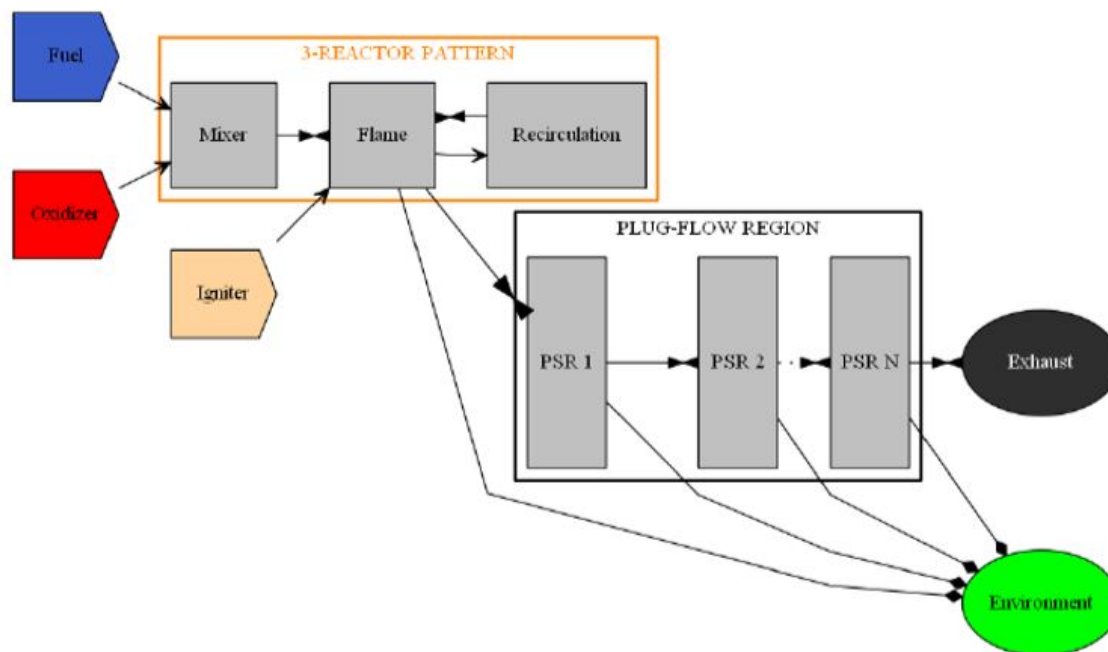


Figure 2.15: The CRN of the main combustor as modeled by Rosati, Fig. courtesy: [108]

2.8.4. Model by Talboom

CRN models for the main combustor and the inter-turbine burner were developed individually by Talboom in [20]. For the inter-turbine burner a "simple" CRN model and an "enhanced" CRN model were developed individually. The "simple" model used different zones to represent the different regions of the combustor. The "enhanced" model was built for the purpose of estimating NO_x emissions better by modeling the mixing of fuel and oxidizer using multiple parallel reactors. Comparison of both the models with experimental results showed that the "enhanced" model was more accurate with NO_x estimation, as intended. Finally a whole CRN for the entire hybrid engine with both combustors was built. This hybrid CRN model also considered the HPT in between the combustors. The main combustor was built based on the experimental setup which operated with LH₂ as fuel. The inter-turbine burner is also built based on the experimental setup which operated in the flameless combustion regime. These CRN models were also developed based on Computational Fluid Dynamic (CFD) studies performed under the AHEAD project. The CRNs which are made using a combination of PSRs and PFRs are shown in figures 2.16 and 2.17.

The Rao and Bhat model for the hybrid engine considered the HPT between the combustors while studying emissions. The CRN of the main combustor which is also shown in figure 2.14 was also followed for this thesis. The model by Rosati did not study the ITB and hence did not consider the HPT. The model by Talboom considered both the combustors with the HPT in between, but used a reactor model which is not the most accurate for representing the HPT. These models also did not shed light on the specific role of the HPT in the emissions from the hybrid engine configuration. Thus, this thesis aims to give more clarity on the role of the HPT in between the combustors in terms of a wide range of operating conditions pertinent to the hybrid engine.

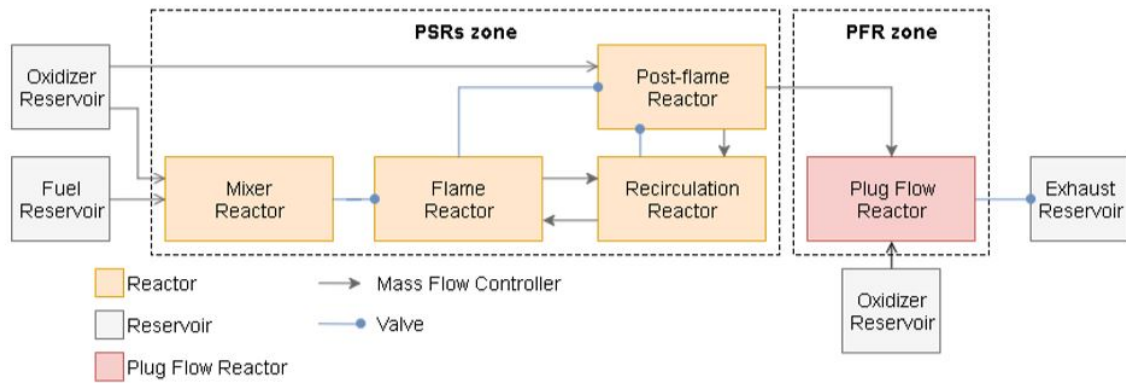


Figure 2.16: CRN for the main combustor developed in [20]

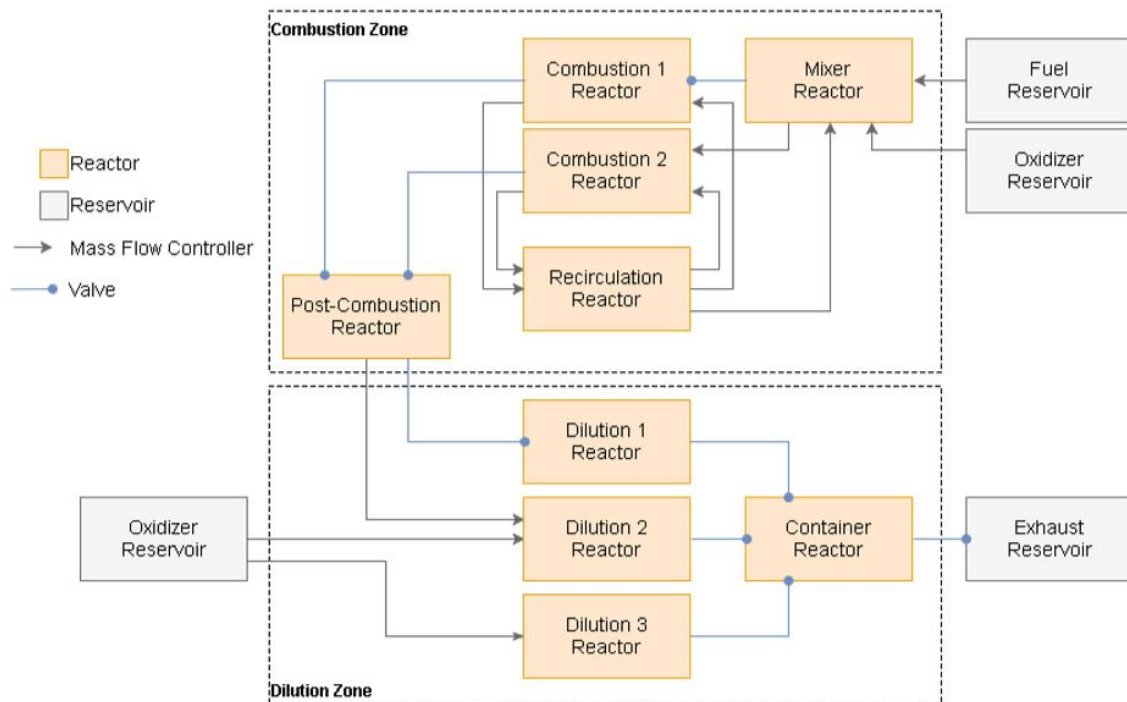


Figure 2.17: CRN for the inter-turbine burner developed in [20]

2.9. Summary

The fundamental aspects of combustion and chemical kinetics are explained in this chapter. This was followed by an extensive discussion of reaction mechanisms pertaining to combustion and also for the formation of emissions. Some of the previous works on modeling and studying the evolution of emissions after the combustor are also presented, thus highlighting the importance of postcombustion behaviour. Finally, previous CRN models which have aimed to model and study the main and/or the inter-turbine burner are presented.

3

Modeling Tools, Method and Validation

This chapter describes the modeling tools i.e the solver, the reactors used, the reactor network architecture employed and the method of the set-up for all test cases. Eventually the reactor network was validated and the results of the same have been presented.

3.1. Modeling tools

Chemistry Solver For the purpose of building the reactor network and solving its chemistry, the solver that has been used in this thesis is the ANSYS CHEMKIN-PRO 18.2. This is not an open-source solver and has been used by employing the university license.

3.1.1. Reactor models used

There are a number of 0D and 1D reactor models and auxiliary components offered by CHEMKIN-PRO 18.2 for reactor network modeling. The following section provides a description of the same:

Inlet The inlet stream is connected to one or more reactors and requires the specification of inlet temperature, composition and mass flow rate. For a fuel-oxidizer mixture, the equivalence ratio and the composition of the fuel and oxidizer can be specified.

Perfectly Stirred Reactor

The Perfectly Stirred Reactor (PSR) is one which corresponds to an ideal reactor with a single inlet, outlet and a fixed volume. In this reactor, perfect mixing is achieved. This means that there are no spatial gradients in temperature and concentration, since the gases inside the reactor are assumed to mix instantaneously once they are inside the reactor. In this reactor, reactions are assumed to happen homogeneously. Therefore, the temperature, composition and residence time govern the extent of the reaction. In case of steady-state, the temperature and composition of the gas at the exit corresponds to that of the interior of the reactor. The illustration of a continuously-stirred reactor is given in figure 3.1.

The governing equations of this reactor are the conservative equations corresponding to mass, species and energy. The PSR is considered to be in steady state. Therefore:

Conservation of mass At steady-state

$$\frac{dm}{dt} = \sum_{in} \dot{m}_{in} - \sum_{out} \dot{m}_{out} = 0 \quad (3.1)$$

Conservation of species Assuming steady state

$$\dot{\omega}_i MW_i V + \dot{m}(Y_{i,in} - Y_{i,out}) = 0 ; \text{for } i = 1, 2, \dots, N \text{ species} \quad (3.2)$$

where,
 $\dot{\omega}_i$ is the net rate of production of the i th species;

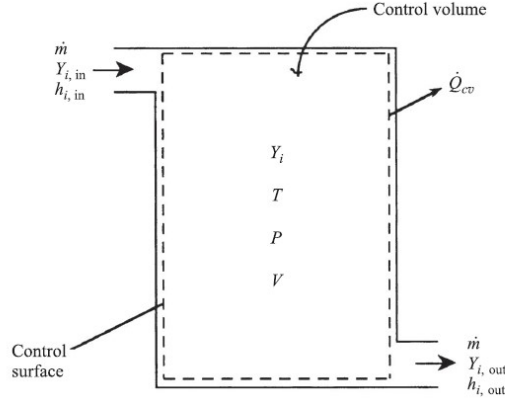


Figure 3.1: The illustration of a perfectly stirred reactor, Figure courtesy: [109].

MW_i is the molecular weight of the i th species;
 V is the reactor volume;
 \dot{m} is the mixture mass flow rate in the reactor;
 $Y_{i,in}$ is the inlet mass fraction of the i th species, and
 $Y_{i,out}$ is the outlet mass fraction of the i th species.

The species net production rate is of the form,

$$\dot{\omega}_i = f([X_i]_{cv}, T) = f([X_i]_{out}, T) \quad (3.3)$$

where the mass fractions and the mole fractions are related by the following way,

$$Y_i = \frac{[X_i]MW_i}{\sum_{j=1}^N [X_j]MW_j} \quad (3.4)$$

Conservation of energy The conservation of energy equation for a steady-state, steady-flow is given as

$$\dot{Q} = \dot{m} \left(\sum_{i=1}^N Y_{i,out} h_i(T) - \sum_{i=1}^N Y_{i,in} h_i(T) \right) \quad (3.5)$$

where,
 \dot{Q} is the heat transfer rate;
 h_i is the absolute enthalpy which is given as the sum of the enthalpy of formation and the sensible enthalpy change, as,

$$\bar{h}_i(T) = \bar{h}_{f,i}^0(T_{ref}) + \int_{T_{ref}}^T c_{p,i} dT \quad (3.6)$$

There are a total of $N+1$ unknowns which correspond to the mass/mole fraction of N species and the temperature T . These are solved by the system of $N+1$ equations obtained from the species conservation and the energy conservation equation. An important parameter for the PSR is the residence time of the gases in the reactor which is given by

$$\tau = \frac{\rho V}{\dot{m}} \quad (3.7)$$

where ρ corresponds to the mixture density which is calculated by,

$$\rho = \frac{PMW_{mix}}{R_u T} \quad (3.8)$$

where P is the pressure in the reactor and R_u is the universal gas constant.

Plug Flow Reactor

A Plug Flow Reactor (PFR) corresponds to an ideal reactor congruous to a steady flow with steady state, and a constant area in which properties are uniform across the flow i.e. perpendicular to the flow direction and only vary along it. Therefore, this is a 1D reactor in the sense that the flow properties are a function of one spatial dimension. There is also no mass and turbulent diffusive transport even in the axial direction, and hence meaning that there is no mixing in the flow direction. The mass flow rate remains constant throughout the reactor. The behaviour of the gas inside the reactor corresponds to an ideal gas, and the flow of gas inside the reactor is assumed to be an ideally friction-free one. A simple schematic of a PFR is given in figure 3.2.

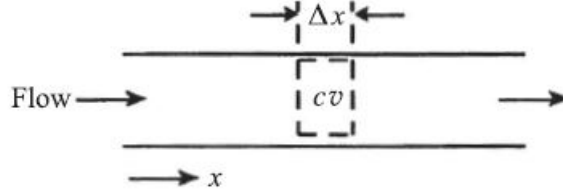


Figure 3.2: The illustration of a plug flow reactor, Figure courtesy: [109].

The governing equations for a PFR pertaining to steady-state and steady-flow conditions are:

Conservation of Mass

$$\frac{d\rho u A}{dx} = 0 \quad (3.9)$$

where,

u is the axial velocity,

ρ is the ideal gas density, and

A is the constant cross-sectional area.

Conservation of x-momentum

$$\frac{dP}{dx} + \rho u \frac{du}{dx} = 0 \quad (3.10)$$

where P represents the local pressure

Conservation of energy

$$\frac{d(h + u^2/2)}{dx} + \frac{\dot{Q}'' Pe}{\dot{m}} = 0 \quad (3.11)$$

where,

h represents the absolute enthalpy;

\dot{Q}'' represents the heat flux function, and

Pe stands for the local perimeter of the reactor.

Conservation of species

$$\frac{dY_i}{dx} - \frac{\dot{\omega}_i MW_i}{\rho u} = 0 \quad (3.12)$$

The above mentioned equations can be expanded to obtain individual derivatives which can then be eliminated by substitution and would eventually lead to the following system of ODEs.

$$\frac{d\rho}{dx} = \frac{\left(1 - \frac{R_u}{C_p MW_{mix}}\right) \rho^2 u^2 \left(\frac{1}{A} \frac{dA}{dx}\right) + \frac{\rho R_u}{u C_p MW_{mix}} \sum_{i=1}^N MW_i \dot{\omega}_i \left(h_i - \frac{MW_{mix}}{MW_i} C_p T\right)}{P \left(1 + \frac{u^2}{C_p T}\right) - \rho u^2} \quad (3.13)$$

$$\frac{dT}{dx} = \frac{u^2}{\rho C_p} \frac{d\rho}{dx} + \frac{u^2}{C_p} \left(\frac{1}{A} \frac{dA}{dx}\right) - \frac{1}{u \rho C_p} \sum_{i=1}^N h_i \dot{\omega}_i MW_i \quad (3.14)$$

$$\frac{dY_i}{dx} = \frac{\omega_i MW_i}{\rho u} \quad (i = 1, 2, \dots, N) \quad (3.15)$$

Another equation that has to be defined is for the residence time,

$$\frac{d\tau}{dx} = \frac{1}{u} \quad (3.16)$$

These plug flow equations which are expressed as spatial coordinates need the following N+3 boundary conditions for solving the above N+3 equations

Boundary conditions

$$T(0) = T_0 \quad (3.17)$$

$$\rho(0) = \rho_0 \quad (3.18)$$

$$Y_i(0) = Y_{i0}; i = 1, 2, \dots, N \quad (3.19)$$

$$\tau(0) = 0 \quad (3.20)$$

Outlet The outlet or exhaust stream is connected to the last reactor. Using the outlet means that the mixture is not processed further.

3.2. Method

This section describes the steps involved in building the Chemical Reactor Network (CRN) model for studying the behaviour of emissions in the axial turbine. This involves the following major tasks. Firstly, the architecture of the CRN has to be decided. This means that the kind of the reactors to be used in the network, the number of reactors, and the way they are to be interconnected need to be found. Secondly, the reactor specifications have to be found. These are given in the following sections.

3.2.1. CRN Architecture

The modeling of an aero-engine combustor using CRN has been practised widely in literature. CRN modeling serves as a computationally viable option for obtaining preliminary estimate of emissions from a combustor design under consideration.

A "Bragg Combustor" is such an idealized representation of a gas turbine combustor. It consists of a primary zone represented by a Perfectly Stirred Reactor (PSR) and a secondary zone represented by a Plug Flow Reactor (PFR). This model is built on the principle that a steady-state and a steady flow combustion system needs to be modeled with two distinct regions - the primary and the secondary zones. Since the primary zone is where there is intense recirculation, it is best represented by a PSR in which the incoming reactant flow undergoes mixing completely with the continuously recirculating products that were already burned. Therefore, this reaction zone has reactants, products and intermediates undergoing mixing. The secondary zone has the main function to allow for the combustion to complete and also to add air for dilution. Such a reaction zone is idealized using a PFR. The Bragg combustor which outlines the basic structure of a reactor network which is representative of a gas turbine combustor is shown in figure 3.3.

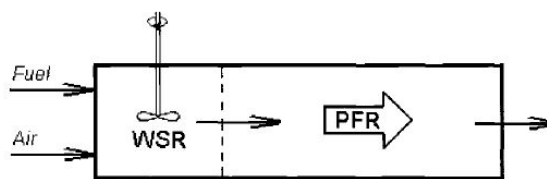


Figure 3.3: The Bragg's combustor. Fig. courtesy: [110]

The Bragg's combustor offers a basic schematic to be considered while creating a reactor network for the combustor. But specific reactor architecture is based on important aspects such as the combustor design and type of the combustor technology. The combustor technology is a major decider towards deciding how the total air mass flow is distributed [111]. Since the High Pressure Turbine (HPT) that is being investigated is the one pertaining to the hybrid engine configuration, the main combustor is a conventional combustor which is similar to the architecture used in [112–114]. The CRN used in [113] has been shown in figure 3.4.

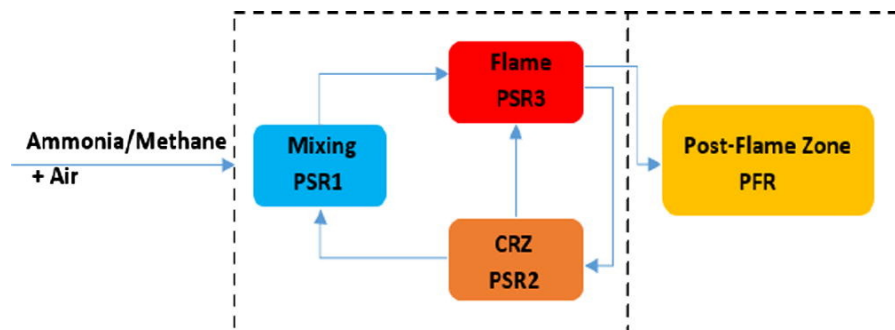


Figure 3.4: The CRN used for gas turbine combustion in [112]

This similar architecture has been used to model the main combustor of the hybrid engine configuration in [107] as shown in figure 3.5.

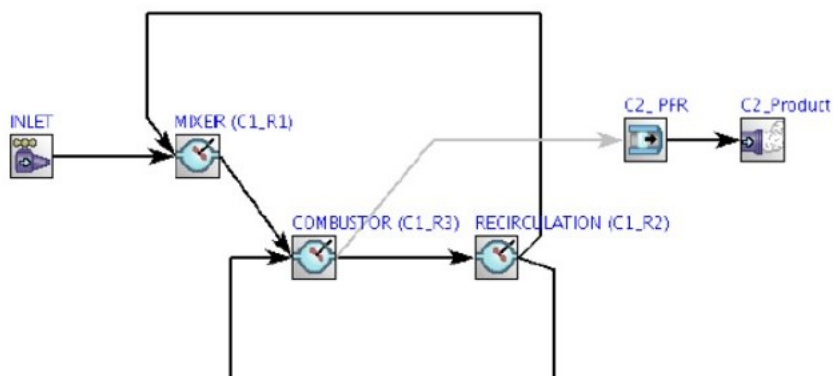


Figure 3.5: The CRN used to model the main combustor of the hybrid engine configuration. Fig. courtesy [20]

Therefore, for this thesis, the main combustor and subsequently the HPT have been modeled using the same architecture. The schematic of the CRN that has been used is shown in figure 3.6. It must be noted that throughout this report, 4 means the combustor exit/ stator inlet and 42 means the stator exit.

3.2.2. Cycle Parameters

Any reactor network requires some necessary inputs in order to be used for estimation of emissions. Once the reactor network architecture has been built, it requires other inputs to be used for emissions estimation. These inputs include cycle temperatures, pressures, air and fuel mass flow rates and volume of the reactors. Since the combustor pertains to the hybrid engine configuration, the cycle parameters for this configuration which have been calculated in [15] and [18] have been used. They are listed in table 3.1. It must be noted that while some of these parameters have been mentioned in the references explicitly, others have been calculated using simple cycle calculations. These were done from the data of individual components available from [15], and the assumption of Mach number at the stator inlet and exit as 0.35 and 1 respectively [116].

For the parametric analysis to be done, the bounds of temperatures and pressures were decided. The highest temperature and pressure correspond to the highest power setting of the hybrid engine configura-

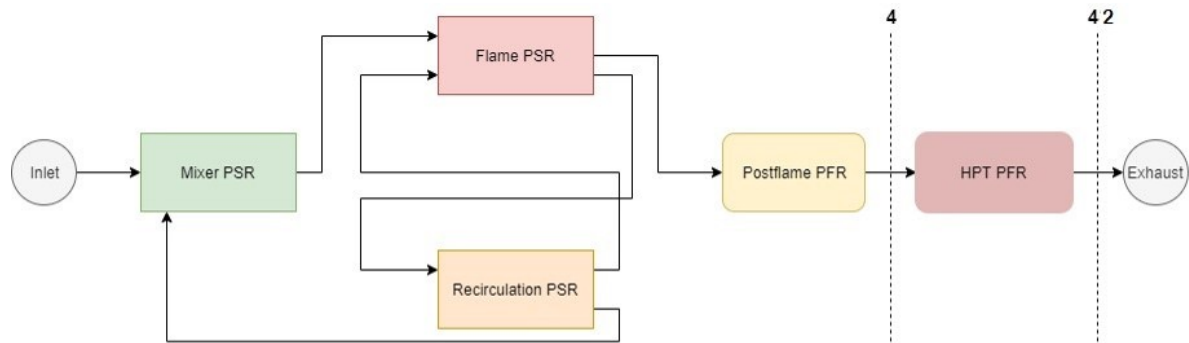


Figure 3.6: The schematic of the main combustor + HPT CRN that has been modeled for this thesis

T_{t3} [K]	P_{t3} [bar]	\dot{m}_a [kg/s]	\dot{m}_f [kg/s]
1042.13	70	55.75	1.48
750	13.93	12.55	0.58

Table 3.1: Cycle parameters corresponding to the hybrid engine

tion. Given that these cycle temperatures, pressures and flow rates are known, the other important parameters to be known are each of the reactor volumes. Although the aforementioned network architecture has been used in literature, the reactor dimensions are not specified. The proper estimation of individual reactor dimensions requires the availability of other specific details of the combustor design. Therefore the reactor volumes were determined based on certain assumptions as described in the following section.

3.2.3. Reactor Dimensions

The following section describes the methods and techniques used for obtaining the reactor dimensions of the CRN architecture. It must be noted that the PSR is a 0D reactor. This means that for this kind of reactor, it is possible to impose either the volume or the residence time (given the mass flow rate). Whereas the PSR is a 1D reactor which has a length dimension and therefore requires the axial length and diameter or cross-sectional area as input, which would then be used to calculate the residence time in the reactor using the given mass flow rate.

The typical residence time in an aero-engine combustor is denoted to be between 3ms to 5ms in [10], but the individual split of the residence time in each reactor has to be known. The approach of imposing reactor residence times instead of reactor volumes has been practiced in [84] and [117]. In [84] the total residence time in the combustor has been split as different fractions for different reactors. Similarly, for a total combustor residence time of 5ms, the individual residence times in the mixer, flame and recirculation reactors are imposed. For the postflame reactor, the fraction of the remaining residence time was used to calculate the volume which was then imposed.

The caveat to be noted here is that, since the residence times of the PSRs are imposed, this means that the overall combustor volume is slightly different for the different thermodynamic conditions investigated. Although that is not the case in an actual engine, this can still be pursued since this assumption is analogous to considering the design point for the combustor operation with respect to residence time.

For the reactor pertaining to the HPT, the axial length corresponding to a stator blade row was obtained from the geometry of the blade which was used in [118]. Since the flow rate and thermodynamic conditions are known, the area was calculated using the relation between mass flow rate and Mach number by following the assumption of a stator inlet Mach of 0.35 and outlet Mach of 1 [116]. These reactor dimensions are given in the following table.

Axial Length	0.17022m
Cross-sectional area	0.01727m ²

Table 3.2: Dimensions of the HPT reactor

3.3. Chemical kinetics study

NO_x analysis

In case of NO_x, there are certain prominent pathways which have been identified and understood from literature. To find the contribution of each of these pathways, a common methodology is to find NO_x emissions with the reactions for each of these pathways disabled. The NO_x emissions with specific pathway disabled and the total NO_x emissions are then compared to give the contribution of that specific pathway. But this methodology comes with its drawbacks too. This comes from the effect of the disabled reactions on the rate of other reactions. While disabling the reactions for the specific NO_x pathway, its interactions with other pathways is also not captured, which leads to an error in the resulting NO_x emissions. Therefore, the assumption that total NO_x emissions is the sum of NO_x from each pathway, is not fully satisfied, since the sum of NO_x from each pathway happens to be lesser than the total NO_x due to the reasons mentioned above.

Nevertheless, this is adopted because the error is close to 10%. Therefore, for the NO_x pathway analysis, the following reactions pertaining to each pathway were disabled:

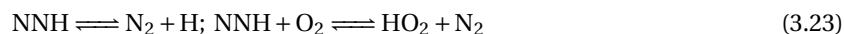
Thermal NO_x



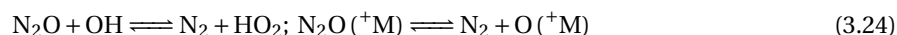
Prompt NO_x



NNH Route

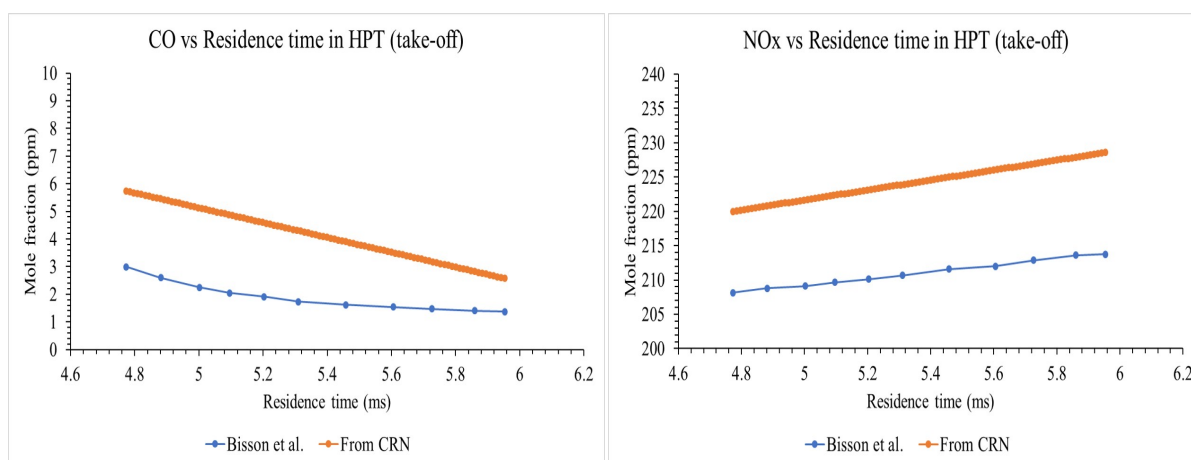


N₂O mechanism



3.4. Model Validation

In order to validate the architecture of the CRN involved in the modeling, the work of Bisson et al.[81] has been used. This work aims to model the behaviour of gaseous aerosol precursors and particles in the CFM56-2C1 turbofan engine. A CRN has been developed to model the whole combustor and also the HPT, LPT and the nozzle. This CRN was validated for the exhaust emission values obtained from the the APEX experimental campaign of the same turbofan engine. The experimental values of emissions from the exhaust were compared to the nozzle outlet emission values from the CRN, for four different power settings of the engine - Idle, Approach, Climbout and Takeoff. In case of NO_x, the emissions had a good match for all 4 conditions. Whereas in case of CO there was a good match for idle and approach conditions, and a decent match for the other two conditions.



(a) The behaviour of CO in the HPT for take-off conditions

(b) The behaviour of NO_x in the HPT for take-off conditions

Figure 3.7: Emissions at takeoff - Bisson et al. vs CRN

In [81] since the focus is on sulfur-related species and gas-phase soot precursors, the reaction mechanism used is a combination of a number of mechanisms which includes the detailed chemistry for all the aforementioned species. The APEX experiment used a highly aromatic fuel, and the CRN of [81] used n-decane as the surrogate for Jet-A1. For the validation of the current CRN, the Aachen Surrogate which consists of 80% n-decane and 20% tri-methyl-benzene to model kerosene was used.

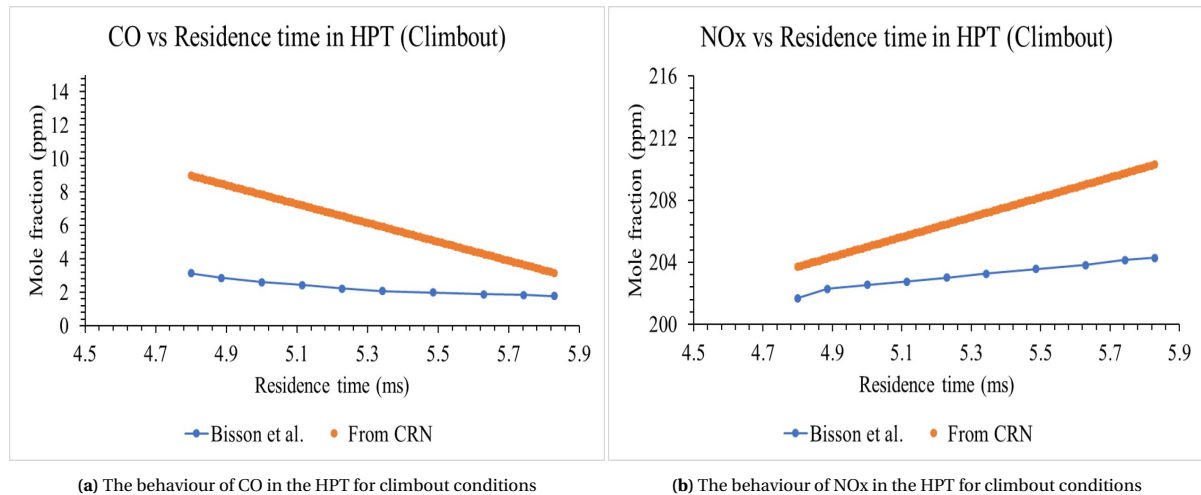


Figure 3.8: Emissions at climbout - Bisson et al. vs CRN

Since the ratio of variation of temperature and pressure for the 4 conditions are also known, they are imposed in the PFR of the HPT. The plots of variation of emissions for these 4 conditions along the whole engine with respect to the residence time are given. These plots were used to obtain data points for the variation of emissions along the HPT which were then compared with the variation of emissions from the current CRN. This comparison has been shown in figures 3.7, 3.8, 3.9, 3.10.

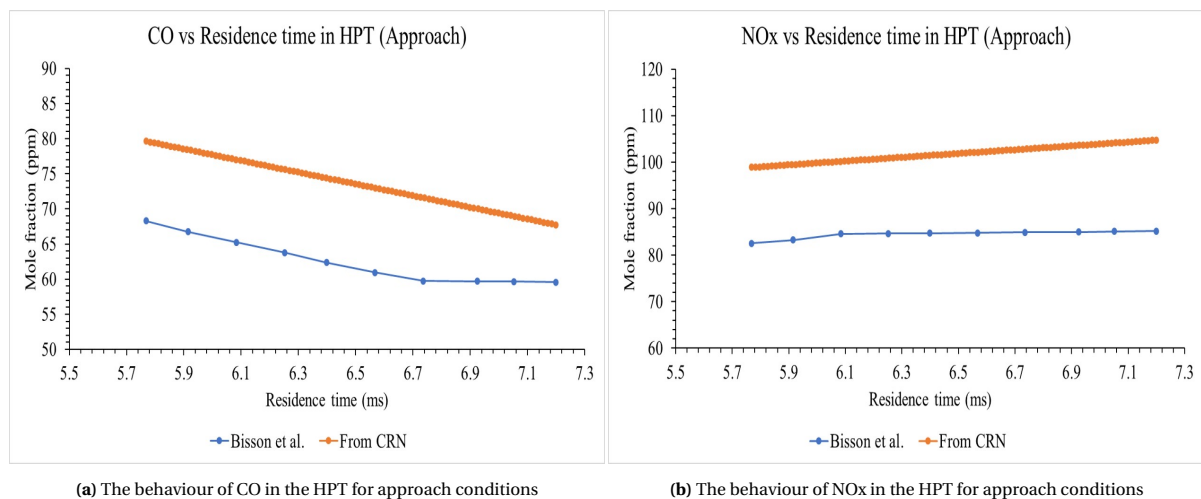
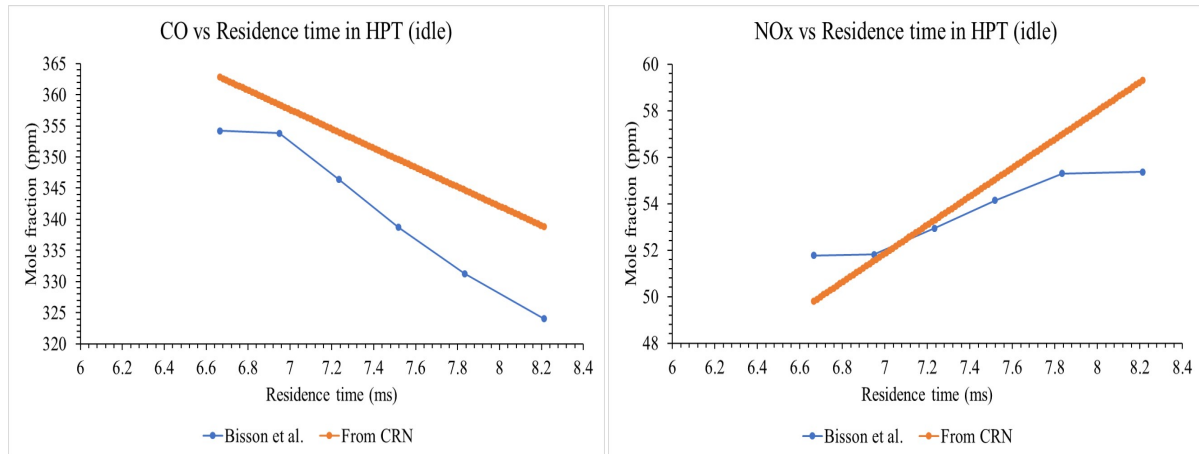


Figure 3.9: Emissions at approach - Bisson et al. vs CRN

The comparison of the results from Bisson et al. [81] and that from the current CRN shows that for all the 4 power settings both the results have matching trend except for the quantitative difference in the order of few ppm. The CRN in [81] consists of a n-parallel PSRs to model the unmixedness of the primary zone. The difference in estimation between the two models may be attributed to the difference in the modeling of the primary zone which leads to difference in the prediction of local equivalence ratio. Another reason can be the difference in the chemical reaction mechanism used for the modeling. Nevertheless, the comparison shows a good match and thus the CRN can be considered to be validated.

3.5. Summary

This chapter began with the discussion of the CRN modeling reactors used for the purpose of this thesis. This was followed by explaining the CRN architecture which was built based on literature. The setup for the simulations also consisted of describing the cycle parameters and the reactor specifications. This was followed by the presentation of validation done for the CRN.



(a) The behaviour of CO in the HPT for idle conditions

(b) The behaviour of NOx in the HPT for idle conditions

Figure 3.10: Emissions at idle - Bisson et al. vs CRN

4

Results and Discussion

4.1. Intent of the parametric analysis

Literature review of previous research has shown that, based on the fuel and the operating conditions of certain parameters, the change or evolution of emission species downstream of the combustor is not a negligible phenomenon. Therefore, it is important to identify these parameters that influence the way emission species behave downstream of the combustor, and also assess the level of influence that they have.

This work has been done by decoupling the detailed chemical kinetics and the fluid mechanics associated with the problem. This is done because of the computational constraints in implementing detailed chemistry in CFD. The CRN modeling allows for incorporating detailed chemistry with economical use of computational resources. CRNs also offer a good amount of flexibility because of the simplicity of 0D/1D modeling.

Previous studies on the evolution of emissions have been done for very specific conditions. They have been done for specific conditions/settings for a specific engine, and how emissions change for those specified conditions of the engine. Although a specific engine has been chosen for the same, it is used in order to achieve modeling that is pertinent and relevant to a combustor. Therefore, the motive was to study the effect of a wide range of conditions on the emissions in a turbine, using the capabilities at disposal. While one parameter is varied, the others are maintained at conditions pertaining to the hybrid engine, in order to assess the individual effect that the variation of the specific parameter has. The effect of each parameter has been analysed individually in order to see the extent of their stand-alone impact, without the coupling of the influence of other parameters.

4.1.1. Parameters considered

Therefore using the described CRN pertaining to a combustor-turbine network, the evolution of species for the following different conditions of parameters have been studied:

- Turbine Inlet Temperatures(TIT)
- inlet pressures
- chemical reaction mechanisms
- residence times
- temperature variation in the HPT
- temperature and pressure change in the HPT

These parameters were identified as those which are capable of having an impact, if any, in how the concentration of emission species change between the turbine inlet and exit. Apart from that, these are also the parameters which are possible to be explored using the 0D/1D modeling capabilities. The schematic of the combined combustor + HPT CRN corresponding to the hybrid engine configuration has been shown in 4.1.

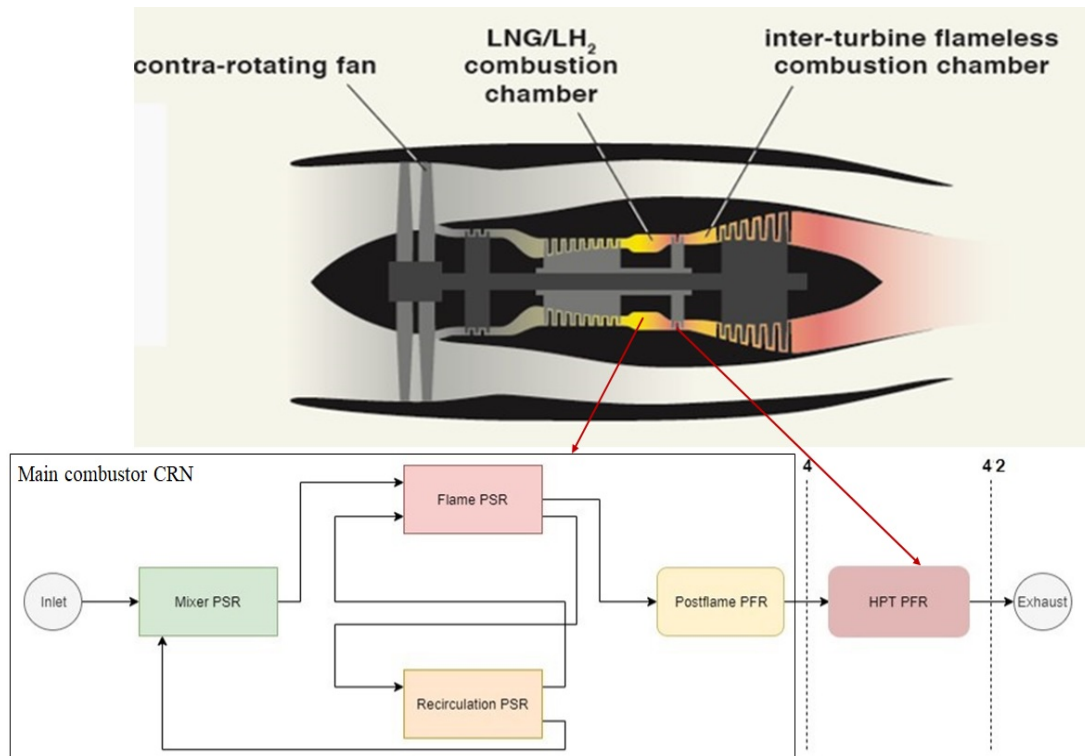


Figure 4.1: The schematic of the main combustor + HPT CRN pertaining to the components of the hybrid engine configuration

4.2. Turbine Inlet Temperatures

The study for turbine inlet temperature was done for the range of temperatures between 1650K to 2200K which is a comprehensive range that is good to encapsulate the turbine inlet temperatures at different instances of the mission profile. The turbine inlet temperatures were obtained as a result of changing the combustor inlet temperature. While the turbine inlet temperature was varied, the pressure was maintained to be 13,93bar corresponding to the cruise pressure at the turbine inlet of the hybrid engine which is obtained from the engine cycle calculations [15]. As mentioned earlier, this is done in order to see the individual impact that temperature has, on the behaviour of emissions in the PFR representative of the HPT. It must be noted that these different turbine inlet temperatures are *maintained throughout the HPT*. Although cycle temperatures and pressures are coupled in the sense that when the pressure is high, the temperature is also high and vice-versa, they have been studied individually in order to see the decoupled impact they have on what happens to CO and NO_x in the HPT.

4.2.1. Evolution of CO with TIT

The variation of CO at 4 and 42 is given in figure 4.2. CO from the combustor is high for lower temperatures. These lower temperatures result in the reaction rate for reactions involving the oxidation of CO to CO₂ to be low. Hence the consumption of CO does not happen quick. As the temperature increases the combustor CO decreases due to faster oxidation of CO to CO₂. This behaviour is observed until a certain temperature beyond which CO begins to increase again. This is because of the dissociation of CO at high temperatures which is a proven phenomenon in high temperatures [119, 120].

For CO at the stator exit, at lower temperatures the high CO from the combustor continues to undergo oxidation in the HPT and therefore at the stator exit CO is almost completely oxidised. As the temperature increases, CO gets closer to attaining equilibrium in the postflame region of the combustor itself. Since the temperature is maintained in the HPT, and since there is no variation in other parameters that can affect this attained equilibrium, CO continues to remain in equilibrium in the HPT also. This phenomenon inside the HPT can be observed in figure 4.3.

This behaviour of CO has been shown previously in [121] and [122], in terms of equivalence ratio which

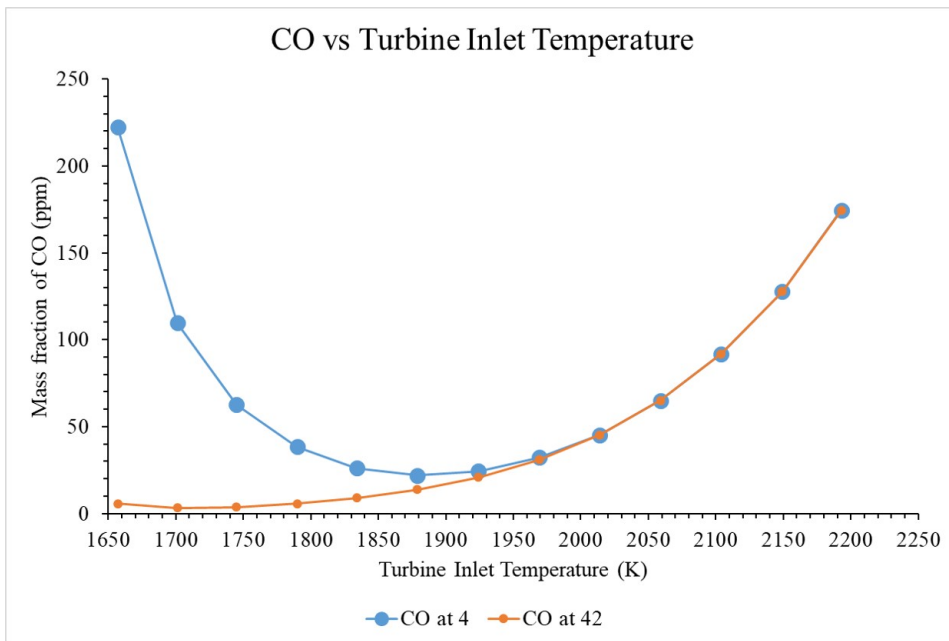


Figure 4.2: CO at the stator inlet (blue curve) and the exit (orange curve) vs TIT

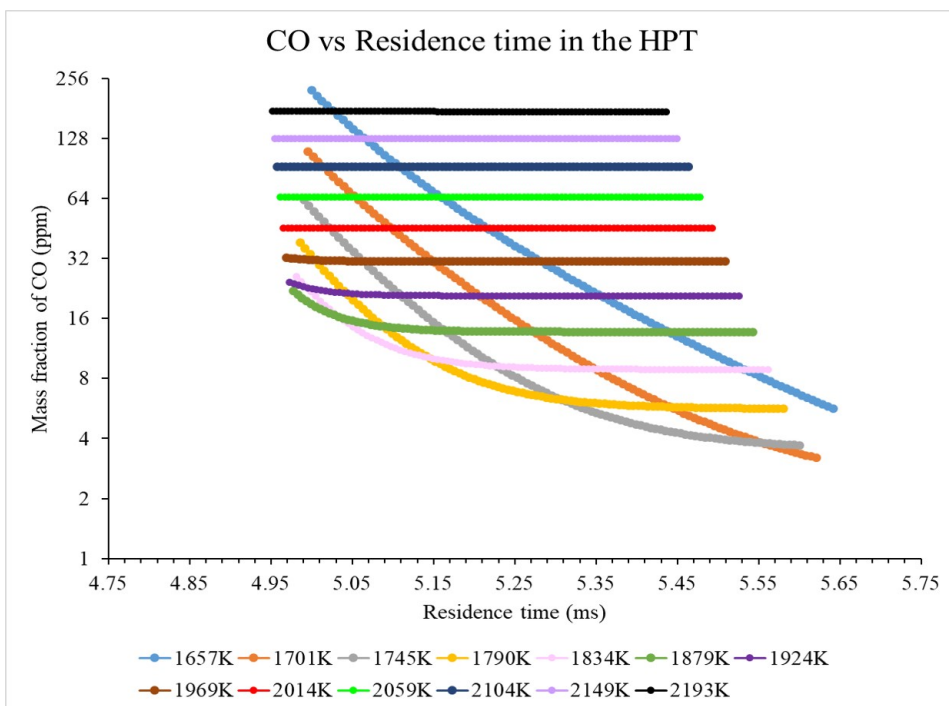


Figure 4.3: CO vs Residence time in the HPT (for different TITs)

is then associated to resulting temperature. The evolution of CO with residence time from [121], for different equivalence ratios is shown in figure 4.4. The evolution of CO with equivalence ratios for both high and low pressure conditions are shown in 4.5. At lower equivalence ratios, the resulting combustion temperatures are low and therefore the oxidation of CO is slow. At higher equivalence ratios, the resulting temperatures are higher leading to higher reaction rates which results in the equilibrium of CO being attained sooner.

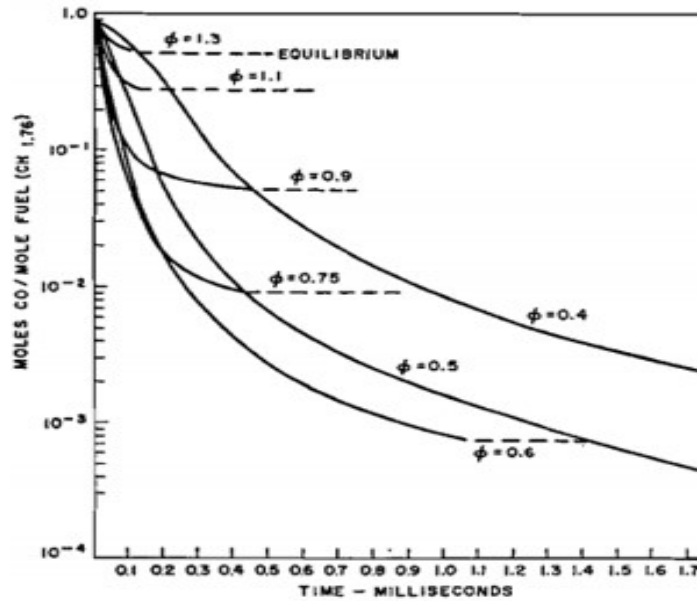


Figure 4.4: CO vs Residence time for different equivalence ratios with combustor inlet conditions i.e. $T_{inlet} = 450K$ and $P = 4atm$. Fig. courtesy [121]

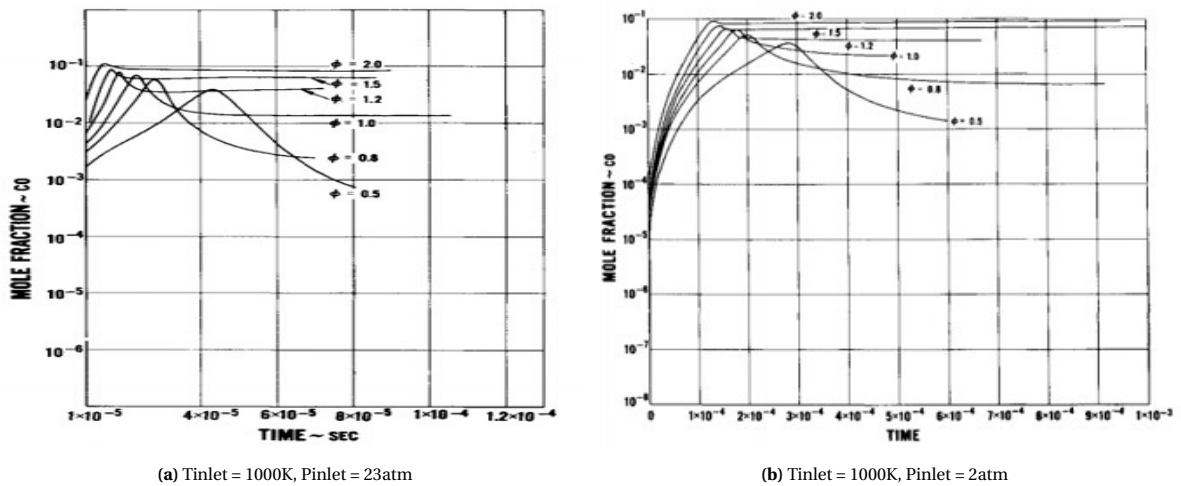


Figure 4.5: CO vs Residence time for different equivalence ratios and for two different combustor inlet pressures. Fig. courtesy [122]

4.2.2. Evolution of NO_x for TIT

In case of NO_x, the output from the combustor increases with increasing temperatures. In the HPT, since these high temperatures are maintained, NO_x increases in the HPT. The fact that the residence time increases from the stator inlet to the exit aids for the increase of NO_x due to the temperature. The increase of temperature leads to NO_x pathways becoming more active which results in higher NO_x. The specific pathways which are dominant in these conditions are also studied. The variation of NO_x at 4 and 42 is given in figure 4.6.

The relative and absolute contributions of the NO_x pathways are shown in figures 4.7 and 4.8. In case of the both the combustor and the HPT, at lower temperatures, specifically between 1657K to 1834K, the N₂O mechanism is dominant in producing NO_x by means of the N₂O intermediate. The importance of the N₂O pathway at low temperatures has been demonstrated in [126]. Upto 1834K, the contribution of the N₂O pathway to the total NO_x is more than 50%. As the temperature increases beyond 1834K, the contribution of thermal NO_x dominates since the thermal pathway is highly favoured by the high operating temperatures which is observed in figures 4.7a and 4.8a. Although the percentage contribution of the N₂O pathway wanes with increasing temperature, the NO_x obtained from this pathway continues to increase gradually with in-

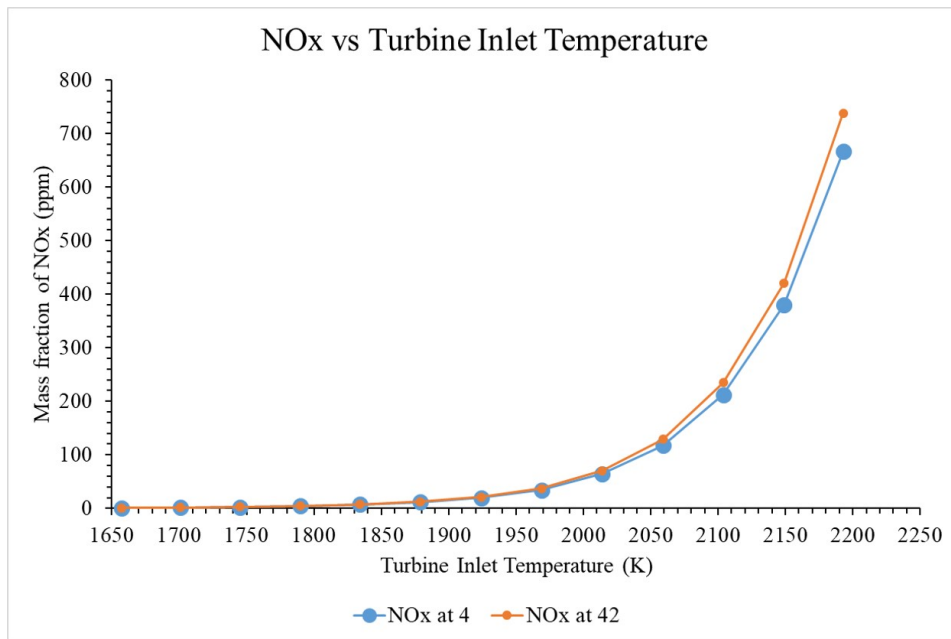
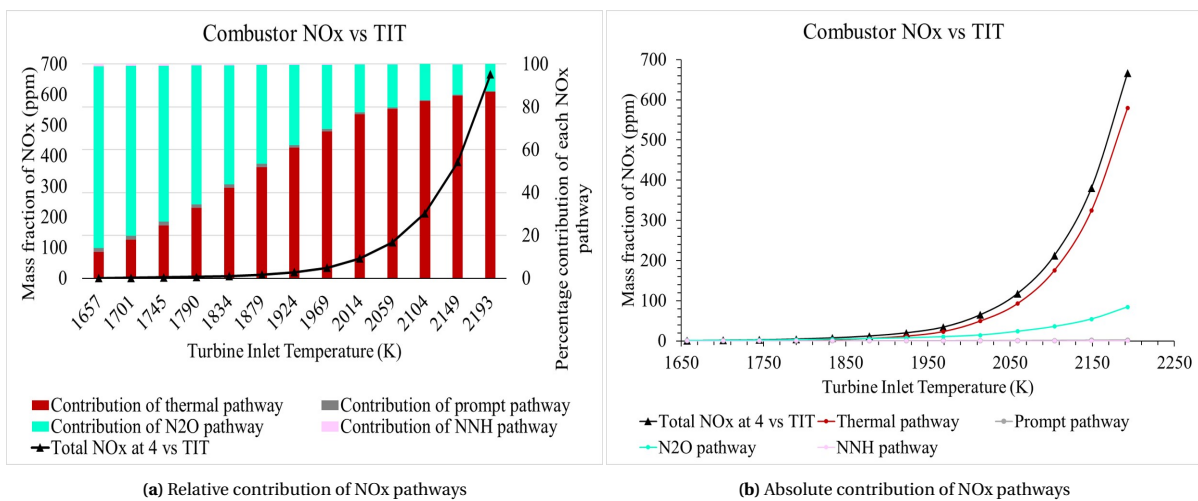


Figure 4.6: NOx at the stator inlet (blue curve) and the exit (orange curve) vs TIT

creasing temperature as seen in figures 4.7b and 4.8b. The contribution of the other two pathways is almost negligible irrespective of the temperature.



(a) Relative contribution of NOx pathways

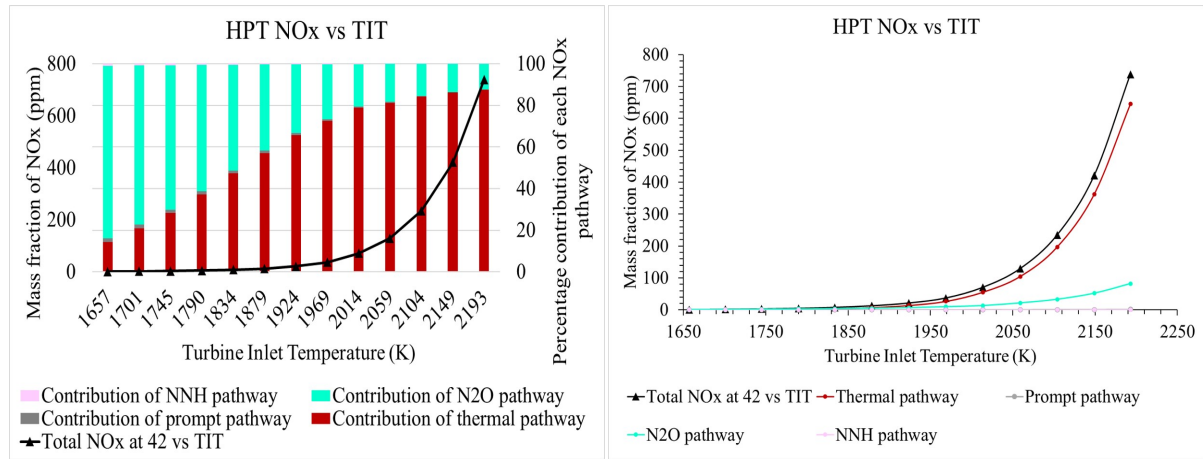
(b) Absolute contribution of NOx pathways

Figure 4.7: Contribution of NOx pathways to the total NOx emissions from the main combustor with TIT

Another interesting thing to look into is the change (increase) in NOx from the combustor into the HPT and the role of each pathway. As can be seen in figure, although at lower temperatures the total NOx was mainly due to the N2O pathway, the increase in NOx even at lower temperatures is dominated by the thermal pathway. This is due to the fact that from the combustor to the HPT, the residence time increases while the temperature is maintained. Therefore the thermal pathway which is already active due to the operating temperature is aided by the residence time increase from 4 to 42. This is also the same reason for the complete dominance of thermal pathway's role in the increase of NOx at higher temperatures.

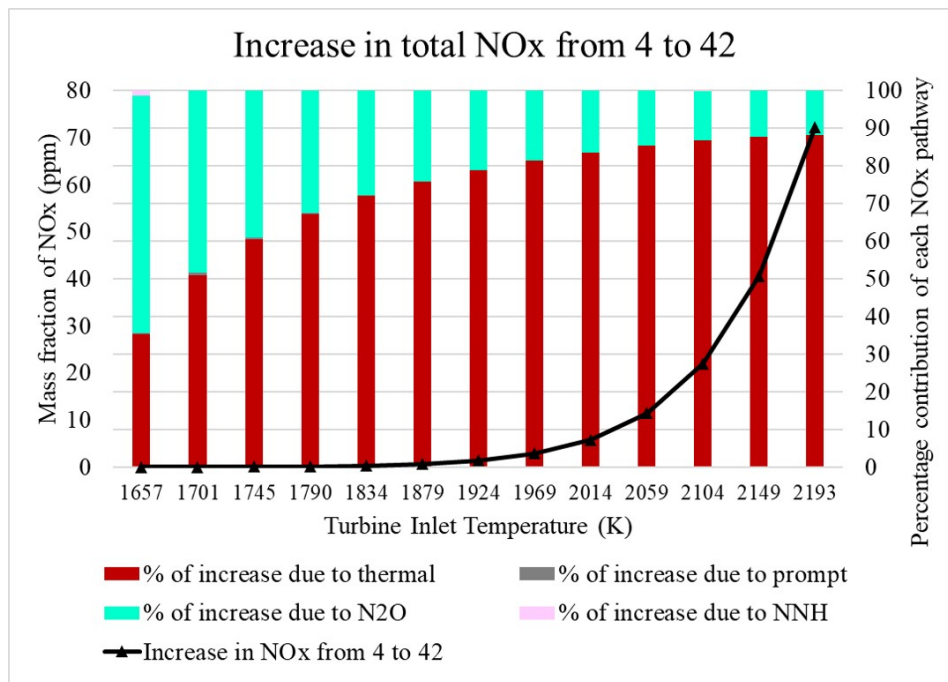
4.3. Inlet Pressures

The combustor and hence the turbine inlet pressures were varied between 10bar to 70bar which is representative of the lowest and highest power settings of the hybrid engine configuration. The investigation for



(a) Relative contribution of NOx pathways

(b) Absolute contribution of NOx pathways

Figure 4.8: Contribution of NOx pathways to the total NOx emissions from the HPT with TIT**Figure 4.9:** Increase of total NOx from the stator inlet to exit with respect to TITs

pressures was done for the highest and lowest TIT in order to see the influence of the operating temperatures too. The range of pressures considered is broad, and so the subsequent residence time for each of these pressures also varies hugely. Therefore the mass flow rates from table 3.1 are used accordingly such that the resulting residence times are indeed pertinent to a realistic combustor. It must be noted that for each case, the considered temperature and pressure are *maintained throughout the HPT*.

4.3.1. Evolution of CO with inlet pressures

For the lowest TIT, as the pressure is increased, CO from the combustor decreases considerably. This is due to the fact that with increasing pressures the formation of CO is suppressed [10]. Due to the low operating temperature, CO continues to be oxidised in the stator and therefore CO at the stator exit is very low. This low CO also keeps decreasing with increasing pressure because the oxidation of CO is increasingly favoured with increasing pressure. The variation of CO at 4 and 42 is given in figure 4.10a.

At the operating condition corresponding to the highest TIT, although the amount of CO from the com-

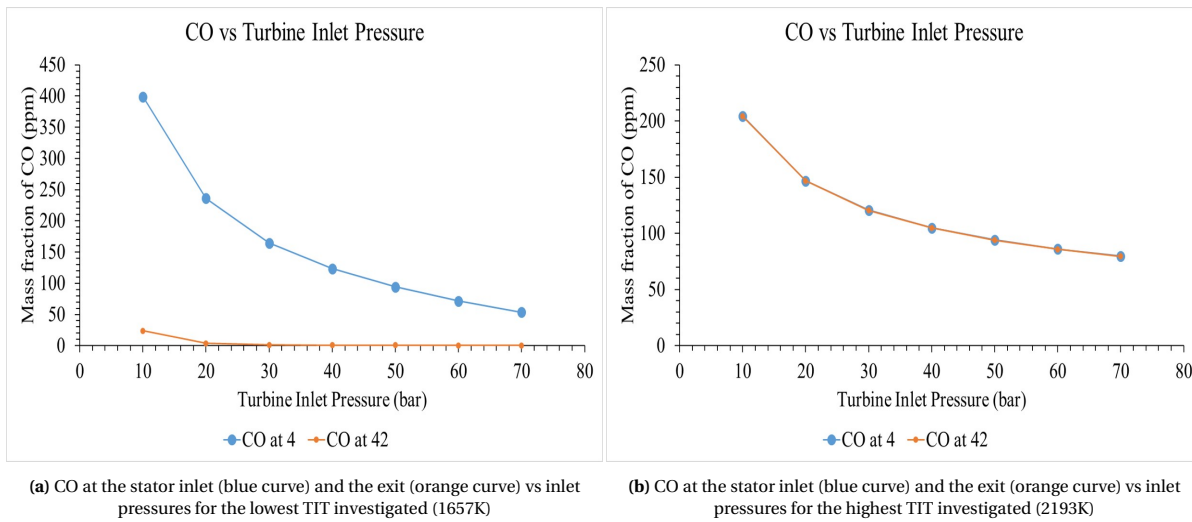


Figure 4.10: CO vs turbine inlet pressures for the highest and lowest TIT

bustor is high, this high CO decreases with increasing pressures. As mentioned before, this is also due to the formation of CO being suppressed with increasing pressures. It was shown that CO from the combustor reaches equilibrium faster with rising temperatures. Since the TIT is high in this case, CO inside the HPT remains in equilibrium because the parameters that can influence this equilibrium remain unaltered in the HPT. Therefore, CO at 42 is exactly the same as CO at 4 as seen in figure 4.10b.

4.3.2. Evolution of NOx with inlet pressures

Low TIT

At the lowest TIT investigated, the formation of NOx is low. This increases gradually with increasing pressures. The dependence of NOx on pressure is found to be influenced by the flame temperature [124]. Due to the operating temperature, the increase of NOx is found to be scant with rising pressure as shown in figure 4.11a. The NOx from the combustor undergoes a very slight increase in the HPT because of the fact that more residence time in the HPT allows for the already active NOx pathways to be active longer.

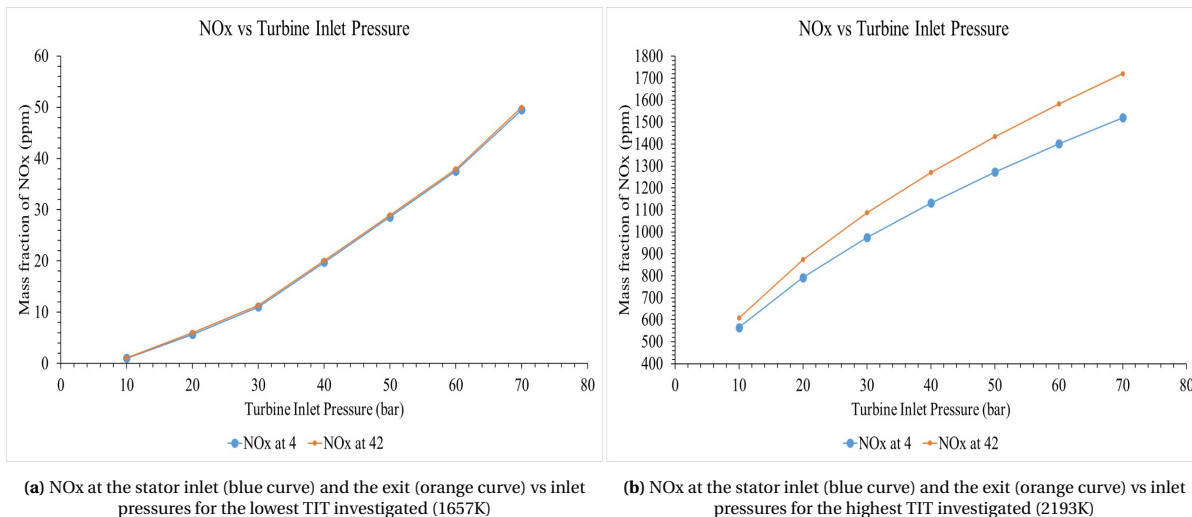


Figure 4.11: NOx vs turbine inlet pressures for the highest and lowest TIT

The specific contribution of NOx pathways to this rise has been investigated. It has been found that because of the low temperature, the N2O pathway is the most active contributor to the total NOx as seen in figure 4.12. For all the pressures, the contribution of the N2O pathway is of 80% and higher due to the low

operating temperature. As the pressure increases, the contribution of the thermal pathway increases slightly, by about 5%, since the rate constants of the initiation reaction of the thermal pathway become sensitive to these rising pressures. Yet, the N₂O pathway has the highest contribution to the NO_x from the combustor.

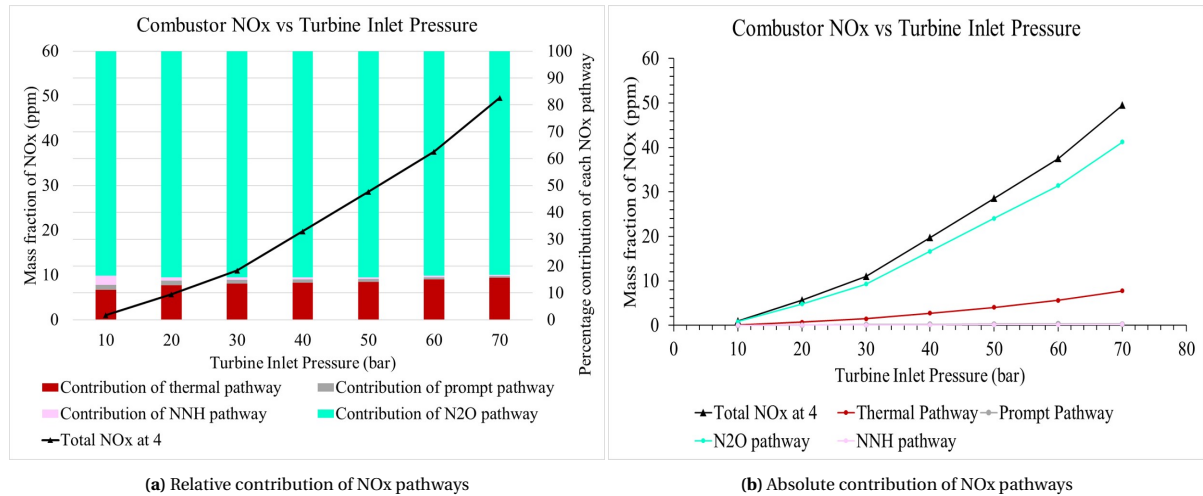


Figure 4.12: Contribution of NO_x pathways to the total NO_x emissions from the combustor for the lowest TIT investigated (1657K)

The same observation holds for the NO_x from the stator exit as well, as shown in figure 4.13. The contribution of the thermal pathway increases more with pressure, in comparison to that for the combustor. While for the combustor the thermal pathway increased by about 5%, in the HPT the contribution rises by about 15%. The increase in NO_x from the stator inlet to the exit has been shown in figure 4.14. Inside the HPT, the increase in NO_x due to thermal pathway rises by 20%. Apart from the fact that the reaction rate constants become sensitive with pressure, the residence time also increases with increasing pressure. This increase in residence time also backs the thermal pathway more with the rising pressures.

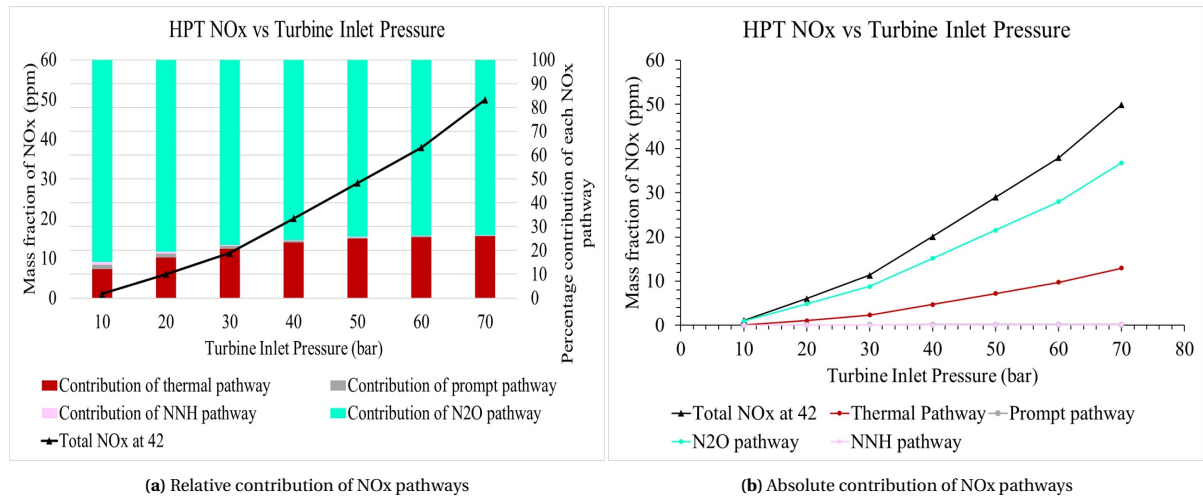


Figure 4.13: Contribution of NO_x pathways to the total NO_x emissions from the HPT for the lowest TIT investigated (1657K)

High TIT

In case of the highest TIT, the NO_x formation from the combustor is high. This high NO_x further increases with increasing pressure. Unlike the previous case, the rise of NO_x with pressure is considerable and not slight as shown in figure 4.11b. This is because of the fact that the increase in NO_x with pressure is influenced by the flame temperature which is very high in this case. As with the low TIT case, the NO_x from the combustor increases more aided by the increasing residence time with pressures.

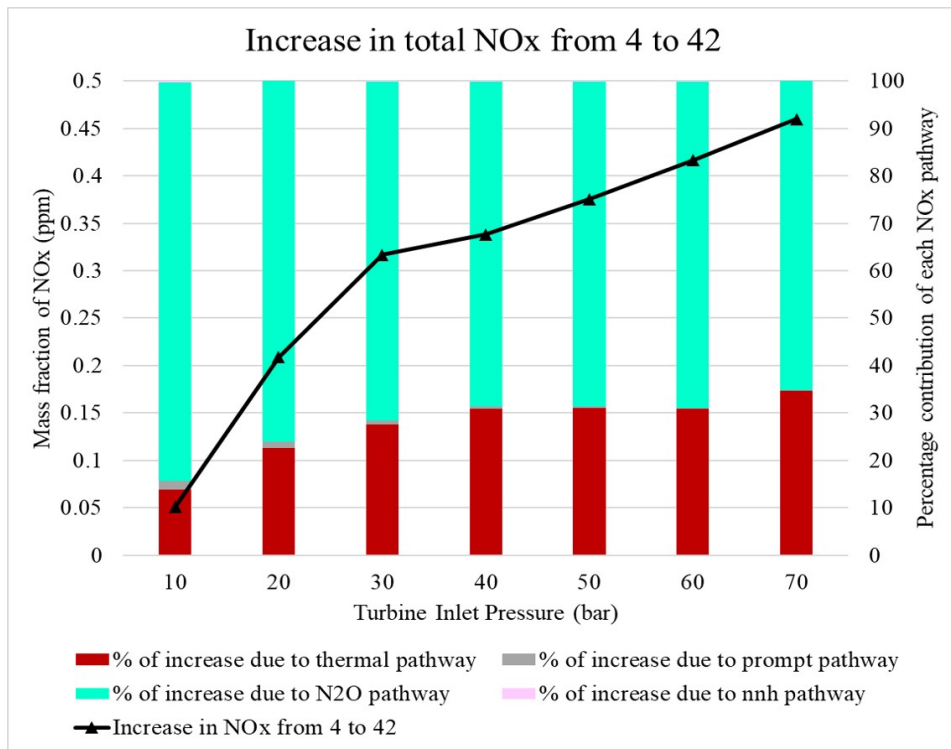


Figure 4.14: Increase of total NOx from the stator inlet to exit with respect to turbine inlet pressures for the lowest TIT investigated (1657K)

Assessing the specific contribution of the pathways leading to NOx shows that the high operating temperature means that thermal pathway is the most dominant player for the NOx obtained from the combustor as seen in figure 4.15. The contribution of thermal NOx is as high as 80%. With increasing pressures, although thermal pathway still remains dominant, the contribution of the N2O pathway becomes more pronounced. This is in line with the behaviour of the N2O mechanism with increasing pressure for lean premixed combustion, as reported by [126]. The role of the N2O pathway rises by upto 10% with increasing pressures, while the contribution of the thermal pathway decreases by the same percentage.

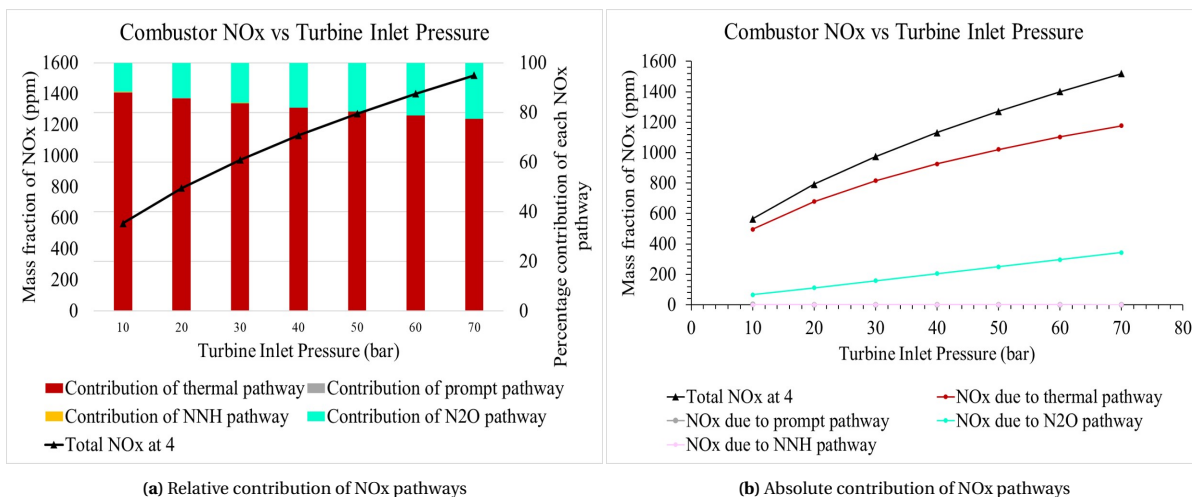


Figure 4.15: Contribution of NOx pathways to the total NOx emissions from the combustor for the highest TIT investigated (2193K)

In case of NOx from the HPT, thermal NOx is the most active contributor of NOx due to the high TIT. The rising pressure leads to the rise of the contribution of the N2O pathway as see in figure 4.16. In comparison

to the combustor NO_x, this behaviour is slightly different in the sense that, with increasing pressures the contribution of the N₂O pathway increases more than it did for the combustor as shown in figure 4.17. While the increasing pressures led to the rise in N₂O pathway contribution by about 10%, inside the stator the rise in the contribution of the N₂O pathway is by upto 20% and therefore the fall in the contribution of the thermal pathway is also by the same percentage. Apart from the increasing pressure favouring the N₂O pathway, the increasing residence time aids for the pathway to be an active contributor for longer.

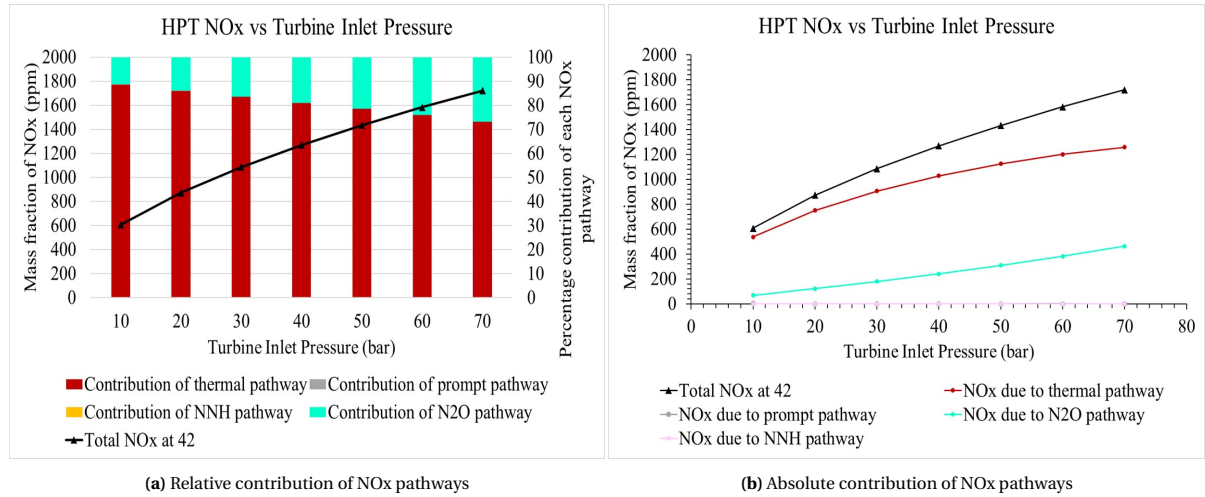


Figure 4.16: Contribution of NO_x pathways to the total NO_x emissions from the HPT for the highest TIT investigated (2193K)

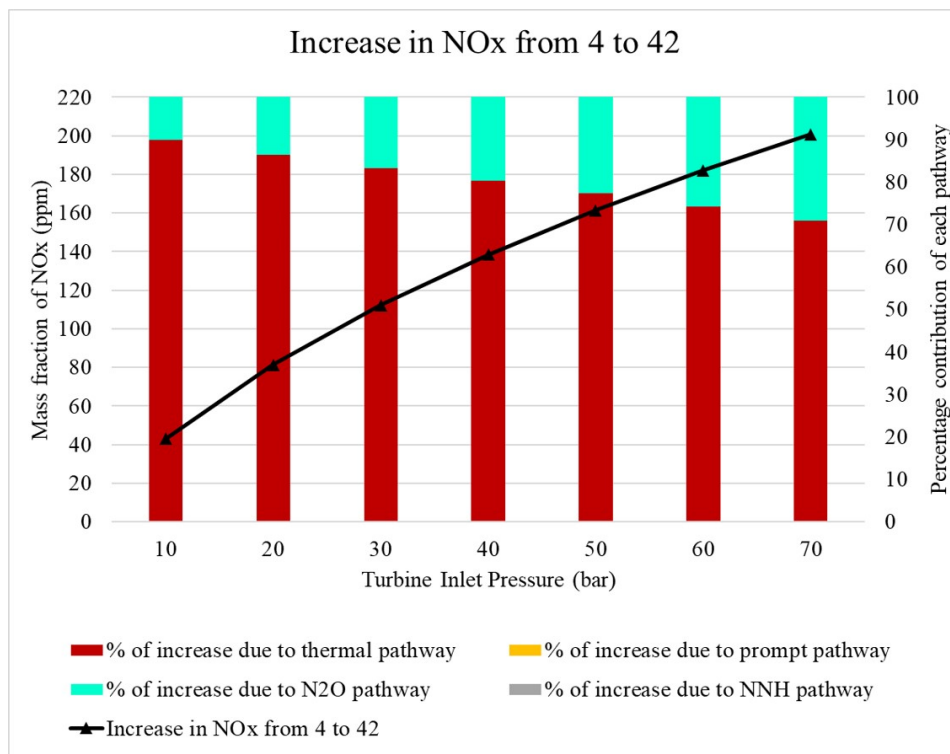


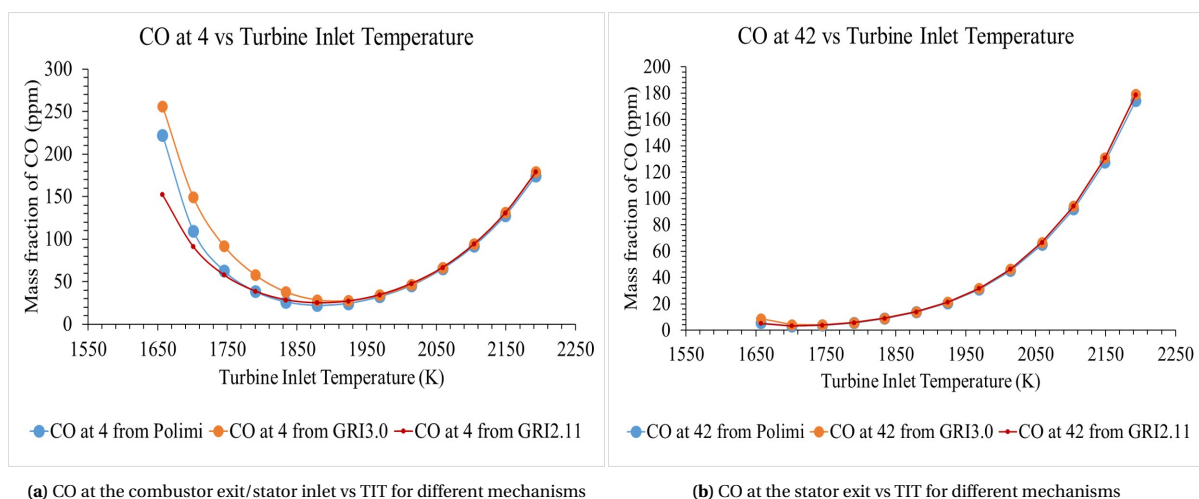
Figure 4.17: Increase of total NO_x from the stator inlet to exit with respect to turbine inlet pressures for the highest TIT investigated (2193K)

4.4. Reaction mechanisms

Chemical reaction mechanisms form the core of using CRNs for emission estimation. The advantage of using CRN modeling stems from the fact that the 0D/1D modeling allows for detailed chemical reaction mechanisms for the estimation of CO and NO_x which are considered minor species due to their low fraction in the exhaust gas stream. Therefore, it is important to gauge how the behaviour of emissions is influenced by the reaction mechanism used. For this purpose three reaction mechanisms have been used for comparison - the Polimi C1-C3 mechanism, the GRI2.11 and the GRI 3.0. It must be noted that the Polimi C1-C3 mechanism with 2141 reactions and 115 species has been used throughout this research. Since temperature is a fundamental parameter for reaction kinetics, these mechanisms were compared by using them for observing the variation with respect to the TIT.

4.4.1. Evolution of CO with different mechanisms

The estimation of the combustor CO by using the 3 different reaction mechanisms is shown in figure 4.18. For lower temperatures, there are differences in the prediction by the different mechanisms. The highest difference is between the two GRI mechanisms by upto a 100ppm. This difference keeps reducing as the temperature increases, and the estimation of CO from the combustor is the same from all the 3 mechanisms. At lower temperatures, the equilibrium of CO is attained slower. This means that the non-equilibrium amount of CO estimated by the different reactions are slightly different from each other and hence the values are different at the combustor exit for these temperatures. As the temperature increases, the equilibrium of CO is attained sooner in the combustor. This equilibrium value of CO is estimated exactly the same by all the 3 mechanisms.



(a) CO at the combustor exit/stator inlet vs TIT for different mechanisms

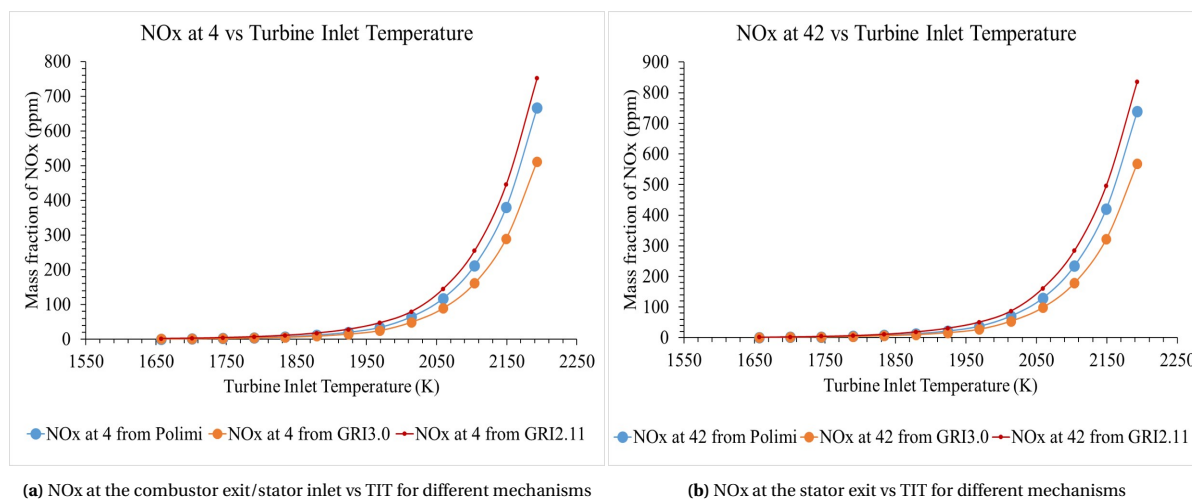
(b) CO at the stator exit vs TIT for different mechanisms

Figure 4.18: CO at the stator inlet and the exit assessed by three different mechanisms with respect to TITs

4.4.2. Evolution of NO_x with different mechanisms

The estimation of NO_x from the combustor by the three different mechanisms is shown in figure 4.19. Contrary to the behaviour of CO, at lower temperatures, the estimation of NO_x by different mechanisms is the same. As temperature increases, the difference in estimation of NO_x by the three mechanisms also increases. This observation holds good for both the cases - i.e. at the stator inlet and the exit as shown in figures 4.19a and 4.19b. The Polimi mechanism and the GRI2.11 mechanism have a closer agreement in the estimation of NO_x. The reason behind these can be better understood by analysing the role of different pathways assessed by each mechanism, which has also been presented below.

The relative contribution of each NO_x pathway in assessing the total NO_x at the stator inlet and exit are shown in figures 4.20 and 4.21. It can be seen that in lower temperatures, the NO_x at the combustor exit/stator inlet as in figure 4.20 has 3 mechanisms contributing to it. At these lower temperatures, the relative contribution of the prompt pathway is more or less the same from the Polimi and the GRI3.0 mechanism, whereas the prompt contribution estimated by GRI2.11 is relatively higher. As temperature increases, the



(a) NOx at the combustor exit/stator inlet vs TIT for different mechanisms

(b) NOx at the stator exit vs TIT for different mechanisms

Figure 4.19: NOx at the stator inlet and the exit assessed by three different mechanisms

agreement in prompt contribution still holds good between the Polimi and GRI3.0 mechanism. This is due to the fact that one of the main changes or improvements made from the GRI2.11 to GRI3.0 was the change in CH kinetics important for the prompt NO_x pathway as a result of new measurements. And the Polimi mechanism was built by using the GRI3.0 as a reference. Therefore the prompt NO_x agreement between the two mechanisms is better in comparison to that with GRI2.11. The same observation holds for NO_x at the stator exit as shown in figure 4.21.

Another thing to be noted is the contribution of thermal NO_x by the three mechanisms. In both figures 4.20 and 4.21 it can be seen that the thermal NO_x contribution at all temperatures except the lowest one, is ascendingly predicted by the GRI3.0, GRI2.11 and the Polimi mechanisms. This is due to the definition of the rate constants of the thermal NO_x initiation reaction from the three mechanisms. As mentioned in section 2.4, each mechanism has a set of elementary reactions for which the preexponential factor A , temperature exponent b and the activation energy E_a are defined after finding them for a range of experimental conditions for which they are validated. These have a direct relationship with the reaction rate as defined in equation 2.26, which in turn affects the reaction rate as given in equation 2.23. These 3 values, pertaining to the thermal NO_x initiation reaction, for all the three mechanisms are defined such that the thermal NO_x reaction rate constant for the same temperature is highest for the Polimi mechanism, followed by GRI2.11 and GRI3.0. Although the contribution assessed by them does not have much differences, the observed difference can be attributed to this reason. In case of the Polimi mechanism, the hydrocarbon part of the mechanism has been validated for pressures between 0.5atm - 60atm and for temperatures between 298K - 470K. The high temperature NO_x mechanisms have been validated for temperatures between 800K - 1450K [64]. As mentioned earlier, the GRI2.11 mechanism is validated for temperatures between 900K and 1400K [35]. Thus the total NO_x values estimated by these two mechanisms are closer to each other. The GRI3.0 mechanism is validated for a broad range of temperatures and pressures (300K-5000K) [37, 38]. Thus, the observed differences can also be attributed to the range of conditions for which the mechanisms are optimized or validated.

4.5. Residence time in the combustor

The residence time, which is another influential parameter in terms of chemical kinetics has also been investigated. The residence time of the combustor has been varied to be between 4.8ms to 6ms. This is done by varying the postflame reactor volume by means of changing the reactor length. This range of residence time is typical for an aero engine combustor and therefore has been investigated for two conditions - the lowest power condition (low TIT and low turbine inlet pressure), and the highest power condition (high TIT and high turbine inlet pressure). It must be noted that temperature and pressure are maintained from the HPT inlet through the exit.



Figure 4.20: Relative contribution of NOx pathways at the combustor exit/stator inlet with TIT, as estimated by three different mechanisms

4.5.1. Evolution of CO with residence time

The variation of CO at the combustor outlet/stator inlet and the stator exit has been for the highest and lowest power conditions are shown in figure 4.23. For the case of the lowest temperature and pressure from figure 4.23a, CO from the combustor (CO at 4, the blue curve) is high at the lower residence times. This CO drastically changes with residence time. This is because of the fact that the chemistry of CO is fast as shown in figure 4.22 and hence a few ms of extra residence time leads to significant oxidation of CO to CO₂. Regardless of how high the amount of CO is from the combustor, it gets almost completely oxidised at the stator exit which is the reason for a huge difference in CO from the stator inlet to the exit for the same residence time (difference between data point values corresponding to the same colour). CO from the stator exit which is already low due to being oxidised completely decreases further with increasing residence time (CO at 42, the orange curve).

In case of the highest temperature and pressure from figure 4.23b, CO from the combustor (CO at 4, the blue curve) is high because of the high operating temperature. This high CO does not change much with increasing residence time. This is because, as shown earlier in figure 4.3, at this high operating temperature CO reaches equilibrium in the postflame region itself and continues to remain in equilibrium since none of the parameters that can affect or disturb this equilibrium (temperature, pressure and composition) are changing. This is also the reason why there is not much difference between the CO at the stator inlet and the stator exit for the same residence time (difference between data point values corresponding to the same colour). CO from the stator exit (CO at 42, the orange curve) also therefore does not change much with increasing residence time.

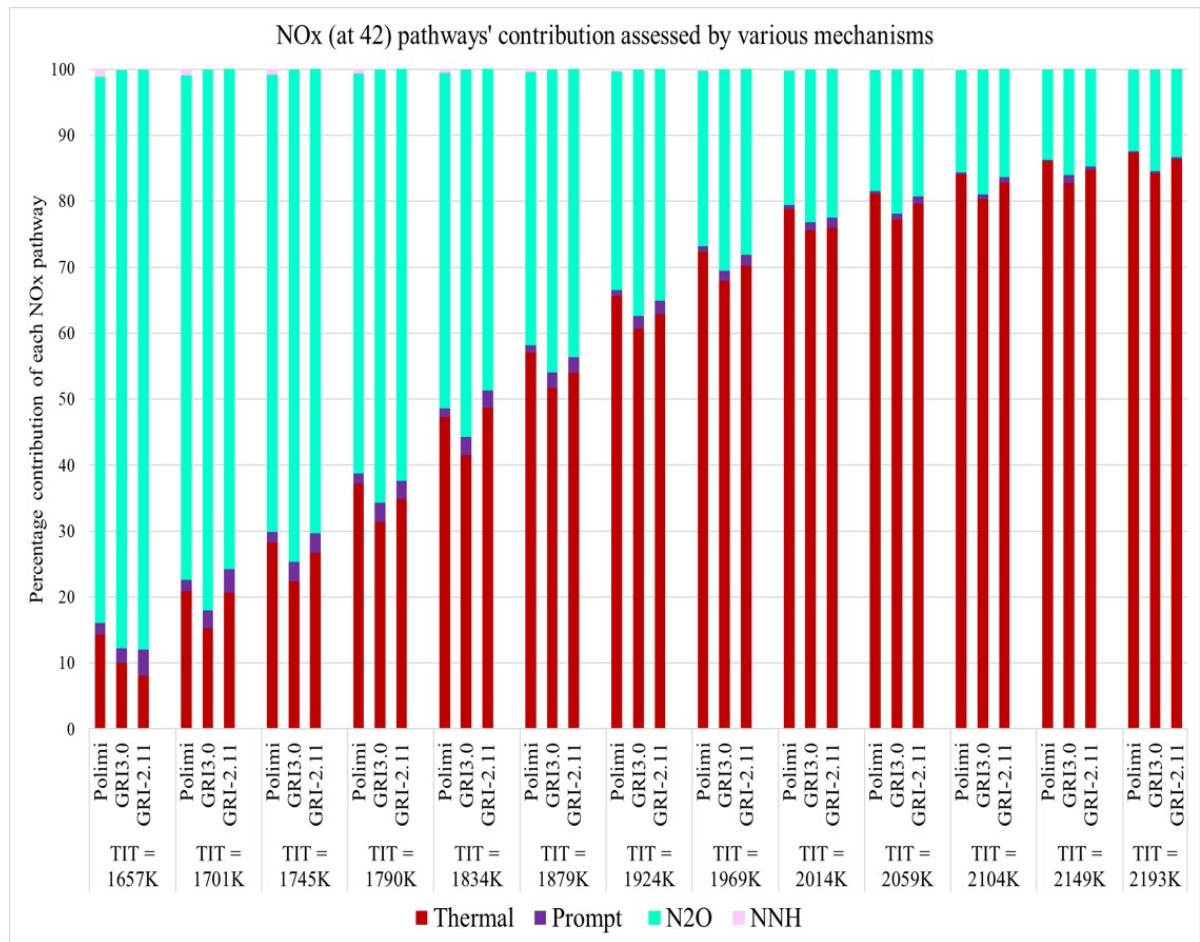


Figure 4.21: Relative contribution of NOx pathways at the stator exit with TIT, as estimated by three different mechanisms

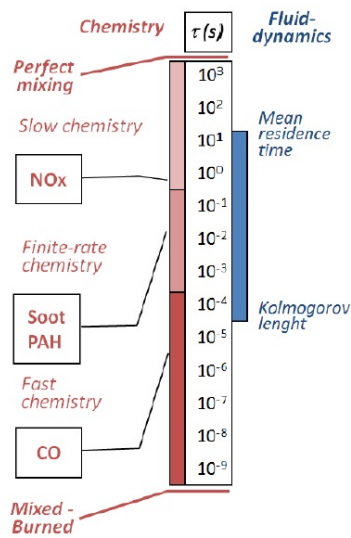


Figure 4.22: Chemical and flow time scales in a turbulent reacting flow, Figure courtesy: [22, 125]

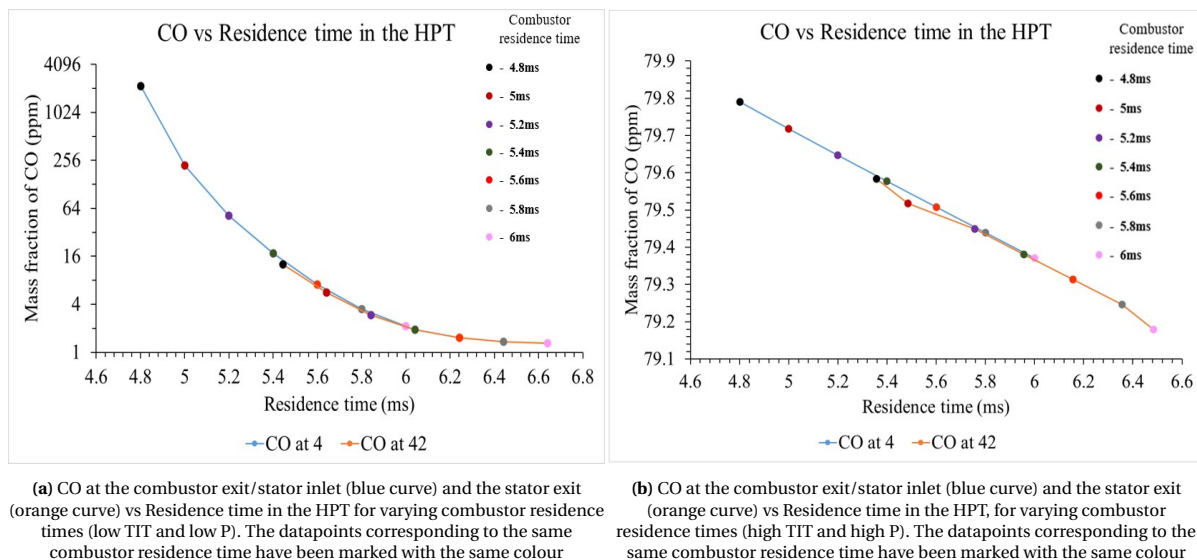


Figure 4.23: CO at the stator inlet and exit vs Residence time in the HPT for different combustor residence times

4.5.2. Evolution of NO_x with residence time

The variation of NO_x with residence time is shown in figure 4.24. At the lowest temperature and pressure from figure 4.24a, the NO_x emissions from the combustor (NO_x at 4, the blue curve) are very low. This low NO_x increases slightly with increasing residence time. This is because of the fact that the residence time gives more time for the progress of NO_x pathways and these are having relatively less reaction rates at this temperature and pressure. This can also be attributed to the slow chemistry of NO_x as shown in figure 4.22. Thus, there is not much difference between NO_x at the combustor exit/stator inlet and the stator exit (difference between data point values corresponding to the same colour). Although the increase in NO_x from the HPT inlet to the exit is not much, NO_x at the stator exit (NO_x at 42, the orange curve) also increases scantily with increasing residence time.

At the highest temperature and pressure as seen in figure 4.24b, NO_x at the combustor exit/stator inlet (NO_x at 4, the blue curve) increases significantly with increasing residence time. This is because the high operating temperature leads to high reaction rates of NO_x pathways, especially the thermal pathway as shown earlier. These reactions with high reaction rates are aided by the increasing residence time to happen longer. Hence the difference between NO_x at the combustor exit/stator inlet and the stator exit (difference between data point values corresponding to the same colour) also increases with increasing residence time. This means that NO_x at the stator exit also increases considerably with increasing residence time.

4.6. Temperature change in the HPT

The HPT is a gas turbine component in which a considerable change in temperature occurs, which, as mentioned earlier, is one of the main reasons why the chemistry cannot be assumed to be frozen past the combustor. This specific phenomenon and its role in influencing the behaviour of emissions has been investigated here. This investigation has also been done for the conditions of the lowest and highest temperature and pressure. The combustor exit temperature and the rotor exit temperature for both the conditions are known. The degree of reaction is the parameter which is defined as the ratio of temperature drop across the rotor to that of across the whole stage [115]. Using the assumption of a degree of reaction of 0.5, which is a sound one for an axial turbine [115, 116], the enthalpy drop across the turbine is equal through the stator and the rotor. Thus, the stator exit temperature was calculated for both conditions. These values are given in the following table 4.1. Thus, the temperatures at the stator inlet and exit mentioned in the table, were imposed across the stator length based on the degree of reaction assumption.

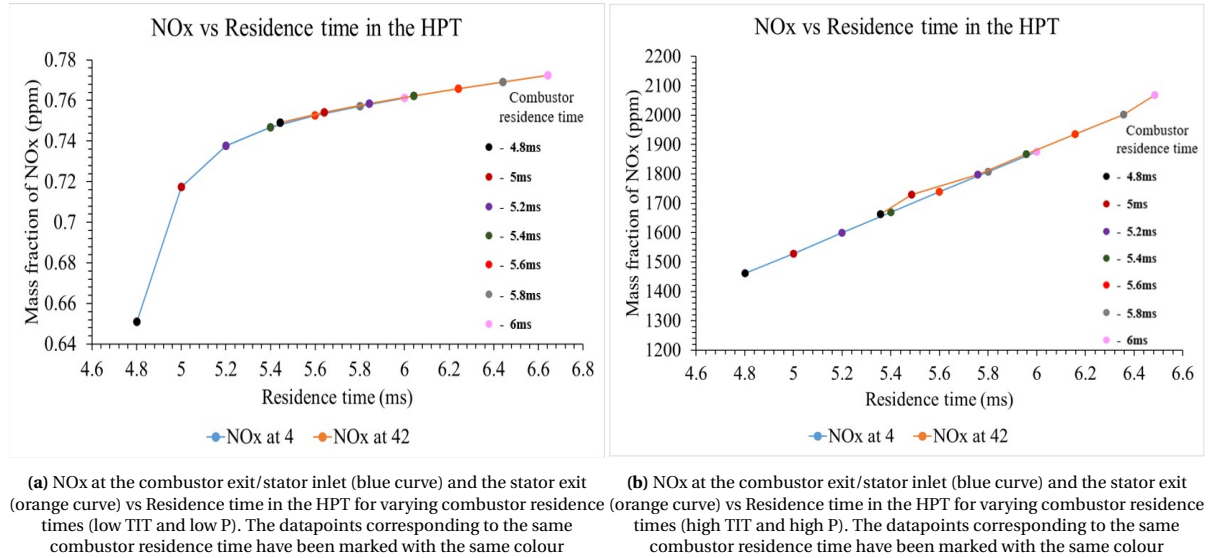


Figure 4.24: NOx at the stator inlet and exit vs Residence time in the HPT for different combustor residence times

T_4	T_{42}
1624K	1286.9K
2149	1505.2K

Table 4.1: The stator inlet and exit temperature values used

4.6.1. Evolution of CO with temperature change

The change in CO along the HPT with and without a temperature change, for the lowest and highest temperatures have been shown in figure 4.25. For the lowest temperature case in figure 4.25a, it can be seen that the curves with and without a temperature change are more or less similar. CO corresponding to temperature change is slightly higher than the one without temperature change. This is due to the fact that when the temperature in the HPT is constantly as high as the TIT (the orange curve), the rate of oxidation of CO to CO₂ is faster. Whereas the decreasing temperature (blue curve) leads to relatively slower reaction rate for the oxidation of CO.

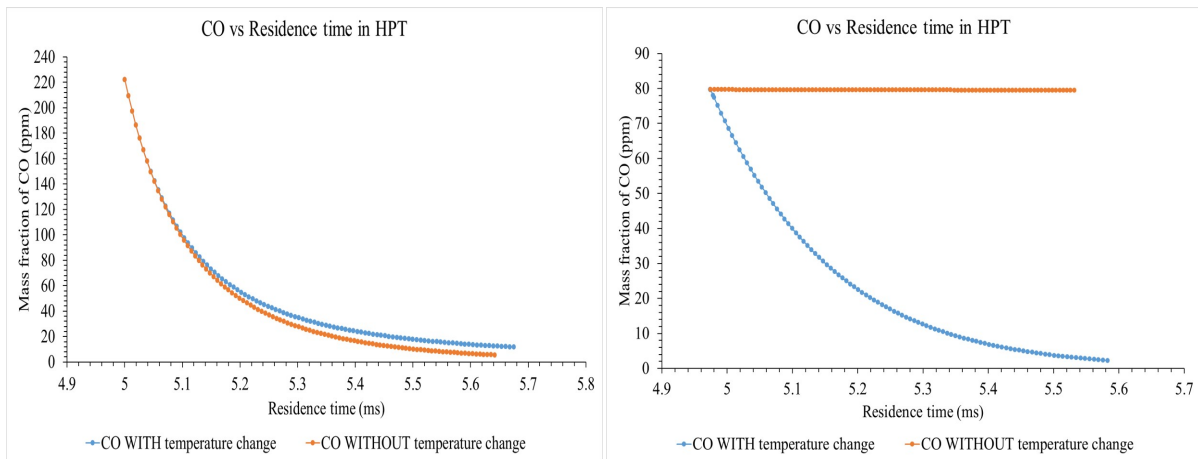
For the case of the highest temperature and pressure as shown in figure 4.25b the behaviour of CO is significantly different. When the temperature is constantly equal to the highest TIT (the orange curve), CO is already in equilibrium from the postflame region itself. Since this equilibrium is maintained due to the unchanging parameters that can affect it (temperature, pressure and concentration), the equilibrium continues in the HPT. Whereas, when there is a temperature change, this equilibrium from the postflame region is no longer retained and thus CO is continuously oxidized to CO₂.

4.6.2. Evolution of NOx with temperature change

The behaviour of NOx with and without temperature change in the in HPT is shown in figure 4.26 for both the lowest and highest temperature and pressure. In both cases, when there is no temperature change and the TIT is constantly maintained in the HPT, the increase in NOx along the HPT is significant. The consistently high temperature increases the reaction rates of the active NOx pathways. Whereas, when there is a temperature change, the rise in NOx with residence time is slowed down due to the slower reaction rates. In case of the low TIT the increase in NOx with temperature change is slight whereas in case of the high TIT, the increase in NOx with temperature change is not negligible.

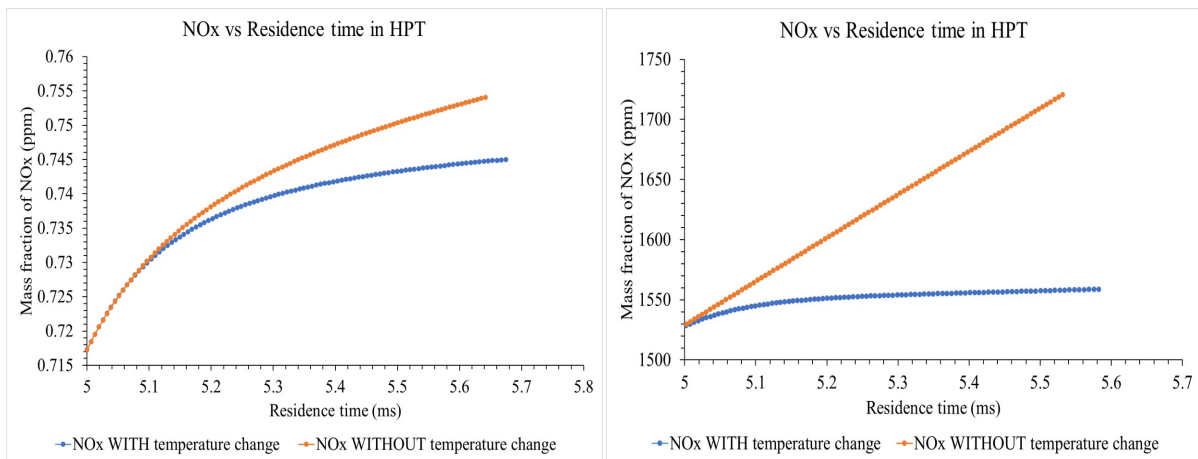
4.7. Temperature and pressure change in the HPT

In a HPT, expansion of the exhaust gases take place in order to provide energy for the HPT to run the compressor. Therefore, along with a temperature fall, the pressure also changes along the HPT. The change in temperature and pressure along a typical turbine is shown in the figure 4.27. The high and low pressure tur-



(a) CO vs residence time along the HPT (low TIT and low P) (b) CO vs residence time along the HPT (high TIT and high P)

Figure 4.25: CO vs Residence time in the HPT with and without temperature change for the lowest and highest temperature and pressure



(a) NOx vs residence time along the HPT (low TIT and low P) (b) NOx vs residence time along the HPT (high TIT and high P)

Figure 4.26: NOx vs Residence time in the HPT with and without temperature change for the lowest and highest temperature and pressure

bines consist of alternate blade rows, the stator and rotor, which have a temperature and pressure variation as shown in the figure since the exhaust gases undergo expansion in the turbine. The cycle pressures are known and the pressure at the stator exit needs to be calculated. Therefore using, the corresponding cycle temperatures, mass flow rates, and the area of the HPT and the assumption of mach number 1 at the stator exit, the pressures at 42 are calculated.

The pressures which were thus calculated are given in the following table 4.2. The temperature change as per table 4.1 and the pressure variation as per table 4.2 were imposed along the HPT reactor length.

P_4	P_{42}
12.85bar	4bar
64.58bar	18.91bar

Table 4.2: The stator inlet and exit pressure values used

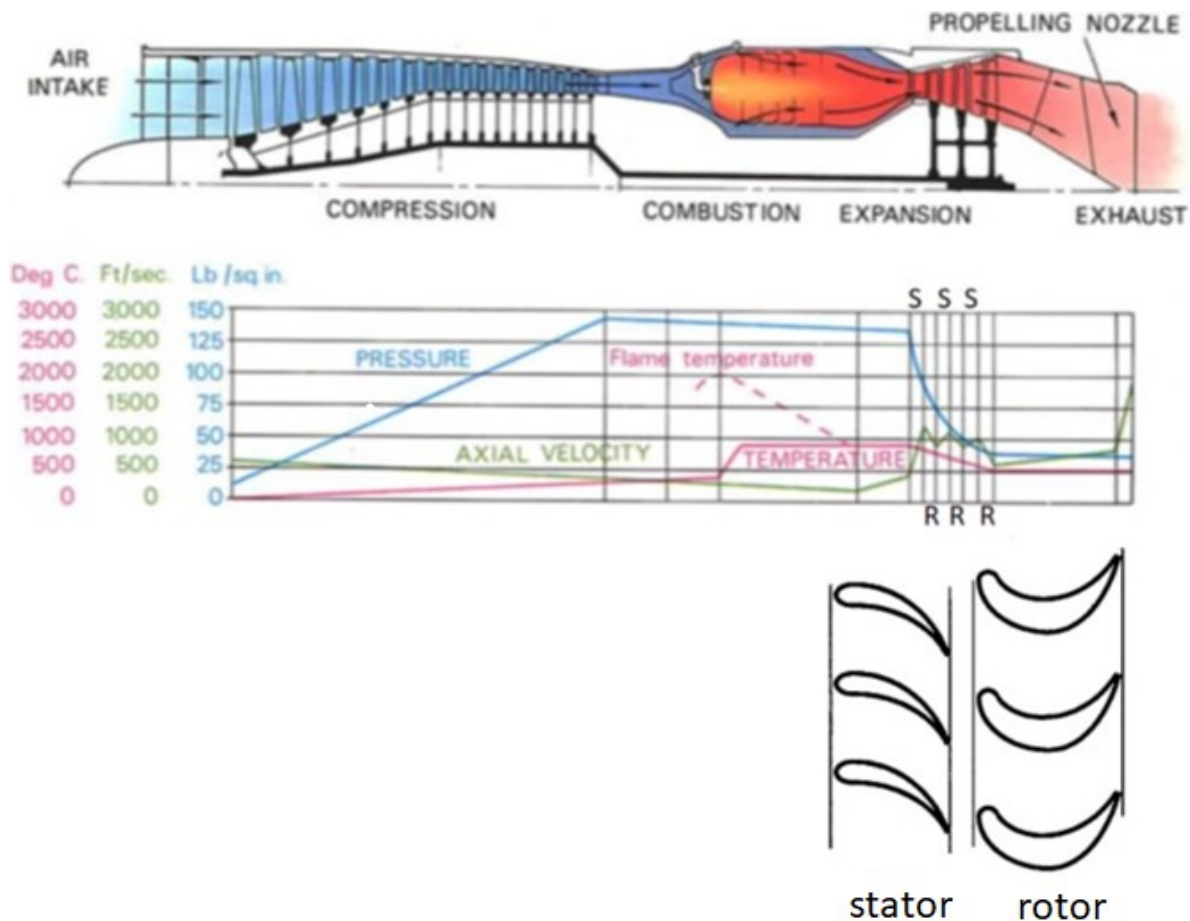


Figure 4.27: A blade row of the turbine of a typical aero-engine depicted along with the representative variation of temperature and pressure along the engine

4.7.1. Evolution of CO with temperature and pressure change in the HPT

The behaviour of CO with and without temperature and pressure change is shown in figure 4.28, for both low and high power cases. For the low power case, CO from the combustor continues to get oxidised in the HPT for all four scenarios. The rate of oxidation of CO is the fastest when the inlet pressure and temperature are consistently maintained (grey curve). When only the expansion is imposed this rate of oxidation is slightly lower (yellow curve). If only the temperature change is considered (orange curve), the rate is affected considerably and thus the CO in the HPT is relatively higher than the former two scenarios. When both expansion and temperature change are considered (blue curve) as in an actual turbine, the rate of oxidation of CO is very slow thus leading to the highest amount of CO out of all the investigated scenarios.

For the high power case, when the temperature and pressure change are not imposed, CO continues to remain in equilibrium (grey curve). When this equilibrium is affected by imposing the pressure expansion, since the pressure is decreasing, the equilibrium is altered to favour the increase in CO. Therefore at a high power case, considering only an expansion causes the increase in CO (yellow curve). In case of considering the temperature change with and without expansion (blue and orange curves respectively), CO gets continuously oxidized to CO_2 .

4.7.2. Evolution of NO_x with temperature and pressure change in the HPT

The change in NO_x in the HPT for the four scenarios are presented in figure 4.29. For both low and high power cases, the rise in NO_x along the HPT is the highest when the inlet temperature and pressure are maintained (grey curve), due to the resulting high reaction rates of the NO_x pathways. This rate is slightly lower when only the pressure decreases in the turbine (yellow curve). The rate is more considerably affected when the

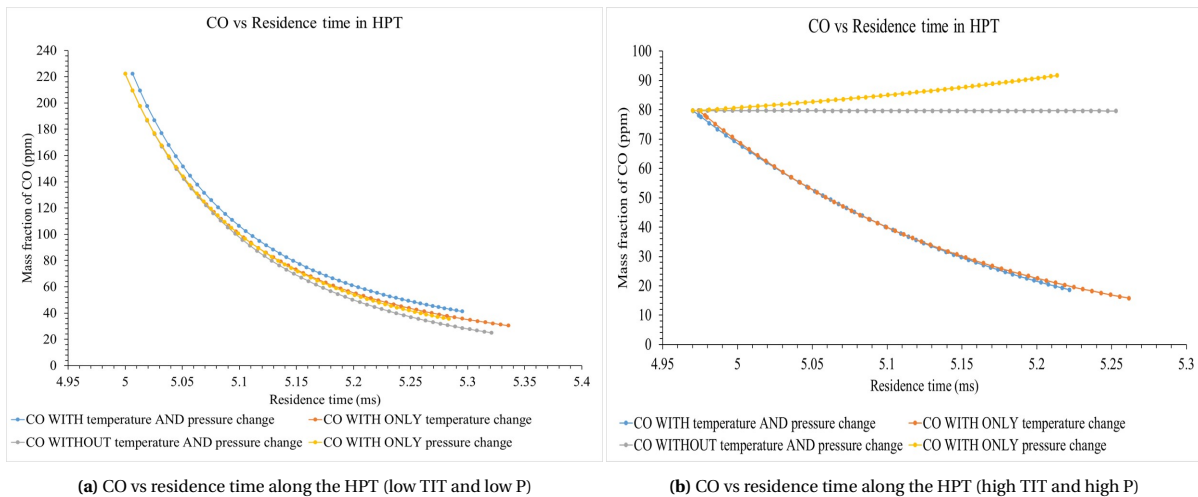


Figure 4.28: CO vs Residence time in the HPT for four scenarios corresponding to the temperature and pressure change for the lowest and highest temperature and pressure

temperature changes along the reactor, with the inlet pressure maintained (orange curve). Thus when there is a temperature change and pressure change as in an actual turbine, the rate of rise in NO_x along the HPT is the slowest out of all scenarios.

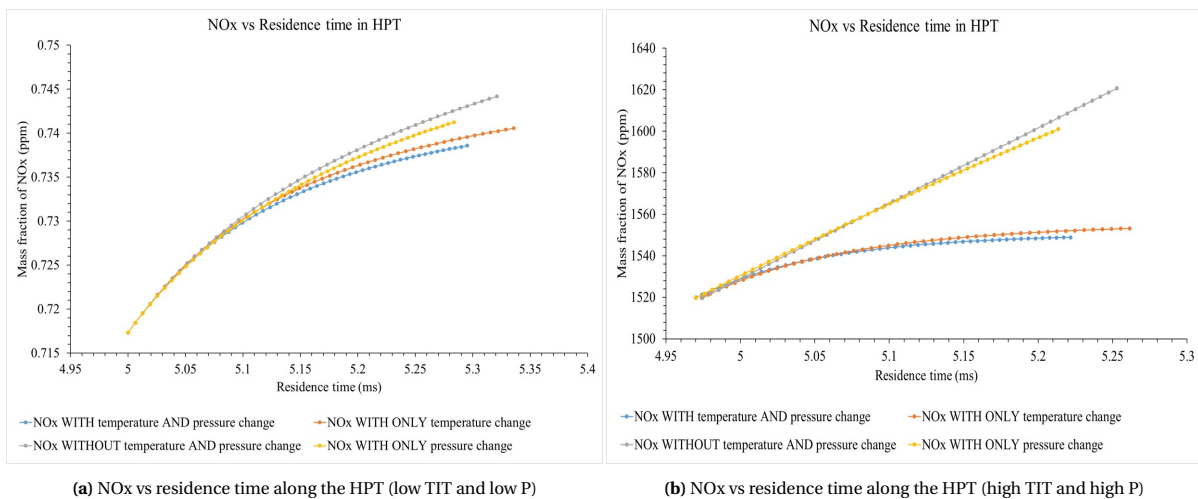


Figure 4.29: NO_x vs Residence time in the HPT for four scenarios corresponding to the temperature and pressure change for the lowest and highest temperature and pressure

4.8. Kerosene vs LNG

The hybrid engine configuration was designed for using cryogenic fuels i.e. LNG or LH₂ for the main combustor. Cryogenic fuels pose a problem of storage in the sense that they are supposed to be stored in cylindrical or spherical tanks. This would lead to problems in terms of volume for a conventional aircraft. But in case of the hybrid engine configuration, the storage issue is resolved due to the integration of the fuselage and the wing, which leads to volume availability for these storage tanks. The secondary combustor or the inter-turbine burner is designed to operate with kerosene or biofuel in the flameless combustion regime. The main motive for choosing cryogenic fuels for the main combustor is that these fuels are inherently better options in terms of emissions, in comparison to conventional aviation fuels like kerosene.

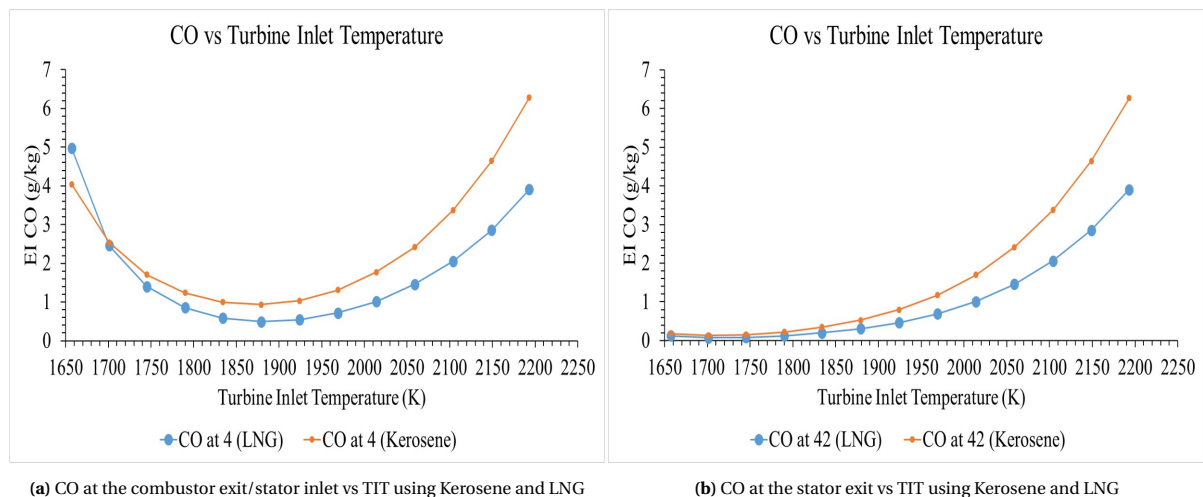
Aviation fuels usually comprise of complex hydrocarbon mixtures. Such fuels consist of a large number of species and therefore the use of detailed reaction mechanisms for these fuels, even with a computationally economical modeling like CRNs is still unrealistic and non-viable. For this purpose fuel surrogates are

employed. A fuel surrogate is, in principle, similar to a reduced mechanism and consists of a mixture of a number of hydrocarbons usually much lesser than the original fuel, and these are used based on their ability to reproduce the most important physical and chemical properties of the original fuel [128].

For a complex fuel, surrogates are created and used after extensive testing of their capacity to be a substitute for the original fuel. In case of kerosene which is also a complex hydrocarbon mixture, the surrogates which are recommended to be used are n-dodecane ($C_{12}H_{26}$) and n-decane ($C_{10}H_{22}$). Using a surrogate instead of real kerosene mainly poses a difference for the postcombustion hydrocarbon profile which can have an effect on the estimation of soot, since the postcombustion amount of aromatics are affected [130, 131]. To model the use of kerosene in the main combustor of the hybrid engine configuration, the Aachen Kerosene surrogate mechanism has been used. This mechanism uses a mixture of 80% n-decane and 20% 1,2 tri-methyl benzene to model kerosene combustion and consists of 163 species and 838 reactions [132]. A quantitative comparison of using LNG in the main combustor against using kerosene in the main combustor has been presented in the following section. The results are presented for cases of inlet temperatures, pressures and temperature change and expansion in the turbine.

Turbine Inlet Temperatures

The outcome of emissions by using kerosene and LNG for the same inlet temperatures have been presented. It can be seen that in terms of CO emissions, except for the lowest TIT, LNG is the better fuel option for the main combustor. This is because of the higher carbon content in kerosene which leads to more carbon branching reactions which subsequently result in the formation of more CO [10, 74]. Whereas using LNG is more beneficial in all cases, in terms of NOx.



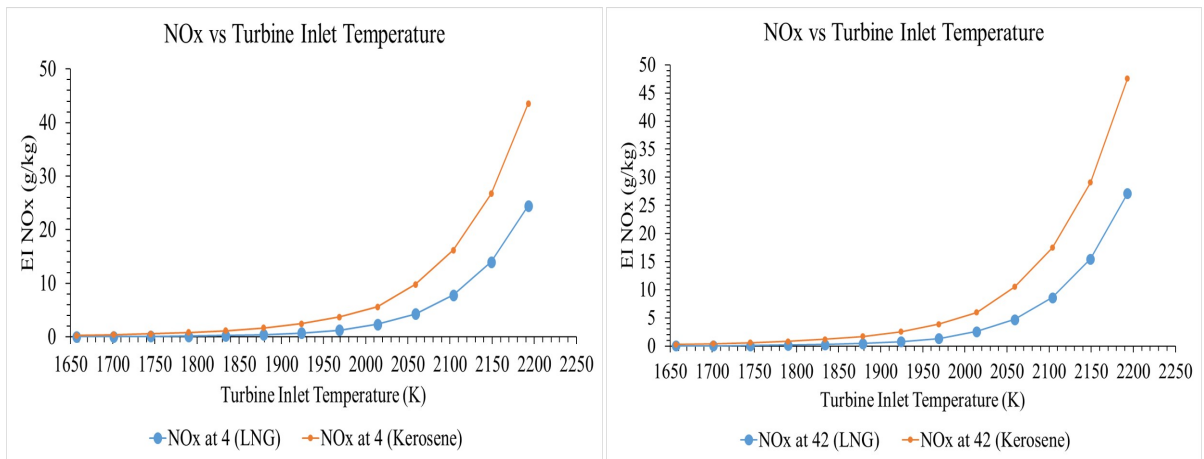
(a) CO at the combustor exit/stator inlet vs TIT using Kerosene and LNG

(b) CO at the stator exit vs TIT using Kerosene and LNG

Figure 4.30: CO at the HPT stator inlet and the exit vs TIT compared for using kerosene and LNG in the main engine of the hybrid combustor

Turbine inlet pressures

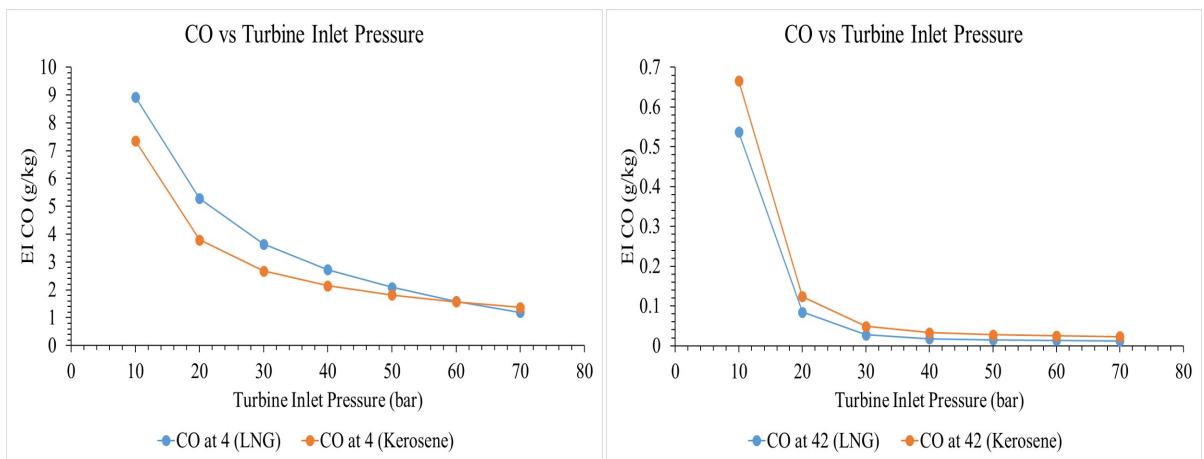
In case of varying pressures, for the lowest TIT, CO from the combustor is higher while using LNG, whereas for the highest TIT LNG is the better option in terms of both NOx and CO.



(a) NOx at the combustor exit/stator inlet vs TIT using Kerosene and LNG

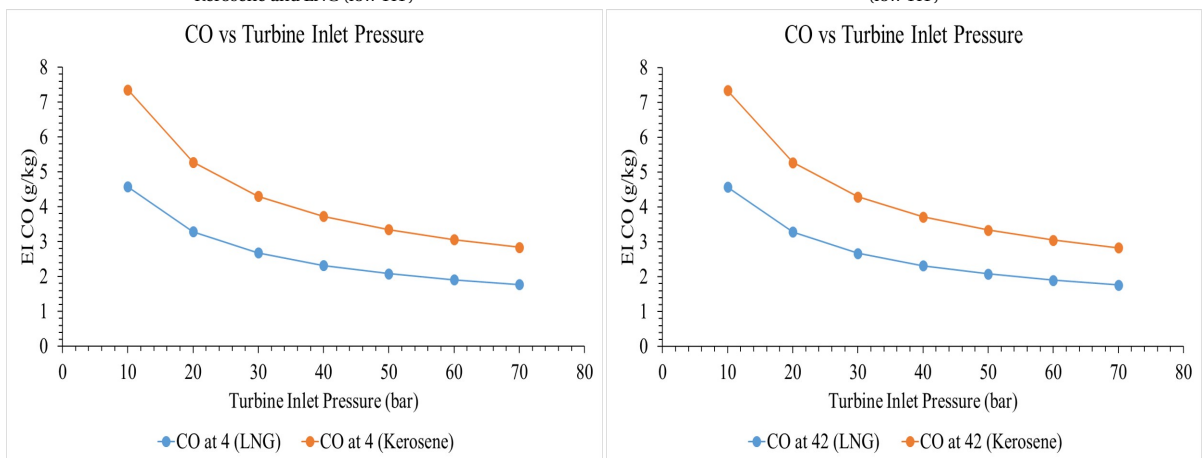
(b) NOx at the stator exit vs TIT using Kerosene and LNG

Figure 4.31: NOx at the HPT stator inlet and the exit vs TIT compared for using kerosene and LNG in the main engine of the hybrid combustor



(a) CO at the combustor exit/stator inlet vs turbine inlet pressure using Kerosene and LNG (low TIT)

(b) CO at the stator exit vs turbine inlet pressure using Kerosene and LNG (low TIT)



(c) CO at the combustor exit/stator inlet vs turbine inlet pressure using Kerosene and LNG (high TIT)

(d) CO at the stator exit vs turbine inlet pressure using Kerosene and LNG (high TIT)

Figure 4.32: CO at the HPT stator inlet and the exit vs turbine inlet pressure compared for using kerosene and LNG in the main engine of the hybrid combustor for the lowest and the highest TITs investigated

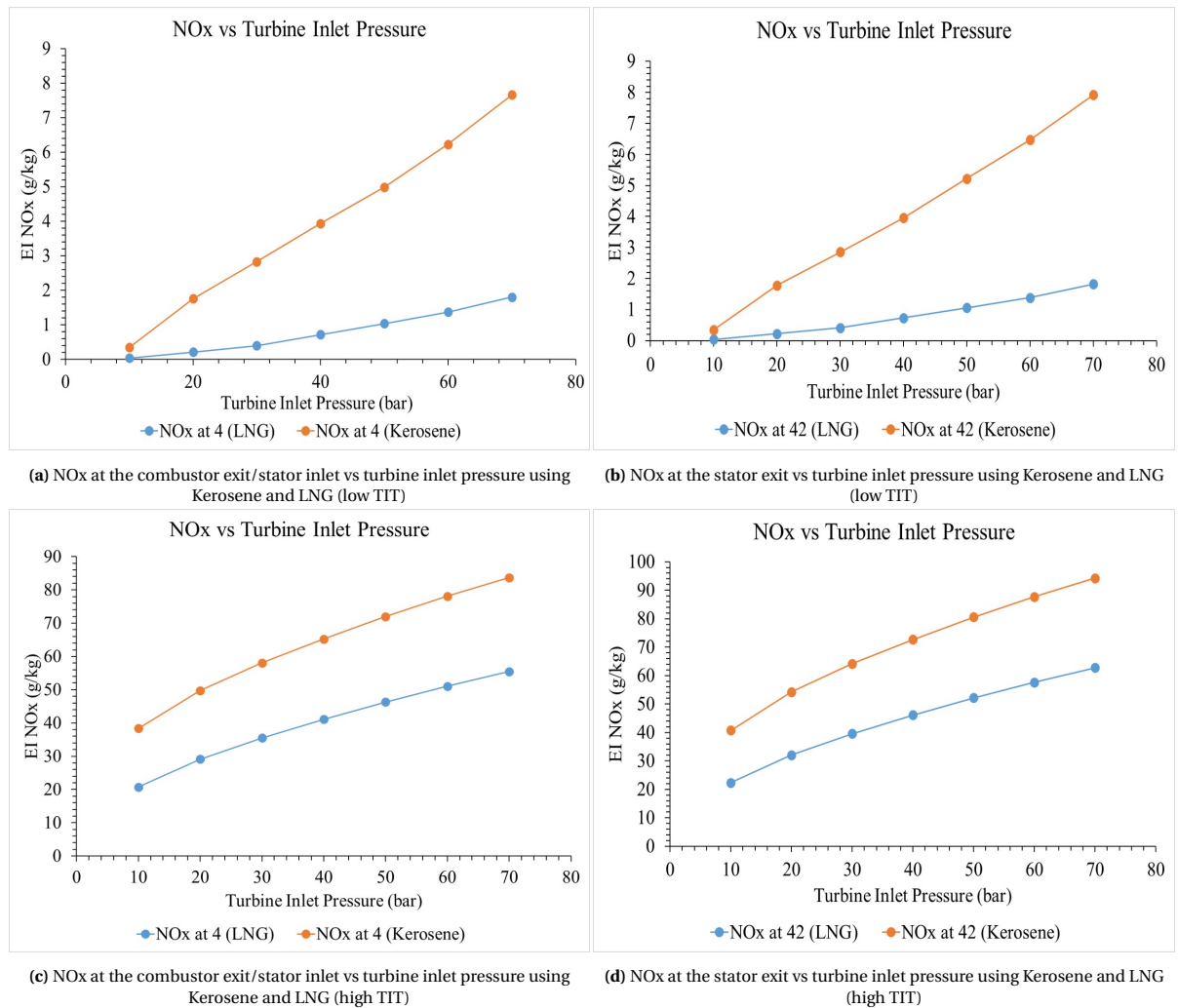


Figure 4.33: NOx at the HPT stator inlet and the exit vs turbine inlet pressure compared for using kerosene and LNG in the main engine of the hybrid combustor for the lowest and the TITs investigated

Temperature and pressure change in the turbine

The change in temperature and pressure in the HPT have also been studied with kerosene. For the same calculated stator inlet and exit pressures and temperatures the behaviour of emissions while using kerosene have been presented below. This has been done for both the highest and the lowest power conditions.

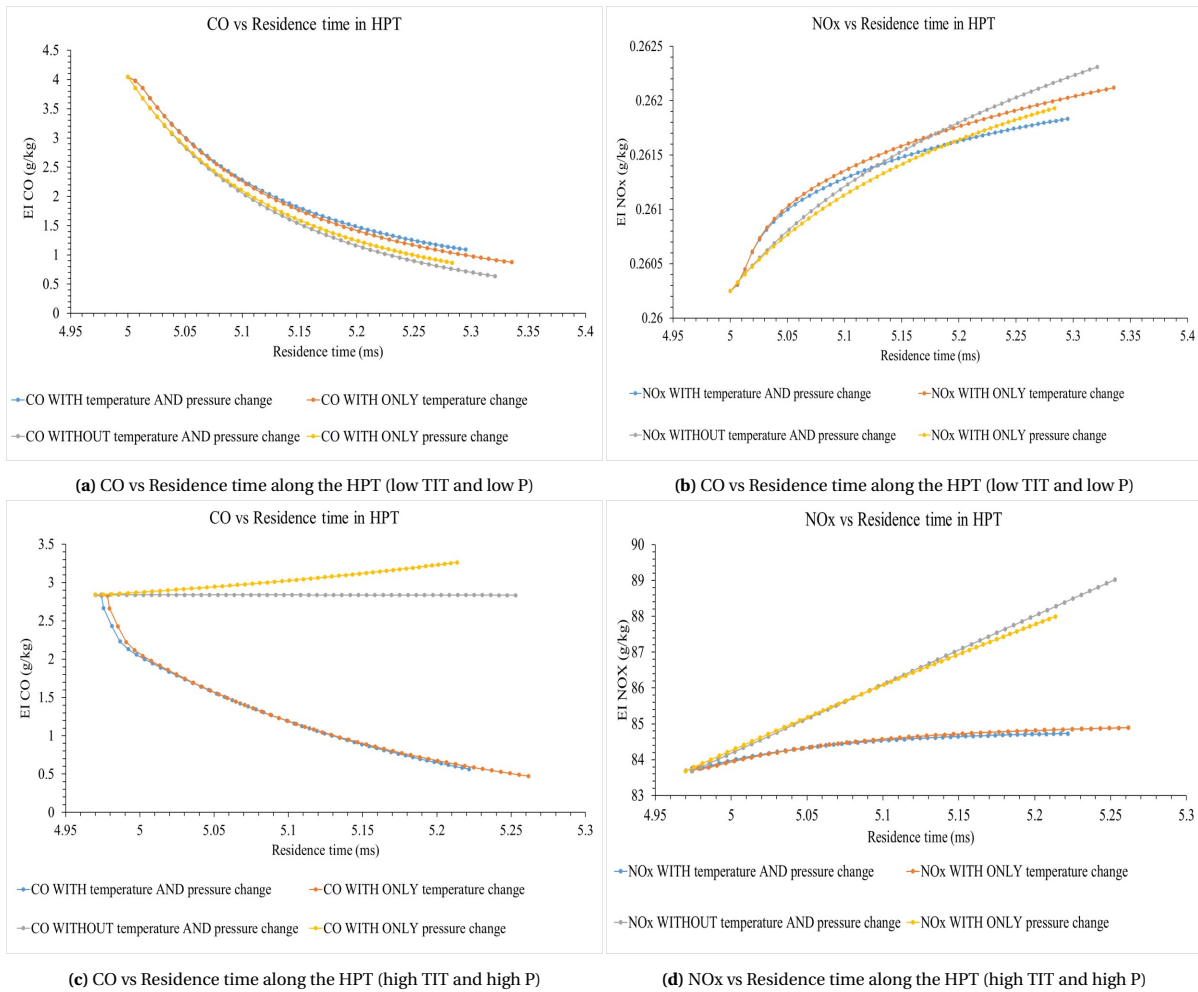


Figure 4.34: CO and NOx vs Residence time in the HPT for four scenarios corresponding to the temperature change and pressure expansion for the lowest and highest temperature and pressure

The use of natural gas for the main combustor of the hybrid engine in comparison to conventional kerosene is clearly beneficial due to the significantly large reduction of emissions as can be seen. While industrial gas turbines predominantly operate with natural gas to satisfy emission requirements to be low, aero-engines typically use only high-quality liquid jet fuels. These fuels usually have a relatively narrow range of properties. The use of natural gas has a great benefit especially in terms of NO_x emissions. The advantage stems mainly from the lower adiabatic flame temperature in case of using natural gas, which has a direct impact in reducing NO_x. The adiabatic flame temperature is lower mainly due to the carbon-hydrogen ratio. In general, in comparison to kerosene, natural gas gives lower emissions even at the same operating temperatures and pressures. This is because of some of the important properties of the fuel such as the carbon-hydrogen ratio, the final products composition, thermal and chemical stability, lesser molecular weight, low carbon formation leading to better outcome in terms of emissions. [129]. Therefore, advanced lean premixing combustor design such as the main combustor of the hybrid engine configuration, which aims for low emissions, can tap into the benefits of using natural gas since it is associated with high thermal stability and thus can be used relatively easier with a multi-point fuel injection system. Lean premixing systems can benefit from natural gas also because it has ignition delay time of almost an order of magnitude longer than conventional aviation fuels thus giving longer time to premix [74].

4.9. Evolution of emissions for a conventional turbofan engine

Though the behaviour of emissions in the novel hybrid engine configuration has been studied, it would also be interesting to look into that of a conventional turbofan engine. For this reason, the CF680 turbofan engine of General Electric has been chosen. This is a high bypass turbofan engine which was initially developed in the 1970s. The engine has a bypass ratio of 5 and an overall pressure ratio of 30.08. The engine comprises of maximum thrust of 249kN. The CF680 engine family has three variants - the 80A, C2 and E1. The cutaway drawing of the C2 variant is given in figure 4.35.

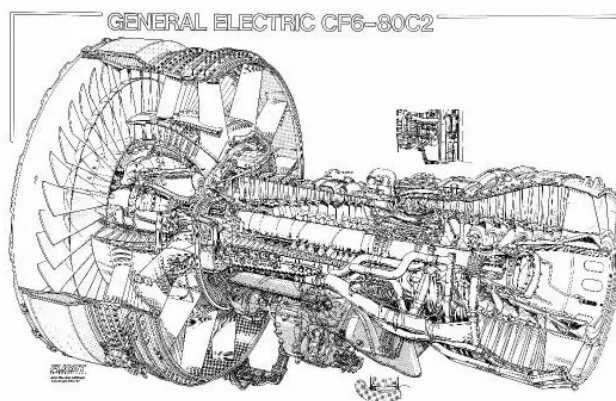


Figure 4.35: The cutaway drawing of the CF680C2 engine

This specific engine has also been used in the work of Telidevara [18] which was focused on building an emission prediction tool for an RQL combustor, and used this engine for comparison and validation of emission predictions. For this purpose, the cycle parameters pertaining to the engine were obtained by using the modeling tool Gasturbine Simulation Program (GSP). These were obtained for four power settings of the engine pertaining to four operating conditions. TUDelt's in-house tool - Aerocomb, was used to obtain the volume of each region in the combustor. Thus, the reactor volumes for each combustion zone are specified. Although the reactor architecture used in [18] is different from what was used in this thesis, the volumes from that CRN were adapted to the reactors of this CRN. The engine cycle parameters corresponding to this engine have been described in table 4.3 and the volume of the reactors have been mentioned in table 4.4.

The CRN for the CF6-80 from [18] had used the Aachen Kerosene surrogate mechanism which has also been used here. This was helpful to check the current CRN's capability in replicating the modeling of the

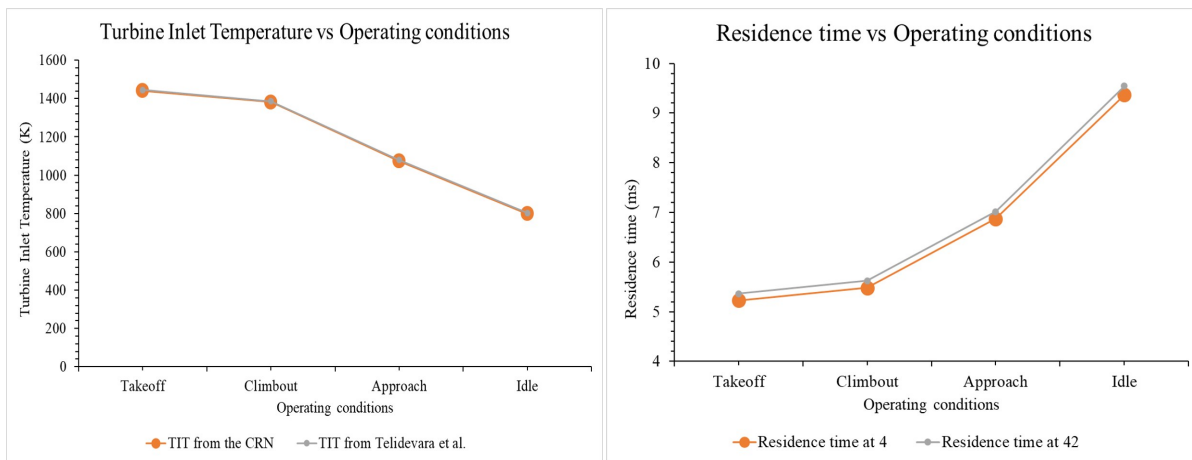
Thrust	Operating condition	$T_{t3}[K]$	$P_{t3}[bar]$	$\dot{m}_3[kg/s]$	$\dot{m}_{f3}[kg/s]$	ϕ
100%	Takeoff	796.56	30.48	124.1	2.29	0.27
85%	Climbout	768.54	26.42	109.97	1.91	0.26
30%	Approach	626.44	12.14	58.06	0.69	0.18
7%	Idle	508.71	5.88	33.05	0.24	0.11

Table 4.3: Cycle parameters corresponding to the four operating conditions for the CF6-80 engine

Reactor	Volume [m^3]
Mixer	1.95e-3
Flame	1.52e-2
Recirculation	4.2e-3
Postflame	4.74e-2

Table 4.4: Reactor volumes corresponding to the CRN for the CF6-80 combustor

CR6-80 engine which was validated in [18]. Thus, the current CRN's effectiveness for the same was estimated by comparing the TIT predicted by the engine with that from [18]. The comparison showed a good fit. One of the main differences between the architecture of both CRNs was that the CRN from [18], which was intended for RQL combustors thus had primary, secondary and dilution air distributions of the total air such the local equivalence ratios achieved are pertinent to that for RQL type. In the current CRN, all of the total air is fed at the mixer reactor. Inspite of this difference, the match between the TIT from both CRNs was still close. The HPT reactor which was used for the hybrid engine configuration has been retained for this CRN. The TIT and the residence time for this engine conditions have been shown in figure 4.36. In order to study the behaviour of emissions along the turbine, the temperature and pressure at the stator exit need to be calculated. Using the cycle parameters and the component data of CF6-80 as mentioned in [127] the stator exit temperatures and pressures were calculated. These are denoted in table 4.5.



(a) Turbine Inlet Temperature vs Operating conditions for the CF6-80 turbofan engine **(b)** Residence time at the stator inlet and the exit vs Operating conditions for the CF6-80 turbofan engine

Figure 4.36: Turbine Inlet Temperature and Residence time of the CF6-80 engine with operating conditions

Operating condition	T_{42} [K]	P_{42} [bar]
Takeoff	1081.57	16.65
Climbout	1036.23	14.36
Approach	699.1	3.45
Idle	585.82	2.89

Table 4.5: Stator exit temperatures and pressures calculated for the CF6-80 operating conditions

Using these, the change in CO and NO_x emissions from the stator inlet to the exit was estimated for the engine. The results are shown in figure 4.37. It can be seen that the change in CO and NO_x emissions is insignificant. This can be attributed to the magnitude of the operating temperature and pressure. Even at the highest power setting, the operating values of temperature and pressure are still relatively small such that for the residence time in the stator, there is not any change in the emission values. Previously, section 2.7 showed studies on the change in emissions for conventional engines. These engines had similar and a little higher operating temperatures and pressures and showed the consequence of these conditions on the behaviour of the emissions, which was shown to be not negligible in some cases. In this case, one of the reasons for this observation, other than the operating conditions can also be the fact that the same HPT reactor was used. While the reactor volumes for all the combustor zones is available, for the HPT the reactor, the one corresponding to the hybrid engine configuration has been used. This reactor has a cross section that is almost 60% smaller than if the HPT reactor dimensions were to be calculated for this relatively low bypass turbofan engine, which leads to considerably lower residence time in the stator.

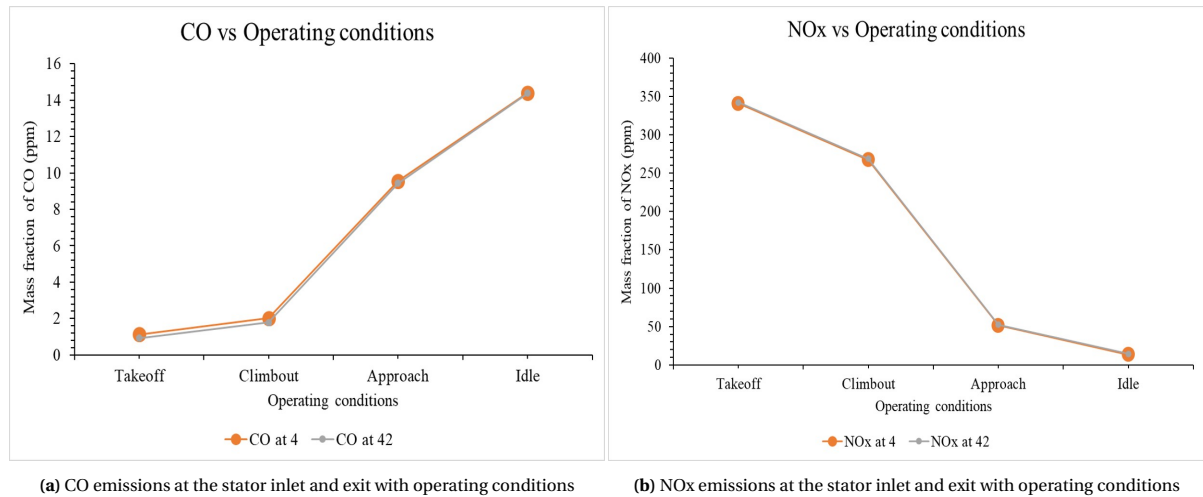


Figure 4.37: The emissions at the stator inlet and exit for different operating conditions of the CF6-80 turbofan engine

4.10. Summary

This chapter provided the extensive results and their relevant discussions. The detailed parametric analysis for the hybrid engine showed the individual role of each parameter in determining the resulting CO and NO_x. The benefits of using LNG over kerosene in the main combustor were also demonstrated quantitatively. The variation of emissions in the HPT for an older engine was also shown.

5

Conclusions and Recommendations

This chapter aims to describe the conclusions that can be drawn from the results discussed in chapter 4. This is preceded by a summary of this report. Furthermore, recommendations for extending the work of this research topic have also been presented here.

5.1. Summary

All kinds of future trend predictions show the never-declining growth of air traffic. On the other hand, the impact of emissions on the environment and human health are also increasingly becoming evident. This has therefore been addressed by aviation authorities and regulatory bodies in the form of stricter regulations and more ambitious targets for future emissions. Thus, there is necessity to develop and improve novel aircraft engine configurations.

In this context, the AHEAD consortium was an ambitious undertaking which aims to develop a multi-fuel, blended wing-body aircraft which would operate with a hybrid engine configuration that has two combustors, and would use alternative fuels by making use of the advantage offered by the blended wing-body. This engine is an ultra high bypass turbofan engine and would have a high overall pressure ratio of 70. This inevitably leads to high operating pressures and temperatures of the gas turbine components. Consequently, the estimation of development trend for the turbine inlet temperature also shows steady increase for future engines coming into service.

While emissions are usually measured at the engine exhaust in case of experimental studies, computational modeling of emissions usually ends with the combustor. This is due to the assumption of frozen chemistry after the combustor. The literature review has shown that the thermodynamic conditions in the high pressure turbine result in an active chemistry in the HPT, and the influence it can have on the emission species cannot be ignored in some cases. Most of previous literature has focused on sulphur and soot emissions, and have done so for only the specific operating conditions of the considered engine. This research work intended to focus on CO and NO_x emissions which are the minor species in the exhaust gases. For more accurate modeling of these minor species the use of detailed chemical reaction mechanisms is more preferable. But using CFD modeling along with detailed chemical reaction mechanisms are computationally expensive. Therefore CRN modeling has been employed in this research. Although the combustor and turbine flow-field are highly simplified by this approach, it can still serve as a good first-estimate for the behaviour of emissions. The CRN architecture was used based on literature and the CRN model was validated using another study which also focused on emissions from a conventional turbofan engine.

Since there is not exact knowledge available on the decoupled influence of every parameter on the behaviour of emissions *after* the combustor, this work focused on doing a parametric analysis in order to see the role of each parameter in detail. Given that the modeling tool is of CRN modeling, the parameters which can be flexibly explored using this tool have been selected and studied. These were the turbine inlet temperatures, inlet pressures, (combustor) residence times, reaction mechanisms, temperature change and expansion corresponding to the HPT. Natural gas is a known better option compared to typical aviation fuels, in terms of emissions. In case of the hybrid engine the level of advantage that LNG provides over the usage of kerosene

has also been demonstrated. Furthermore, the change in emissions along the HPT of a conventional turbofan has also been looked into. This sheds light on the fact that, although the chemistry from older engines can be considered to be frozen, the same assumption cannot hold good in case of a futuristic architecture like the hybrid engine. As engine development trends predict, the operating pressures and temperatures keep increasing for future aircraft engines, and the hybrid engine design is a good demonstration of that fact. In these high operating conditions the increase of NO_x with residence time in the HPT cannot be ignored. Although it may be argued that CO emissions decrease after the combustor and are therefore not important to be considered, in the specific context of the hybrid engine it is still important to consider this changed CO concentration because the exhaust of the main combustor, after passing through the HPT, becomes the "oxidizer" at the inlet of the inter-turbine burner. Therefore, accurate modeling of the inlet conditions of the inter-turbine burner are important to gauge its effectiveness in achieving the ambitious emission standards desired to be met by the hybrid engine configuration. Doing this would help to attain better understanding on possible improvements that can be done to the inter-turbine burner and its operation.

5.2. Conclusions

Previous research which shows the change in emissions downstream of the combustor attribute this to the aerothermodynamics and chemical kinetics that are prevalent. Since CRN modeling was chosen, there is more flexibility at disposal, to explore a broad range of parameters and operating conditions. Thus, the following research question was then studied using the 0D/1D reactor modeling:

How do CO and NO_x evolve after the combustor and what are the parameters that influence this evolution the most?

- The turbine inlet temperature was investigated for a large range which can hold well for future engine configurations. These temperatures were maintained consistently throughout the HPT. The results showed that the change in chemistry of CO between the combustor exit and the stator exit can be significant or not depending on the operating temperature. In case of low TITs, the change in CO between the two stations is so significant that ignoring it would lead to wrong assumptions in studying the inlet conditions of the inter-turbine burner. Whereas for high TITs, the quicker equilibrium attained by CO leads to insignificant differences in CO between the two stations. NO_x emissions, on the other hand, increase between the stator inlet and the exit for all temperatures. But whether the amount of increase is significant or not, is determined by the operating temperature. In case of low temperatures the (insignificant) increase is mainly due to the N₂O pathway, whereas increasing temperatures strengthen the thermal pathway.
- For the wide range of investigated pressures, the temperature determined the behaviour of CO and NO_x. CO from the combustor decreases with increasing pressures. But whether there is a significant change between the stator inlet and the exit depends on the temperature. At low temperatures CO continues to be oxidized in the stator and therefore the difference between CO from the inlet and exit cannot be neglected, and doing so may lead to miscalculations corresponding to the HPT. For higher temperatures, CO reaches equilibrium and thus undergoes meagre change in the HPT. In case of NO_x, it increases with increasing pressures, and the increase between the stator inlet and the exit is the highest when the operating temperature is also high because of the thermal pathway, and also the N₂O pathway whose contribution rises with pressures.
- Since temperature has been found to have a major impact in the behaviour of both emissions, the sensitivity of the reaction mechanism used has been studied for varying TITs. This showed that the trend of behaviour predicted by all mechanisms were the same and the use of a specific mechanism can, in principle, likely lead to more accurate quantitative results if the conditions being investigated are within the range in which the reaction mechanism was optimized for. In this case, the GRI3.0 and the Polimi mechanisms are better suited and therefore present more reliable results.
- When the combustor residence time is studied, temperature again decides the outcome in a major way. CO is known to decrease with increasing residence times which holds true in this study also, for both

low and high temperatures. CO is associated with fast chemistry and therefore a small amount of higher residence time also leads to significant change in the amount of CO obtained from the combustor and also the amount of CO from the stator exit, in case of low operating temperature. The equilibrium at high temperature is maintained except for minute changes between the stator inlet and exit, with increasing residence time. NOx increases with increasing residence time and results in significant change in amount between the stator inlet and exit in case of high temperature.

- If the change in pressure and temperature were to be considered as in a real HPT it goes on to show the considerable change in the concentration of CO and NOx between the stator inlet and the exit. For both the highest and lowest power settings, the difference in CO between the stator inlet and the exit is significant. Thus, assuming an inlet concentration of CO for the inter-turbine burner equal to that at the main combustor exit would lead to inconsistency which is not negligible. In case of NOx, while the lowest condition leads to a minor change in composition, the highest condition leads to a change in NOx which if ignored can lead to improper assessment of the inter-turbine burner's ability to lead to very low NOx values. This outcome is in contrast to what was obtained for the CF6-80 turbofan engine. Even at its highest power setting the change in NOx and CO in the HPT was not considerable. That is because of the temperature and pressure which is associated with its highest power setting. Future aircraft engines aim for high operating pressures and temperatures and the hybrid engine is an example of one such futuristic engine configuration. While it may have been right to ignore the chemistry after the combustor for an engine like the CF6-80, employing the same practice would lead to prediction of emissions with debatable accuracy. The use of alternative fuels like LNG over the use of kerosene has also been shown to be advantageous in all scenarios especially in terms of NOx emissions.

Thus the aforementioned research question and analysis following it lead to the explained behaviour of CO and NOx in the HPT with the temperature playing to be the most important deciding parameter in terms of how significant or not the change between the emissions in the stator inlet and exit are. This is followed by the operating pressure as another significant deciding parameter. The change in both of these in the HPT, thus has non-ignorable effects on emission concentration.

5.3. Recommendations for future research

The work from this research topic is subject to certain limitations which have been suggested as ideas to address in case of continuing research on similar lines.

- **Modeling the rotor and inclusion of turbine cooling air:** - This work has been done considering the change that happens until the stator exit. An expected extension of this work is to also model the rotor of the turbine. This can lead to interesting outcomes if the inclusion of the turbine cooling air is also implemented. Turbine blade cooling can have locally beneficial effects for NOx and in contrast adverse effects on CO, according to literature. This would be interesting to be analysed in the context of emission behaviour evolution in the HPT.
- **Investigation for combustion using LH2:** - The use of LH2 in the main combustor has also been conceived and studied previously. While this work studied the evolution of emissions from the exhaust of the main combustor using LNG as the fuel, the same investigation for when LH2 is used as fuel can also lead to interesting outcome in terms of which fuel would be a better option and to what extent that holds.
- **Incorporating unmixedness modeling:** - The combustor CRN has reactors which are based on the assumption of perfect mixing. But this assumption leads to the over estimation of rates of progress in some reactions. Especially NOx estimations can be overestimated due to the thermal NOx in case of a perfect mixing assumption. Literature has shown the effective way of modeling unmixedness by using a number of PSRs in parallel, to model the flame zone, with a normal distribution of local equivalence ratios. This can also be adapted for improving the current estimation of emissions.
- **Hybrid CRN-CFD model:** - While the CRN modeling helps to include detailed mechanisms, the influence of the flow-field can be captured much better by the use of CFD. Thus, a CRN modeling the main combustor can be used with detailed reaction mechanisms to get the combustor outlet concentration

of exhaust species. These can be used to give inlet conditions for CFD modeling of the turbine which would incorporate detailed flow-field and aerothermodynamic aspects and the impact of these on the chemistry in the turbine can be studied using reduced mechanisms of the detailed mechanism used in the CRN modeling. This can shed more light on the specific effects of aerothermodynamics in the turbine, apart from only temperature and pressure variation.

- **Stator-rotor interaction:** - In case of a hybrid CRN-CFD model being employed, the stator-rotor interaction in the single stage axial turbine would be an interesting thing to look into. The analysis of the phenomenon of stator/rotor interaction has been accomplished by various researchers. Almost all of these have emphasized the complex flow field in a turbine cascade due to the interaction of the wake flow with the secondary flows, the tip flows, the profile/boundary layer flows, and cooling flows (in case of a cooled turbine). Due to these complex interactions, the associated flow field is highly unsteady. It also results in losses in the form of entropy, total pressure losses and total temperature losses. Therefore, modeling this phenomenon as steady or quasi-steady is not recommended in case of priority for realistic results. This complex flow field also results in turbulent interactions within the cascade, leading to local hot spots/streaks of very high temperature, high heat transfer, high thermal load, and high losses. Depending on the row gap between the stator and the rotor rows, the heat transfer can be upto 25% higher. In case of a cooled turbine blade, these unsteady flow interactions can reduce the adiabatic film effectiveness by as much as 64% when compared to a steady modeling of the cooled blade. This complex flow field and the interactions in turn have a significant effect on the aerodynamics of the cascade, mainly in the form of pressure perturbations. Therefore, as a result of the turbulent interactions, stagnation pressure and temperature fluctuations, change in heat transfer, and change in aerodynamics due to the secondary flow interactions, the exhaust species from the combustor are subjected to inherent, significant unsteady aerothermal effects. Thus it is important to model the flow unsteadiness while modeling the exhaust flow in the first stage of the HPT.
- **Combustor-turbine interaction:-** Another interesting aspect to look into is the combustor-turbine interaction. This is relatively a very new field of research and has a lot to be explored. Preliminary research on combustor-turbine interaction shows the effect of the combustor hot streaks traveling downstream to the turbine and especially to the pressure side of the rotor leading to overheating of the blade. These hot streaks can show significant local effects in terms of emissions which reverberate downstream as well. Thus, in case of computational resources being extensively available for detailed CFD modeling, the main combustor and the HPT can be modeled together which can lead to significant and interesting finds.

Bibliography

- [1] *Global Market Forecast 2018-2037*, Airbus 2018, <https://www.airbus.com/aircraft/market/global-market-forecast.html>
- [2] M. Marisol and R.M. Harrison, *Aircraft engine exhaust emissions and other airport-related contributions to ambient air pollution: a review*, *Atmospheric Environment*(2014), Vol. 95, pp: 409-455.
- [3] International Air Transport Association, *Local Air Quality* <https://www.iata.org/policy/environment/Pages/laq.aspx>
- [4] European Commission, *Reducing emissions from aviation* https://ec.europa.eu/clima/policies/transport/aviation_en
- [5] *Aviation and Global Atmosphere*, Intergovernmental Panel on Climate Change, 1999.
- [6] International Civil Aviation Organization, <https://www.icao.int/environmental-protection/Pages/default.aspx>
- [7] ICAO - Aircraft Engine Emissions Databank, <https://www.easa.europa.eu/easa-and-you/environment/icao-aircraft-engine-emissions-databank>
- [8] Advisory Council for Aviation Research and Innovation in Europe, *Flight-path 2050*, <https://www.acare4europe.org/sria/flightpath-2050-goals/protecting-environment-and-energy-supply-0>
- [9] B. Owen, D.S. Lee, L. Lim, *Flying into the future: Aviation Emissions Scenarios to 2050*, *Environmental Science and Technology*, 2010, 44 (7), pp 2255–2260, DOI:10.1021/es902530z
- [10] A. H. Lefebvre, D. R. Ballal, *Gas Turbine Combustion - Alternative Fuels and Emissions*, CRC Press, Taylor Francis group.
- [11] E. Bernini, *Advances in Gas Turbine Technology*, Intechopen publications, DOI: 10.5772/664.
- [12] Advanced Hybrid Engine for Aircraft Development - AHEAD Project, <http://www.ahead-euproject.eu/project-description/>.
- [13] A.G. Rao, F. Yin, J.P. van Buijtenen, *A hybrid engine concept for multi-fuel blended wing body*, *Aircraft Engineering and Aerospace Technology: An International Journal* 86/6 (2014) 483–493, DOI: 10.1108/AEAT-04-2014-0054.
- [14] A.A.V. Perpignan, A.G. Rao, D.J.E.M. Rokaerts, *Flameless combustion and its potential towards gas turbines*, *Progress in Energy and Combustion Science*, Vol. 69, pp: 28-62, DOI:<https://doi.org/10.1016/j.pecs.2018.06.002>.
- [15] F. Yin, *Modeling and Characteristics of a Novel Multi-fuel Hybrid Engine for Future Aircraft*, PhD Thesis, TUDelft, DOI: 10.4233/uuid:344b7d9c-f54c-4836-87ca-28582231a3d3, 2016.
- [16] B. Droste, R. Van Gent,, M. Straathof, D. Steenhuizen, M. Kotsonis, F. Geuskens, S. Shroff, A. Gangoli Rao, C. Lada, D. Dewanji, H. Yu, M. Schroijsen, J. Hoekstra, *CleanEra: A Collection of Research Projects for Sustainable Aviation*, Delft University Press, DOI:<http://resolver.tudelft.nl/uuid:e3108e2d-0708-46e9-bdc1-17a5e44cf224>.
- [17] A.M. Savel'ev, A.M. Starik, N.S. Titova, *Investigation of the Dynamics of Formation of Environmentally Harmful Gases in Elements of a Gas Turbine Engine*, *High Temperature*, Vol. 37, pp: 470-478.
- [18] Siddharth Telidevara, *Emission Predictions in RQL-based aero-engines*, Master of Science Thesis, Delft University of Technology, 2015.

- [19] Y. Levy, V. Erenburg, V. Sherbaum, I. Gaissinski, *Flameless Oxidation Combustor Development for a sequential combustion hybrid turbofan engine*, Proceedings of the ASME Turbo Expo 2016: Turbomachinery Technical Conference and Exposition. Volume 4B: Combustion, Fuels and Emissions. Seoul, South Korea. June 13–17, 2016, DOI:<https://doi.org/10.1115/GT2016-58079>
- [20] M.G. Talboom, “Chemical Kinetics Study of the Hybrid Combustion System”, Master of Science Thesis, Delft University of Technology, 2017.
- [21] Gibbs Free Energy, Chemistry, OpenStax, PressBooks, DOI: <https://opentextbc.ca/chemistry/chapter/16-4-free-energy/>
- [22] D. Winterborne, A. Turan, *Advanced Thermodynamics for Engineers*, Second edition, Elsevier Publications.
- [23] T. Hasegawa, *Combustion Performance in a Semiclosed Cycle Gas Turbine for IGCC Fired With co-Rich Syngas and Oxy-Recirculated Exhaust Streams*, ASME Journal of Engineering of Gas Turbines and Power, Vol.134, Issue 9, DOI: <https://doi.org/10.1115/1.4006985>
- [24] A.B. Lebedev, A.N. Secundov, A.M. Starik, N.S. Titova, A.M. Schepin, *Modeling of gas turbine combustor emission*, Proceedings of the Combustion Institute, Vol. 32, Issue 2, pp: 2491-2497, DOI: <https://doi.org/10.1016/j.proci.2008.05.015>.
- [25] M. Baratta, A. Ferrari, Q. Zhang, *Multi-zone thermodynamic modeling of combustion and emission formation in CNG engines using detailed chemical kinetics*, Fuel, Vol. 231, pp: 396-403, DOI: <https://doi.org/10.1016/j.fuel.2018.05.088>.
- [26] E. Neshat, D. Honnery, R.K. Saray, *Multi-zone model for diesel engine simulation based on chemical kinetics mechanism*, Applied Thermal Engineering, Vol. 121, pp: 351-360, DOI: <https://doi.org/10.1016/j.applthermaleng.2017.04.090>.
- [27] V. Golovitchev, Chalmers Univ of Tech, Gothenburg, Sweden, <http://www.tfd.chalmers.se/~valeri/MECH.html>.
- [28] J. Li, Z.W. Zhao, A. Kazakov, M. Chaos, E.L. Dryer, J.J. Scire, *A comprehensive kinetic mechanism for CO, CH₂O and CH₃OH combustion*, International Journal of Chemical Kinetics, Vol. 39, Issue 3, DOI: <https://doi.org/10.1002/kin.20218>.
- [29] X. Zhen, Y. Wang, *Numerical analysis on original emissions for a spark ignition methanol engine based on detailed chemical kinetics*, Renewable Energy, Vol. 81, pp: 43-51, DOI: <https://doi.org/10.1016/j.renene.2015.03.027>.
- [30] Maghbouli, R.K. Saray, S. Shafee, J. Ghafouri, *Numerical study of combustion and emission characteristics of dual-fuel engines using 3D-CFD models coupled with chemical kinetics*, Fuel, vol. 106, pp: 98-105, DOI: <https://doi.org/10.1016/j.fuel.2012.10.055>.
- [31] Z. Zheng, M. Yao, *Charge stratification to control HCCI: experiments and CFD modeling with n-heptane as fuel*, Fuel, DOI: <https://doi.org/10.1016/j.fuel.2008.09.002>.
- [32] T.P. Coffee, *Kinetic mechanisms for premixed, laminar, steady state methane/air flames*, Combustion and Flame, Vol. 55, Issue 2, pp: 161-170, DOI: [https://doi.org/10.1016/0010-2180\(84\)90024-5](https://doi.org/10.1016/0010-2180(84)90024-5).
- [33] P. Benard, V. Moureau, G. Lartigue, Y. D'Angelo, *Large-Eddy Simulation of a hydrogen enriched methane/air meso-scale combustor*, International Journal of Hydrogen Energy, Vol. 42, Issue 4, pp: 2397-2410, DOI: <https://doi.org/10.1016/j.ijhydene.2016.11.206>.
- [34] S. Arun, S. Raghuram, R. Sreenivasan, V. Raghavan, *Effect of hydrogen addition in the co-flow of a methane diffusion flame in reducing nitric oxide emissions*, International Journal of Hydrogen Energy, Vol. 37, Issue 24, pp: 19198-19209, DOI: <https://doi.org/10.1016/j.ijhydene.2012.10.016>.
- [35] GRI Mech 2.11, *Combustion Berkeley*, <http://combustion.berkeley.edu/gri-mech/new21/version21/text21.html#performance>.

- [36] B.A.V. Bennet, Z. Cheng, R.W. Pitz, M.D. Smooke, *Computational and experimental study of oxygen-enhanced axisymmetric laminar methane flames*, *Combustion Theory and Modelling*, Vol. 12, Issue 3, pp: 497-527, DOI: <https://doi.org/10.1080/13647830701843296>
- [37] Explosion Dynamics Laboratory, California Institute of Technology, http://shepherd.caltech.edu/EDL/PublicResources/sdt/cti_mech.html
- [38] GRI Mech 3.0, *Combustion Berkeley*, <http://combustion.berkeley.edu/gri-mech/version30/text30.html>
- [39] G.P. Smith, D.M. Golden, M. Frenklach, N.W. Moriarty, B. Eiteneer, M. Goldenberg, et al. *GRI-Mech 3.0*, http://www.me.berkeley.edu/gri_mech/.
- [40] K. Zaker, M.H. Askari, A. Jazayeri, R. Ebrahimi, B. Zaker, M. Ashjaee, *Open cycle CFD investigation of SI engine fueled with hydrogen/methane blends using detailed kinetic mechanism*, *International Journal of Hydrogen Energy*, Vol. 40, Issue 40, pp: 14006-14019, DOI: <https://doi.org/10.1016/j.ijhydene.2015.08.040>.
- [41] S. Zabarnick, J. Zelina, *Chemical Kinetics of NOx production in a well-stirred reactor*, Intersociety Energy Conversion Engineering Conference, International Energy Conversion Engineering Conference (IECEC), DOI: <https://doi.org/10.2514/6.1994-3828>.
- [42] P. Glarborg, R.J. Kee, J.F. Grcar, A.J. Miller, *PSR: A Fortran Program for modeling well-stirred reactors*, Sandia National Laboratories, SAND86-8209, https://www.researchgate.net/profile/P_Glarborg/publication/236418395_PSE_a_Fortran_program_for_modeling_well-stirred_reactors/links/58864f95aca272b7b44cccf7/PSE-a-Fortran-program-for-modeling-well-stirred-reactors.pdf.
- [43] R.J. Kee, F.M. Rupley, J.A. Miller, *Chemkin -II: A Fortran Chemical Kinetics Package for the Analysis of Gas Phase Chemical Kinetics*, Sandia National Laboratories, SAND89-8909, <https://www.osti.gov/biblio/5681118-chemkin-ii-fortran-chemical-kinetics-package-analysis-gas-phase-chemical-kinetics>.
- [44] K.J. Hughes, T. Turanyi, A.R. Clague, M.J. Pilling, *Development and testing of a comprehensive chemical mechanism for the oxidation of methane*, *International Journal of Chemical Kinetics*, Vol.33, Issue 9, DOI: <https://doi.org/10.1002/kin.1048>
- [45] T. Weydahl, M. Poyyapakkam, M. Seljeskog, N.E.L. Haugen, *Assessment of existing H₂/O₂ chemical reaction mechanisms at reheat gas turbine conditions*, *International Journal of Hydrogen Energy*, Vol. 36, Issue 18, pp: 12025-12034, DOI: <https://doi.org/10.1016/j.ijhydene.2011.06.063>.
- [46] I.G. Zseli, T. Turanyi, *Investigation and reduction of two methane combustion mechanisms*, *Archivum Combustionis*, Vol. 21, Issue 3, pp: 173-177, DOI: <https://www.infona.pl/resource/bwmeta1.element.baztech-article-BWM2-0009-0035/tab/summary>
- [47] Q.D. Wang, *An updated detailed reaction mechanism for syngas combustion*, *Royal Society of Chemistry Advances*, Vol. 4, pp: 4564-4585, DOI: <https://doi.org/10.1039/C3RA45959D>.
- [48] J. Strohle, T. Myhrvold, *An evaluation of detailed reaction mechanisms for hydrogen combustion under gas turbine conditions*, *International Journal of Hydrogen Energy*, Vol. 32, Issue 1, pp: 125-135, DOI: <https://doi.org/10.1016/j.ijhydene.2006.04.005>.
- [49] A.A. Konnov, *Detailed Reaction Mechanism for Small Hydrocarbons Combustion*, Release 0.5, <http://homepages.vub.ac.be/~akonnov/>.
- [50] A.A. Konnov, *Remaining uncertainties in the kinetic mechanism of hydrogen combustion*, *Combustion and Flame*, Vol. 152, Issue 4, pp:507-528, DOI: <https://doi.org/10.1016/j.combustflame.2007.10.024>.
- [51] M.O. Conaire, H.J. Curran, J.M. Simmie, W.J. Pitz, C.K. Westbrook, *A comprehensive modeling study of hydrogen oxidation*, *International Journal of Chemical Kinetics*, Vol. 36, Issue 11, pp: 603-622, DOI: <https://doi.org/10.1002/kin.20036>.

- [52] C. Xu, A.A. Konnov, *Validation and analysis of detailed kinetic models for ethylene combustion*, Energy, Vol. 43, Issue 1, pp: 19-29, DOI: <https://doi.org/10.1016/j.energy.2011.11.006>.
- [53] A.A. Konnov, *Implementation of the NCN pathway of prompt-NO formation in the detailed reaction mechanism*, Combustion and Flame, Vol. 156, Issue 11, pp: 2093-2105, DOI: <https://doi.org/10.1016/j.combustflame.2009.03.016>.
- [54] H. Wang, X. You, A.V. Joshi, S.G. Davis, A. Laskin, F. Egolfopoulos, C.K. Law, *USC Mech Version II, High Temperature Combustion Reaction Model of H₂/CO/Cl-C₄ Compounds*, http://ignis.usc.edu/USC_Mech_II.htm, http://ignis.usc.edu/Mechanisms/USC-Mech%20II/USC_Mech%20II.htm, May 2007.
- [55] H. Wang, E. Dames, B. Sirjean, D. A. Sheen, R. Tango, A. Violi, J. Y. W. Lai, F. N. Egolfopoulos, D. F. Davidson, R. K. Hanson, C. T. Bowman, C. K. Law, W. Tsang, N. P. Cernansky, D. L. Miller, R. P. Lindstedt, *A high-temperature chemical kinetic model of n-alkane (up to n-dodecane), cyclohexane, and methyl-, ethyl-, n-propyl and n-butyl-cyclohexane oxidation at high temperatures, JetSurF version 2.0, September 19, 2010*, <http://web.stanford.edu/group/haiwanglab/JetSurF/JetSurF2.0/index.html>.
- [56] G. Blanquart, H. Pitsch, *Thermochemical Properties of Polycyclic Aromatic Hydrocarbons (PAH) from G3MP2B3 Calculations*, The Journal of Physical Chemistry A, Vol. 111, Issue 28, pp: 6510-6520, DOI: <https://doi.org/10.1021/jp068579w>.
- [57] G. Blanquart, P. Peiprot-Desjardins, H. Pitsch, *Chemical mechanism for high temperature combustion of engine relevant fuels with emphasis on soot precursors*, Combustion and Flame, Vol. 156, Issue 3, pp: 588-607, DOI: <https://doi.org/10.1016/j.combustflame.2008.12.007>.
- [58] K. Narayanaswamy, G. Blanquart, H. Pitsch, *A consistent chemical mechanism for oxidation of substituted aromatic species*, Combustion and Flame, Vol. 157, Issue 10, pp: 1879-1898, DOI: <https://doi.org/10.1016/j.combustflame.2010.07.009>.
- [59] Caltech Mechanism, <http://www.theforce.caltech.edu/CaltechMech/index.html>.
- [60] Y. Li, C-W. Zhou, K.P. Somers, K. Zhang, H.J. Curran, *The Oxidation of 2-Butene: A High Pressure Ignition Delay, Kinetic Modeling Study and Reactivity Comparison with Isobutene and 1-Butene*, Proceedings of the Combustion Institute, Vol. 36, Issue 1, pp: 403-411, DOI: <https://doi.org/10.1016/j.proci.2016.05.052>.
- [61] Aramco Mech 2.0, <http://www.nuigalway.ie/combustionchemistrycentre/mechanismdownloads/aramcomech20/>.
- [62] G.P. Smith, Y. Tao, and H. Wang, *Foundational Fuel Chemistry Model Version 1.0 (FFCM-1)*, <http://nanoenergy.stanford.edu/ffcm1>, <https://web.stanford.edu/group/haiwanglab/FFCM1/pages/download.html>.
- [63] N.M. Marinov, W.J. Pitz, C.K. Westbrook, M. Hori, N. Matsunaga, *An Experimental and Kinetic Calculation of the Promotion Effect of Hydrocarbons on the NO-NO₂ Conversion in a Flow Reactor*, Proceedings of the Combustion Institute, Vol. 27, Issue 1, pp: 389-396, DOI: [https://doi.org/10.1016/S0082-0784\(98\)80427-X](https://doi.org/10.1016/S0082-0784(98)80427-X), <https://combustion.llnl.gov/mechanisms/effect-of-no-addition-to-hydrocarbons/c1c4-hydrocarbons-with-no-addition>.
- [64] E. Ranzi, A. Frassoldati, R. Grana, A. Cuoci, T. Faravelli, A.P. Kelley, C.K. Law, *C1-C3 mechanism - Version 1412*, <http://creckmodeling.chem.polimi.it/menu-kinetics/menu-kinetics-detailed-mechanisms/menu-kinetics-c1-c3-mechanism>.
- [65] N. Peters, B. Rogg, *Reduced Kinetic Mechanisms for Applications in Combustion Systems*, Lecture notes in Physics, Springer, DOI: <https://www.springer.com/gp/book/9783662139523>.
- [66] M.D. Smooke, *Reduced Kinetic Mechanisms and Asymptotic Approximations for methane-air flames*, Lecture notes in Physics, Springer.

- [67] X. Jiang, D. Mira, D.L.Cluff, *The combustion mitigation of methane as a non-CO₂ greenhouse gas*, Progress in Energy and Combustion Science, Vol. 66, pp: 176-199, DOI: <https://doi.org/10.1016/j.pecs.2016.06.002>.
- [68] C.K. Westbrook, F.L. Dryer, *Chemical kinetic modeling of hydrocarbon combustion*, Progress in Energy and Combustion Science, Vol. 10, Issue 1, pp:1-57, DOI: [https://doi.org/10.1016/0360-1285\(84\)90118-7](https://doi.org/10.1016/0360-1285(84)90118-7).
- [69] J.M. Simmie, *Detailed Chemical Kinetic models for the combustion of hydrocarbon fuels*, Progress in Energy and Combustion Science, Vol. 29, Issue 6, pp: 599-634, DOI: [http://dx.doi.org/10.1016/S0360-1285\(03\)00060-1](http://dx.doi.org/10.1016/S0360-1285(03)00060-1).
- [70] J. Warnatz, U. Mass, R.W.Dibble, *Combustion - Physical and Chemical Fundamentals, Modeling and Simulation, Experiments, Pollutant Formation*, 4th Edition, Springer International.
- [71] K. Mazaheri, A. Shakeri, *Numerical optimization of laboratory combustor geometry for NO suppression*, Applied Thermal Engineering, Vol. 102, pp: 1328-1336, DOI: <https://doi.org/10.1016/j.applthermaleng.2016.04.027>.
- [72] J.C. Hewson, M. Bollig, *Reduced mechanisms for NO_x emissions from hydrocarbon diffusion flames*, International Symposium on Combustion, Vol. 26, Issue 2, pp: 2171-2179, DOI: [https://doi.org/10.1016/S0082-0784\(96\)80043-9](https://doi.org/10.1016/S0082-0784(96)80043-9).
- [73] C.J. Sung, C.K. Law, J.-Y. Chen, *Augmented reduced mechanisms for NO emission in methane oxidation*, Combustion and Flame, Vol. 125, pp: 906-919, DOI: [https://doi.org/10.1016/S0010-2180\(00\)00248-0](https://doi.org/10.1016/S0010-2180(00)00248-0).
- [74] Tim.C.Lieuwen, Vigor Yang, *Gas Turbine Emissions*, Cambridge Aerospace Series, Cambridge University Press.
- [75] W.C. Gardiner Jr., *Gas-Phase Combustion Chemistry*, Springer International.
- [76] Moskaleva.L.V, Lin.M.C, *The Spin-Conserved Reaction CH + N₂ → H + NCN: A major pathway to Prompt NO studied by Quantum/Statistical Theory calculations and Kinetic Modeling of Rate Constant*, Proceedings of the Combustion Institute, 28: 2393-401.
- [77] Bartok. W, Engleman. V.S., Goldstein. R, del Valle EG, *Basic Kinetic studies and modeling of Nitrogen Oxide formation in combustion processes*, AIChE Symposium Series 68(126):30, 1972.
- [78] Glarborg. P, Miller. J.A, Kee. R.J, *Kinetic Modeling and Sensitivity Analysis of Nitrogen Oxide formation in well-stirred reactors*, Combustion Flame 65:177, 1986.
- [79] Bowman C.T, *Kinetics of Pollutant Formation and Destruction in Combustion*, Progress in Energy Combustion and Science, 1:33-45.
- [80] A.M. Starik, A.M. Savel'ev, N.S. Titova, U. Schumann, *Modeling of sulfur gases and chemiions in aircraft engines*, Aerospace Science and Technology, Vol. 6, Issue 1, pp: 63-81, DOI: [https://doi.org/10.1016/S1270-9638\(02\)01150-1](https://doi.org/10.1016/S1270-9638(02)01150-1).
- [81] J. Bisson, P. Seers, M. Huegel, F. Garnier, *Numerical prediction of gaseous aerosol precursors and particles in an aircraft engine*, Journal of Propulsion and Power, Vol. 32, Issue 4, pp: 918-928, DOI: [10.2514/1.35943](https://doi.org/10.2514/1.35943).
- [82] C.C. Wey, B.A. Anderson, C. Wey, R.C. Miake-Lye, P. Whitefield, R. Howard, *Overview on the Aircraft Particle Emissions Experiment (APEX)*, Journal of Propulsion and Power, Vol. 23, Issue 3, pp. 898-905, DOI:<https://doi.org/10.2514/1.26406>.
- [83] *Chemical Kinetic Mechanisms for Combustion Applications*, Department of Mechanical and Aerospace Engineering, University of California, San Diego, CA, <http://web.eng.ucsd.edu/mae/groups/combustion/mechanism.html>.

- [84] G.C. Moniruzzaman, F. Yu, *A 0D aircraft engine emission model with detailed chemistry and soot micro-physics*, Combustion and Flame, Vol. 159, Issue 4, pp: 1670-1686, DOI: <https://doi.org/10.1016/j.combustflame.2011.11.006>.
- [85] P. Dakhel, S.P. Lukachko, I.A. Waitz, R.C. Miake-Lye, R.C. Brown, *Postcombustion Evolution of Soot Properties in an Aircraft Engine*, Journal of Propulsion and Power, Vol. 23, Issue 5, pp: 942-948, DOI: <https://doi.org/10.2514/1.26738>.
- [86] C.W. Wilson, A. Petzold, S. Nyeki, U. Schrumann, R. Zellner, *Measurement and prediction of emissions of aerosols and gaseous precursors from gas turbine engines (PartEmis): an overview*, Aerospace Science and Technology, Vol. 8, Issue 2, pp: 131-143, DOI: <https://doi.org/10.1016/j.ast.2003.10.006>.
- [87] A.R. Clague, C.W. Wilson, M. Pourkashanian, L. Ma, *Chemical Kinetic Modelling of the Evolution of Gaseous Aerosol Precursors Within a Gas Turbine Engine*, ASME Turbo Expo: Power for Land, Sea and Air, Vol. 1, pp: 443-451, DOI: [10.1115/GT2004-53704](https://doi.org/10.1115/GT2004-53704).
- [88] S.P. Lukachko, I.A. Waitz, R.C. Miake-Lye, R.C. Brown, M.R. Anderson, *Production of sulfate aerosol precursors in the turbine and exhaust nozzle of an aircraft engine*, Journal of Geophysical Research Atmospheres, Vol. 103, Issue D13, pp: 16159-16174, DOI: [10.1029/98JD00684](https://doi.org/10.1029/98JD00684).
- [89] A.M. Savel'ev, A.M. Starik, N.S. Titova, *Investigation of the Dynamics of Formation of Environmentally Harmful Gases in Elements of a Gas Turbine Engine*, High Temperature, Vol. 37, pp: 470-478.
- [90] A.M. Savel'ev, A.M. Starik, N.S. Titova, *Investigation of the Dynamics of Formation of Environmentally Harmful Gases in Elements of a Gas Turbine Engine*, High Temperature, Vol. 37, pp: 470-478.
- [91] S.C. Hunter, *Formation of SO₃ in gas turbines*, ASME Journal of Engineering for Power, Vol. 104, pp: 44-50, DOI: [10.1115/1.3227262](https://doi.org/10.1115/1.3227262).
- [92] B.W. Harris, *Conversion of Sulfur Dioxide to Sulfur Trioxide in Gas Turbine Exhaust*, ASME Journal of Engineering for Gas Turbines and Power, Vol. 112, Issue 4, DOI: [10.1115/1.2906209](https://doi.org/10.1115/1.2906209).
- [93] R.C. Brown, M.R. Anderson, R.C. Miake-Lye, C.E. Kolb, A.A. Sorokin, Y.Y. Buriko, *Aircraft exhaust sulfur emissions*, Geophysical Research Letters, Vol. 23, pp: 3603-3606, DOI: <https://doi.org/10.1029/96GL03339>.
- [94] T. Godin, S. Harvey, P. Stouffs, *High-Temperature Reactive Flow of Combustion Gases in an Expansion Turbine*, ASME Journal of Turbomachinery, Vol. 119, Issue 3, pp: 554-561, DOI: [10.1115/1.2841157](https://doi.org/10.1115/1.2841157).
- [95] B. Leide, P. Stouffs, *Residual Reactivity of Burned Gases in the Early Expansion Process of Future Gas Turbines*, ASME Journal of Engineering for Gas Turbines and Power, Vol. 118, Issue 1, pp: 54-60, DOI: [10.1115/1.2816549](https://doi.org/10.1115/1.2816549).
- [96] R.C. Miake-Lye, M. Martinez-Sanchez, R.C. Brown, C.E. Kolb, *Plume and wake dynamics, mixing and chemistry behind a high-speed civil transport aircraft*, Journal of Aircraft, Vol. 30, Issue 4, pp: 467-479, DOI: <https://doi.org/10.2514/3.46368>.
- [97] F. Arnold, J. Scheid, Th. Stilp, H. Schlager, M.E. Reinhardt, *Measurements of jet aircraft emissions at cruise altitude I: The odd-nitrogen gases NO, NO₂, HNO₂ and HNO₃*, Geophysical Research Letters, Vol. 19, Issue 24, pp: 2421-2424, DOI: <https://doi.org/10.1029/92GL02926>.
- [98] N.G. Dautov, A.M. Starik, *The influence of nonequilibrium effects in elements of hypersonic ramjet engines on the formation of harmful gas components*, High Temperature, Vol. 33, Issue 2, pp: 276-284.
- [99] B. Karcher, M.M. Hirschberg, P. Fabian, *Small-scale chemical evolution of aircraft exhaust species at cruising altitudes*, Journal of Geophysical Research, Vol. 101, Issue D10, pp: 15169-15190, DOI: <https://doi.org/10.1029/96JD01059>.
- [100] M.R. Anderson, R.C. Miake-Lye, R.C. Brown, C.E. Kolb, *Calculation of exhaust plume structure and emissions of the ER 2 aircraft in the stratosphere*, Journal of Geophysical Research, Vol. 101, Issue D2, DOI: <https://doi.org/10.1029/95JD02366>.

- [101] A.B. Lebedev, A.M. Starik, N.S. Titova, *Numerical investigation of non-equilibrium photochemical processes in the wake of subsonic aircraft*, High Temperature, Vol. 36, Issue 1, pp: 75-89.
- [102] S.P. Lukachko, I.A. Waltz, R.C. Miake-Lye, R.C. Brown, *Engine Design and Operational Impacts on Particulate Matter Precursor Emissions*, Journal of Engineering for Gas Turbines and Power, Vol. 130.
- [103] L. Ma, M.C. Pourkashanian, C.W. Wilson, *A CFD Model for Reacting Flows in an Aero-Engine Hot End Simulator*, ASME Turbo Expo: Power for Land, Sea and Air, Vol. 2, pp: 29-39, DOI: [10.1115/GT2005-68077](https://doi.org/10.1115/GT2005-68077).
- [104] A.R. Clague, C.W. Wilson, M. Pourkashanian, L. Ma, *Chemical Kinetic Modelling of the Evolution of Gaseous Aerosol Precursors Within a Gas Turbine Engine*, ASME Turbo Expo: Power for Land, Sea and Air, Vol. 1, pp: 443-451, DOI: [10.1115/GT2004-53704](https://doi.org/10.1115/GT2004-53704).
- [105] T.H. Nguyen, F. Garnier, *3D Modeling and Simulation of physicochemical transformations in a High Pressure Turbine of an aircraft engine*, ASME, ASME International Mechanical Engineering Congress and Exposition, Vol. 1, Advances in Aerospace Technology, DOI: [10.1115/IMECE2014-40190](https://doi.org/10.1115/IMECE2014-40190).
- [106] T.H. Nguyen, P. Nguyen-Tri, X. Vancassel, F. Garnier, *Aero-thermodynamic and chemical process interactions in an axial high-pressure turbine of aircraft engines*, International Journal of Engine Research, DOI: <https://doi.org/10.1177/1468087418772228>.
- [107] Abhishek Bhat and Arvind Gangoli Rao, "AHEAD Deliverable 2.1 Annex: Prediction of emissions from AHEAD engine variants using detailed chemistry and reaction models", Technical report, 2012.
- [108] B. Rosati, *Prediction of Emissions from Combustion systems using OD and 1D reacting flow models - Chemical Reactor Network Modeling*, Master of Science Thesis, Delft University of Technology, 2015.
- [109] Stephen R Turns, *An Introduction to Combustion: Concepts and Applications*, McGraw Hill Publications.
- [110] J.D. Mattingly, W.H. Heiser, D.T. Pratt, K.M. Boyer, B.A. Haven, *Aircraft Engine Design*, Third Edition, AIAA Education Series, DOI: <https://doi.org/10.2514/4.105173>
- [111] S.A. Shakariyants, J.P. van Buijtenen, W.P.J. Visser, *Generic Geometry Definition of the Aircraft Engine Combustion Chamber*, Proceedings of the ASME Turbo Expo 2004: Power for Land, Sea, and Air. Volume 2: Turbo Expo 2004, pp: 173-180, DOI: <https://doi.org/10.1115/GT2004-53522>
- [112] H. Xiao, A. Valera-Madina, R. Marsh, P.J. Bowen, *Numerical study assessing various ammonia/methane reaction models for use under gas turbine conditions*, Vol.196, pp: 344-351, DOI: <https://doi.org/10.1016/j.fuel.2017.01.095>
- [113] Rutar, T., and Malte, P. C. (September 24, 2002). "NO_x Formation in High-Pressure Jet-Stirred Reactors With Significance to Lean-Premixed Combustion Turbines ." ASME. J. Eng. Gas Turbines Power. October 2002; 124(4): 776–783. <https://doi.org/10.1115/1.1492829>
- [114] V. Fichet, M. Kanniche, P. Plion, O. Gicquel, *A reactor network model for predicting NO_x emissions in gas turbines*, Fuel, Vol. 89, Issue 9, pp: 2202-2210, DOI: <https://doi.org/10.1016/j.fuel.2010.02.010>
- [115] Philip P. Walsh, Paul Fletcher, *Gas Turbine Performance*, Blackwell Science, Blackwell Publishing Company Ltd.
- [116] S.L. Dixon, C.A. Hall, *Fluid Mechanics and Thermodynamics of Turbomachinery*, Sixth Edition, Elsevier, DOI: <https://doi.org/10.1016/C2009-0-20205-4>
- [117] D. Kroninger, M. Lipperheide, M. Wirsum, *Effects of Hydrogen Fueling on NO_x emissions – A reactor model approach for an Industrial Gas Turbine Burner*, Proceedings of the ASME Turbo Expo 2017: Turbomachinery Technical Conference and Exposition. Volume 4B: Combustion, Fuels and Emissions, 2017, DOI: <https://doi.org/10.1115/GT2017-64401>
- [118] A.A.V. Perpignan, *Emission Modelling from a Multi-Fuel Dual Combustor Gas Turbine*, PhD Thesis, TUDelft, DOI: <https://doi.org/10.4233/uuid:094af2d0-3fb0-4067-9706-888592d15760>, 2020.

- [119] R.W. Fenning, H.T. Tizard, *The dissociation of carbon dioxide at high temperatures*, Proceedings of the Royal Society Publishing, Vol. 115, Issue 771, DOI:<https://doi.org/10.1098/rspa.1927.0095>.
- [120] L.B. Ibragimova, G.D. Smekhov, O.P. Shatalov, A.V. Eremin, V.V. Shumova, *Dissociation of CO₂ molecules in a wide temperature range*, High Temperature, Vol. 38, Issue 1, pp: 33-36, DOI:<https://doi.org/10.1007/BF02755563>.
- [121] A.R. Morr et al., *Measurements and Predictions of Carbon Monoxide Emissions from an Industrial Gas Turbine*, Journal of Combustion Science and Technology, Vol.11, Issue 3-4, pp: 97-109, DOI:<https://doi.org/10.1080/00102207508946689>
- [122] L.D. Aceto, R. Kollrack, *Primary Zone Carbon Monoxide Levels for Gas Turbines Part I-Premixed Combustion*, AIAA Journal, Vol.12, Issue 4, 1974, DOI:<https://doi.org/10.2514/3.49269>
- [123] S.M. Correa, *A Review of NO_x Formation Under Gas-Turbine Combustion Conditions*, Journal of Combustion Science and Technology, Vol.87, Issue 1-6, pp: 329-362, DOI:<https://doi.org/10.1080/00102209208947221>
- [124] G.L. Leonard, S.M. Correa, *NO_x Formation in Lean Premixed High-Pressure Methane Flames*, Second ASME Fossil Fuel Combustion, pp:69-74.
- [125] A.G. Rao, D.J.E.M. Roekaerts, A. Bohlin, *Lectures - Combustion in Propulsion and Power Technologies*, Delft University of Technology.
- [126] D.G. Nicol, R.C. Steele, N.M. Marinov, P.C. Malte, *The Importance of the Nitrous Oxide Pathway to NO_x in Lean-Premixed Combustion*, Journal of Engineering for Gas Turbines and Power, Vol.117, Issue 1, pp: 100-111, DOI:<https://doi.org/10.1115/1.2812756>
- [127] G. Doulgeris, T. Korakianitis, E. J. Avital, P. Pilidis, P. Laskaridis, *Effect of jet noise reduction on gas turbine engine efficiency*, Proceedings of the Institution of Mechanical Engineers, Part G: Journal of Aerospace Engineering, Vol. 227, Issue 9, DOI: <https://doi.org/10.1177/2F0954410012456925>.
- [128] E. G. Eddings, S. Yan, W. Ciro, A. F. Sarofim, *Formulation of a surrogate for the simulation of jet fuel pool fires*, Journal of Combustion Science and Technology, Vol.177, Issue 4, pp: 715-739, DOI:<https://doi.org/10.1080/00102200590917248>
- [129] S. Blakey, L. Rye, C.W. Wilson, *Aviation gas turbine alternative fuels: A review*, Proceedings of the Combustion Institute, Vol.33, Issue 2, pp:2863-2885, DOI:<https://doi.org/10.1016/j.proci.2010.09.011>
- [130] X. You, F.N. Eglolfopoulos, H. Wang, *Detailed and simplified kinetic models of ndodecane oxidation: The role of fuel cracking in aliphatic hydrocarbon combustion* Proceedings of the Combustion Institute, Vol. 32, Issue 1, pp: 403-410, DOI:<https://doi.org/10.1016/j.proci.2008.06.041>
- [131] T. Edwards, L.Q. Maurice, *Surrogate mixtures to represent complex aviation and rocket fuels*, Journal of Propulsion and Power, Vol.17, Issue 2, pp: 461-466, DOI:<https://doi.org/10.2514/2.5765>
- [132] S. Honnet, K. Seshadri, U. Niemann, N. Peters, *A surrogate fuel for Kerosene* Proceedings of the Combustion Institute, Vol.32, Issue 1, pp: 485-492, DOI:<https://doi.org/10.1016/j.proci.2008.06.218>